

Quantifying the sensitivity of post-glacial sea level change to laterally varying viscosity

Ophelia Crawford^{1*}, David Al-Attar¹, Jeroen Tromp^{2,3}, Jerry X. Mitrovica⁴,
Jacqueline Austermann^{1,5}, Harriet C. P. Lau⁴

¹*Bullard Laboratories, Department of Earth Sciences, University of Cambridge, Madingley Road, Cambridge, CB3 0EZ, UK*

²*Department of Geosciences, Princeton University, Princeton, NJ 08544, USA*

³*Program in Applied & Computational Mathematics, Princeton University, Princeton, NJ 08544, USA*

⁴*Department of Earth and Planetary Sciences, Harvard University, 20 Oxford Street, Cambridge, MA 02138, USA*

⁵*Lamont Doherty Earth Observatory, Columbia University, Palisades, NY 10964, USA*

*E-mail: oc251@cam.ac.uk

6 May 2018

SUMMARY

We present a method for calculating the derivatives of measurements of glacial isostatic adjustment (GIA) with respect to the viscosity structure of the Earth and the ice sheet history. These derivatives, or kernels, quantify the linearised sensitivity of measurements to the underlying model parameters. The adjoint method is used to enable efficient calculation of theoretically exact sensitivity kernels within laterally heterogeneous earth models that can have a range of linear or non-linear viscoelastic rheologies. We first present a new approach to calculate GIA in the time domain, which, in contrast to the more usual formulation in the Laplace domain, is well suited to continuously varying earth models and to the use of the adjoint method. Benchmarking results show excellent agreement between our formulation and previous methods. We illustrate the potential applications of the kernels calculated in this way through a range of numerical calculations relative to a spherically symmetric background model. The complex spatial patterns of the sensitivities are not intuitive, and this is the first time that such effects are quantified in an efficient and accurate manner.

Key words: Sea level change; Dynamics of lithosphere and mantle; Transient deformation; Numerical modelling; Inverse theory

1 INTRODUCTION

Over glacial cycles, sea level varies in both space and time due to the melting of ice sheets. The way in which the Earth responds to such a change in surface load depends on the details of the ice sheet history and also the structure of the Earth – in particular, its viscosity structure. It is therefore possible to use measurements of the response, known as glacial isostatic adjustment (GIA), to learn about both of these aspects, and there have been many such studies, from Haskell (1935) to more recent work (e.g., Nakada & Lambeck 1989; Mitrovica 1996; Lambeck et al. 1998; Peltier 2004; Argus et al. 2012; Nakada et al. 2015; Lau et al. 2016).

In order to use measurements of GIA in this way, there are two aspects of the problem that require consideration. The first of these is forward modelling where, given an ice history and earth model, the response of the Earth is calculated. The second is, as mentioned above, using measurements of the response to say something about the ice history and viscosity structure – the inverse problem.

In modelling GIA, we require a method of calculating the viscoelastic deformation of the Earth due to changes in ice load that includes a number of effects. Firstly, the deformation must be coupled to sea level. A changing ice distribution will lead to a changing water distribution, and the deformation associated with this redistribution will alter the shape of the two surfaces that bound sea level – the solid surface of the Earth and the gravitational equipotential surface that defines the sea surface. The impact of the Earth's rotation must also be considered. The evolving surface mass load will perturb the Earth's moment of inertia both by the direct effect of mass redistribution and by the deformation driven by this redistribution. Therefore, the

Earth's rotation rate will change in order to conserve the total angular momentum of the system. Such a change will result in deformation in both bounding surfaces of sea level. We therefore require a gravitationally and rotationally self-consistent way of modelling sea level change. It has also been shown that it is important to include the effects of shoreline migration in order to model GIA accurately (e.g., Mitrovica & Milne 2003). Most studies of GIA solve the forward problem through use of the so-called sea level equation, which was introduced by Farrell & Clark (1976) with further developments by a number of authors (e.g., Johnston 1993; Lambeck et al. 1998; Milne & Mitrovica 1998; Milne et al. 1999; Mitrovica & Milne 2003; Kendall et al. 2005). It is also common to solve the equations of motion in the Laplace transform domain (Peltier 1974); however, this method is not well suited to Earth structures with lateral variations or continuous radial variations (e.g., Fang & Hager 1995; Han & Wahr 1995; Boschi et al. 1999).

When considering the inverse problem, it would be useful to have a way of calculating the derivatives of measurements with respect to the parameters we wish to determine. Such derivatives provide a measure of the sensitivity of a given measurement to the model and have a number of potential applications within the inverse problem. Firstly, they could be used within a gradient-based optimisation method to find a model that minimises some data misfit function (e.g., Nocedal & Wright 1999). The derivatives could also be used to quantify the uncertainty in such a model and hence to provide understanding of which parts of the model are well constrained. Finally, the derivatives could enable construction of measurements which provide sensitivity to a particular part of the model space in the manner of Backus & Gilbert (1968).

We would expect the Earth's viscosity to vary continuously, both radially and laterally, and there is increasing evidence that the neglect of lateral variations is incompatible with observations and can lead to significant errors within inferences of paleo-climatological interest (e.g., Lambeck & Chappell 2001; A et al. 2013; Van der Wal et al. 2015; Creveling et al. 2017). We would therefore like to be able to calculate continuous, three-dimensional derivatives of measurements with respect to the viscosity structure. Furthermore, we would like to be able to calculate derivatives with respect to ice sheet history. While there now exist a range of computational tools for modelling GIA within laterally heterogeneous Earth models (e.g., Zhong et al. 2003; Wu 2004; Latychev et al. 2005), it is less clear how they can be used effectively within inverse studies to investigate Earth structure and ice sheet history. Forward calculations within three-dimensional models are sufficiently time consuming and involve such a large number of parameters that methods based on trial-and-error or grid-searches are unfeasible.

As an alternative, the adjoint method (e.g., Lions 1970) provides an efficient way of calculating the derivatives we desire and has been used in a number of geophysical applications (e.g., Bunge et al. 2003; Tromp et al. 2005; Li et al. 2011; Crawford et al. 2017). The first application of adjoint methods to GIA was Al-Attar & Tromp (2014), who considered the sensitivity of viscoelastic deformation to surface loads and the viscosity structure. Since then, Martinec et al. (2015) applied the method in order to calculate the sensitivity of measurements to viscosity for GIA including sea level. Furthermore, Larour et al. (2017) have recently calculated the sensitivity of specific locations to present-day mass loss, but address only elastic, and not viscoelastic, deformation. This paper also makes use of a technique known as automatic differentiation as opposed to deriving the adjoint equations.

In this paper, we present a method for forward modelling GIA in the time domain in compressible and heterogeneous earth models. The evolution equations we derive can be numerically integrated without requiring us to solve the sea level equation. We consider only a Maxwell rheology, but the method is applicable to transient linear rheologies and non-linear rheologies through extensions discussed in Crawford et al. (2017). We note that in this paper we do not include the rotation of the Earth; this extension will be the subject of future work. Our forward formulation allows us to apply the adjoint method to the inverse problem, and we use this method to derive equations for the sensitivity of measurements of GIA to both the viscosity structure of the Earth and to the ice sheet history. In order to do this, we build on the work of Al-Attar & Tromp (2014) by including gravitationally self-consistent sea level change. Our formulation is entirely independent of that of Martinec et al. (2015), and is more general and convenient for practical GIA applications. In particular, we present kernels for three-dimensional viscosity perturbations and with respect to ice sheet history. Furthermore, in contrast to Larour et al. (2017), we derive the exact adjoint equations, an approach that is more elegant and flexible than, and offers numerical advantages over, automatic differentiation. The forward and inverse aspects are illustrated with numerical examples calculated in a spherically symmetric earth model.

2 THE GIA FORWARD PROBLEM

We consider the viscoelastic deformation of an earth model possessing surface oceans and ice sheets. In doing so, we follow previous work (e.g., Mitrovica & Milne 2003; Kendall et al. 2005) in making several assumptions. Firstly, we assume that the oceans and ice sheets are sufficiently thin that their interaction with the solid earth can be accurately represented through an associated surface load. Furthermore, we assume that the water surface is defined everywhere by the same gravitational equipotential and so neglect the possibility of isolated bodies of water. We also assume that, prior to the commencement of the deformation, the Earth is in hydrostatic equilibrium. This assumption cannot strictly be valid if the earth model possesses lateral variations in its density structure or if there is aspherical topography on any internal or external boundaries (Dahlen

& Tromp 1998). In particular, a truly hydrostatic earth model would either have to be covered by a global ocean or none at all, and so could not possess both continental and oceanic regions on its surface. However, it is expected that the departure from hydrostatic equilibrium due to realistic lateral variations will be small, and we therefore neglect additional terms in the equations of motion associated with deviatoric pre-stress (Dahlen & Tromp 1998).

The GIA problem is typically solved through the so-called sea level equation, which is generally solved iteratively. Here, however, we present a different approach; we derive coupled evolution equations that capture the same physics but can be solved numerically using an explicit time-stepping scheme. This is an advantage in itself; however, the main motivation for the development of this rate-formulation is its suitability to the application of adjoint methods. The forward method presented in this section is valid in compressible and laterally heterogeneous earth models. We calculate gravitationally self-consistent sea level change, and include shoreline migration.

2.1 Deformation of the solid Earth

We first consider the equations of motion governing the response of the solid Earth to a general surface load. In this context, the “solid Earth” is the part of the model that remains after removal of the oceans and ice sheets; in spite of its name, this can include fluid layers within the Earth, such as a fluid outer core. In what follows, we make extensive use of Al-Attar & Tromp (2014) and also Dahlen (1974), Dahlen & Tromp (1998) and Tromp & Mitrovica (1999).

2.1.1 Equations of motion

We consider the motion of the solid Earth relative to its initial, or reference, configuration at $t = t_0$, which we denote by $M \subseteq \mathbb{R}^3$ with external boundary ∂M . The material particles within this earth model are labelled by \mathbf{x} , their position at the initial time. The earth model has a number of fluid and solid regions that we write as M_F for the former and M_S for the latter. These regions are separated by smooth, non-intersecting, closed surfaces called internal boundaries which consist of four subsets – Σ_{SS} , Σ_{SF} , Σ_{FS} and Σ_{FF} , where the first (second) subscript indicates whether the region on the inside (outside) of the boundary is solid (S) or fluid (F). The union of all boundaries, both internal and external, is written Σ . For times $t \geq t_0$, the deformation of the solid earth is described by

$$\mathbf{r}(\mathbf{x}, t) = \mathbf{x} + \mathbf{u}(\mathbf{x}, t), \tag{2.1}$$

where $\mathbf{r}(\mathbf{x}, t)$ is the spatial point now occupied by the material particle \mathbf{x} and we call $\mathbf{u}(\mathbf{x}, t)$ the displacement. We assume that the displacement is small and so, in what follows, will consider linearised equations of motion. We write $\phi^E(\mathbf{r}, t)$ for the Eulerian gravitational potential at the spatial point $\mathbf{r}(\mathbf{x}, t)$ and time t , and decompose this field as

$$\phi^E(\mathbf{r}, t) = \Phi(\mathbf{r}) + \phi(\mathbf{r}, t), \tag{2.2}$$

where $\Phi(\mathbf{r})$ is the gravitational potential of the reference earth model which satisfies Poisson’s equation,

$$\nabla^2 \Phi = 4\pi G \rho. \tag{2.3}$$

ϕ is the gravitational potential perturbation and, to first order, $\phi(\mathbf{r}, t) = \phi(\mathbf{x}, t)$. Following Dahlen (1974), ϕ satisfies the modified Poisson’s equation,

$$(4\pi G)^{-1} \nabla^2 \phi = \begin{cases} -\nabla \cdot (\rho \mathbf{u}), & \mathbf{x} \in M_S, \\ g^{-1} \phi \partial_n \rho, & \mathbf{x} \in M_F, \\ 0, & \mathbf{x} \in \mathbb{R}^3 \setminus M, \end{cases} \tag{2.4}$$

where ∂_n is the directional derivative along the outward normal to the level surfaces of density ρ and g is the magnitude of the gravitational acceleration. The latter is defined through

$$\nabla \Phi = g \hat{\nu}, \tag{2.5}$$

where $\hat{\nu}$ is thus the local vertical direction.

We have the initial conditions $\mathbf{u}(\mathbf{x}, t_0) = 0$ and $\phi(\mathbf{r}, t_0) = 0$ which follow from the above definitions. As mentioned, we assume that the earth model is in hydrostatic equilibrium initially. In a non-rotating earth model, this assumption implies that the level surfaces of density ρ , pressure p and gravitational potential Φ are concentric spheres. This means that on internal or external boundaries, we must have

$$\nabla \Phi = g \hat{\mathbf{n}}, \tag{2.6}$$

where $\hat{\mathbf{n}}$ is the outward unit normal vector, and so the local vertical direction $\hat{\nu}$ coincides with $\hat{\mathbf{n}}$ on such boundaries.

Neglecting inertial terms, the deformation due to a time-dependent surface loading, $\sigma(\mathbf{x}, t)$, satisfies the quasi-static momentum equation, given by

$$-\nabla \cdot \mathbf{T} + \nabla(\rho \mathbf{u} \cdot \nabla \Phi) - \nabla \cdot (\rho \mathbf{u}) \nabla \Phi + \rho \nabla \phi = \mathbf{0}, \tag{2.7}$$

where \mathbf{T} is the incremental Lagrangian-Cauchy stress tensor and ρ is the density. We also have boundary conditions for the system, which, following Al-Attar & Tromp (2014), are

$$\hat{\boldsymbol{\nu}} \cdot \mathbf{T} = -\sigma \nabla \Phi, \quad \mathbf{x} \in \partial M, \quad (2.8)$$

$$[\hat{\boldsymbol{\nu}} \cdot \mathbf{T}]_+^+ = \mathbf{0}, \quad \mathbf{x} \in \Sigma_{SS}, \quad (2.9)$$

$$\hat{\boldsymbol{\nu}} \cdot \mathbf{T}^+ = \rho^- [\mathbf{u}^+ \cdot \nabla \Phi + \phi] \hat{\boldsymbol{\nu}}, \quad \mathbf{x} \in \Sigma_{FS}, \quad (2.10)$$

$$\hat{\boldsymbol{\nu}} \cdot \mathbf{T}^- = \rho^+ [\mathbf{u}^- \cdot \nabla \Phi + \phi] \hat{\boldsymbol{\nu}}, \quad \mathbf{x} \in \Sigma_{SF}, \quad (2.11)$$

$$[\mathbf{u}]_+^+ = \mathbf{0}, \quad \mathbf{x} \in \Sigma_{SS}, \quad (2.12)$$

$$[\phi]_+^+ = 0, \quad \mathbf{x} \in \Sigma, \quad (2.13)$$

$$[(4\pi G)^{-1} \hat{\boldsymbol{\nu}} \cdot \nabla \phi]_+^+ - \rho^- \hat{\boldsymbol{\nu}} \cdot \mathbf{u}^- = 0, \quad \mathbf{x} \in \partial M, \quad (2.14)$$

$$[(4\pi G)^{-1} \hat{\boldsymbol{\nu}} \cdot \nabla \phi + \rho \hat{\boldsymbol{\nu}} \cdot \mathbf{u}]_+^+ = 0, \quad \mathbf{x} \in \Sigma_{SS}, \quad (2.15)$$

$$[(4\pi G)^{-1} \hat{\boldsymbol{\nu}} \cdot \nabla \phi]_+^+ + [\rho]_+^+ \hat{\boldsymbol{\nu}} \cdot \mathbf{u}^+ = 0, \quad \mathbf{x} \in \Sigma_{FS}, \quad (2.16)$$

$$[(4\pi G)^{-1} \hat{\boldsymbol{\nu}} \cdot \nabla \phi]_+^+ + [\rho]_+^+ \hat{\boldsymbol{\nu}} \cdot \mathbf{u}^- = 0, \quad \mathbf{x} \in \Sigma_{SF}, \quad (2.17)$$

where $+$ and $-$ indicate whether a term is evaluated on the outer or inner side of a discontinuity respectively. We note that the load, σ , appears only through equation (2.8), the equation for the traction on the surface of the Earth. We further require the gravity perturbation to tend to 0 as \mathbf{x} tends to infinity.

2.1.2 Linear viscoelasticity

We require a constitutive equation to describe the rheology of the viscoelastic mantle. Following Al-Attar & Tromp (2014), for an isotropic and linear viscoelastic material with bulk modulus κ and time-dependent shear relaxation function $\mu(t)$ we can write

$$\mathbf{T}(t) = \kappa \nabla \cdot \mathbf{u}(t) \mathbf{I} + \int_{t_0}^t 2\mu(t-t') \dot{\mathbf{d}}(t') dt', \quad (2.18)$$

where a dot over a symbol indicates differentiation with respect to time and

$$\mathbf{d} = \mathbf{e} - \frac{1}{3} \text{tr}(\mathbf{e}) \mathbf{I} \quad (2.19)$$

is the deviatoric part of the linearised strain tensor

$$\mathbf{e} = \frac{1}{2} [\nabla \mathbf{u} + (\nabla \mathbf{u})^T]. \quad (2.20)$$

In equation (2.19), $\text{tr}(\cdot)$ indicates the trace of the matrix. For a Maxwell solid, the shear relaxation function can be written as

$$\mu(t) = \mu_0 e^{-t/\tau}, \quad (2.21)$$

where μ_0 is the unrelaxed shear modulus and τ is the Maxwell relaxation time. It will be useful to define the internal variable

$$\mathbf{m}(t) = \frac{1}{\tau} \int_{t_0}^t e^{-(t-t')/\tau} \mathbf{d}(t') dt', \quad (2.22)$$

which can be seen to satisfy

$$\dot{\mathbf{m}} + \frac{1}{\tau} (\mathbf{m} - \mathbf{d}) = \mathbf{0}. \quad (2.23)$$

We can therefore rewrite equation (2.18) as

$$\mathbf{T} = \kappa \nabla \cdot \mathbf{u} \mathbf{I} + 2\mu_0 (\mathbf{d} - \mathbf{m}). \quad (2.24)$$

From this, we can see that the deviatoric stress, $\boldsymbol{\tau}$, is given by

$$\boldsymbol{\tau} = 2\mu_0 (\mathbf{d} - \mathbf{m}). \quad (2.25)$$

These results can readily be extended to other linear viscoelastic and non-linear viscoelastic materials as described in Crawford et al. (2017).

2.1.3 Rate formulation

In order to incorporate time dependence and a viscoelastic rheology into equation (2.7), we follow the method of Al-Attar & Tromp (2014). Differentiating equation (2.7) and using equations (2.23) and (2.24), we obtain

$$\nabla \cdot (\kappa \nabla \cdot \dot{\mathbf{u}} + 2\mu_0 \dot{\mathbf{d}}) + \nabla \cdot \left[\frac{2\mu_0}{\tau} (\mathbf{m} - \mathbf{d}) \right] - \nabla \cdot (\rho \dot{\mathbf{u}} \cdot \nabla \Phi) + \nabla \cdot (\rho \dot{\mathbf{u}}) \nabla \Phi - \rho \nabla \dot{\phi} = \mathbf{0}. \quad (2.26)$$

We can also differentiate (2.4) and the boundary conditions (2.8) – (2.17). These, along with equation (2.26), constitute the rate formulation in strong form of the viscoelastic loading problem.

2.2 Sea level

We now require the form of the surface load for GIA and the equations governing the time evolution of sea level.

2.2.1 Sea level definitions

We first define ∂M_t to be the outer surface of the solid earth at time t and this is given by

$$\partial M_t = \{\mathbf{x} + \mathbf{u}(\mathbf{x}, t) \mid \mathbf{x} \in \partial M\}. \tag{2.27}$$

Sea level $SL(\mathbf{x}, t)$ is defined at every point on this surface. We assume that the oceans remain in hydrostatic equilibrium throughout the deformation and so the sea surface is an equipotential surface of the gravitational field. We will write the value of the gravitational potential on this surface at a given time as $\Phi_G(t)$. $SL(\mathbf{x}, t)$ is therefore determined implicitly for $\mathbf{x} \in \partial M$ through the equation

$$\phi^E(\mathbf{x} + \mathbf{u}(\mathbf{x}, t) + SL(\mathbf{x}, t)\hat{\nu}(\mathbf{x}, t), t) = \Phi_G(t), \tag{2.28}$$

i.e., sea level is the distance from the solid surface to the gravitational equipotential which defines the sea surface along the direction of the local vertical at the surface.

Above each point on the solid earth surface, there can be an ice sheet of height $I(\mathbf{x}, t)$ and an ocean of height $S(\mathbf{x}, t)$, where these heights are measured in the direction of the local vertical and cannot be negative. We note that, in the GIA literature, I is commonly taken to be the change in ice thickness from the initial value (e.g., Mitrovica & Milne 2003), but we find our definition to be more convenient. The load at the surface comprises both the ocean and ice sheet; we can write

$$\sigma(\mathbf{x}, t) = \rho_w S(\mathbf{x}, t) + \rho_i I(\mathbf{x}, t), \tag{2.29}$$

where ρ_w and ρ_i are the densities of water and ice respectively. Where $S(\mathbf{x}, t)$ and $I(\mathbf{x}, t)$ are simultaneously positive, the ice sheet (or, in this case, ice shelf) floats buoyantly on top of the ocean and so, assuming local isostatic equilibrium between the ocean and ice sheet, we must have

$$\rho_w S(\mathbf{x}, t) + \rho_i I(\mathbf{x}, t) = \rho_w SL(\mathbf{x}, t). \tag{2.30}$$

We note that floating ice here is dynamically equivalent to the presence of the same mass of water. In the case $I(\mathbf{x}, t) = 0$, this equation simplifies to $SL(\mathbf{x}, t) = S(\mathbf{x}, t)$.

Where there is an ocean present, $S(\mathbf{x}, t) > 0$ and so, from equation (2.30), $\rho_w SL(\mathbf{x}, t) > \rho_i I(\mathbf{x}, t)$. Conversely, where there is no ocean present, $S(\mathbf{x}, t) = 0$ and it must therefore hold that $\rho_w SL(\mathbf{x}, t) \leq \rho_i I(\mathbf{x}, t)$. We therefore define the ocean set by

$$\mathcal{O}_t = \{\mathbf{x} \in \partial M \mid \rho_w SL(\mathbf{x}, t) > \rho_i I(\mathbf{x}, t)\}, \tag{2.31}$$

which comprises all those locations where there is an ocean present (including an ocean covered by a buoyant ice sheet). We are then able to define the ocean function by

$$C(\mathbf{x}, t) = \begin{cases} 1, & \mathbf{x} \in \mathcal{O}_t, \\ 0, & \mathbf{x} \notin \mathcal{O}_t, \end{cases} \tag{2.32}$$

which is equivalent to that of Mitrovica & Milne (2003) and reduces to that of Farrell & Clark (1976) in the absence of floating ice sheets. Using the ocean function, we can now write

$$S(\mathbf{x}, t) = C(\mathbf{x}, t) \left[SL(\mathbf{x}, t) - \frac{\rho_i}{\rho_w} I(\mathbf{x}, t) \right], \tag{2.33}$$

which holds at all locations. We can also rewrite equation (2.29) as

$$\sigma = \rho_w C SL + \rho_i (1 - C) I, \tag{2.34}$$

and so, recalling that the ocean function itself depends on SL and I , we see explicitly the non-linear dependence of the surface load on sea level and ice height in the GIA problem.

It will be useful to consider the form of the boundary of the ocean set, which we will write as $\partial \mathcal{O}_t$. From equation (2.31), we can see that this is defined by

$$\partial \mathcal{O}_t = \{\mathbf{x} \in \partial M \mid \rho_w SL(\mathbf{x}, t) = \rho_i I(\mathbf{x}, t)\}. \tag{2.35}$$

Writing ∇_1 for the tangential gradient operator on ∂M , we shall assume that

$$\forall \mathbf{x} \in \partial \mathcal{O}_t : \nabla_1 [\rho_w SL(\mathbf{x}, t) - \rho_i I(\mathbf{x}, t)] \neq \mathbf{0}. \tag{2.36}$$

It then follows from the regular value theorem (e.g, Spivak 1970) that $\partial \mathcal{O}_t$ forms a one-dimensional submanifold on ∂M .

Physically, this result means that the ocean basins have well-defined boundaries on which the ocean locally lies on one side. We can decompose $\partial\mathcal{O}_t$ into locations for which $I(\mathbf{x}, t) = 0$ or for which $I(\mathbf{x}, t) > 0$. In the former case, the boundary to the ocean basin is where the gravitational equipotential that describes the sea surface intersects the solid surface, while for the latter, the boundary lies at the grounding line of the ice sheet. While this simple isostatic relation for the grounding line position is not strictly consistent with ice dynamics (e.g., Schoof 2007), it will be sufficient for our purposes.

2.2.2 The evolution of sea level

In the forward GIA problem, the evolution of the ice sheets is prescribed. It will prove useful to write this as

$$I(\mathbf{x}, t_0) = I_0(\mathbf{x}), \quad (2.37)$$

$$\dot{I}(\mathbf{x}, t) = \dot{I}_1(\mathbf{x}, t), \quad (2.38)$$

i.e., we have the initial ice distribution and the time derivative of the ice sheet thickness at all times. This uniquely defines $I(\mathbf{x}, t)$. Given the initial earth model and ice distribution, we can, in principle, calculate the initial sea level from equation (2.28) with no deformation and so

$$\Phi(\mathbf{x} + SL(\mathbf{x}, t_0)\hat{\nu}, t_0) = \Phi_G(t_0), \quad (2.39)$$

where Φ itself depends on SL . In practice, however, our knowledge of the initial earth model can never be perfect and the above procedure need not lead to sensible values for the initial sea level. We therefore choose to prescribe the initial sea level, and we will write this as

$$SL(\mathbf{x}, t_0) = SL_0(\mathbf{x}). \quad (2.40)$$

We could also, by iteration, find an initial sea level which gives a suitably correct present day sea level (Kendall et al. 2005). We discuss how to perform such calculations using the adjoint method in section 3.5.3.

We now wish to calculate how the sea level evolves with time due to variations in ice thickness. In doing so, we will relate the rate of change of sea level to the deformation of the solid Earth. Differentiating equation (2.28) with respect to time, and retaining only first-order terms in \mathbf{u} and ϕ , we find

$$\dot{S}L = -\frac{1}{g}(\dot{\mathbf{u}} \cdot \nabla\Phi + \dot{\phi}) + \frac{\dot{\Phi}_G}{g}. \quad (2.41)$$

To determine the second term on the right hand side in this equation, we will use the fact that the total mass of water and ice on the surface of the Earth must be conserved. This can be written as

$$\int_{\partial M} (\rho_w \dot{S} + \rho_i \dot{I}) \, dS = 0, \quad (2.42)$$

where we have neglected the difference between the local vertical $\hat{\nu}$ and the outward unit normal vector $\hat{\mathbf{n}}$, which is consistent with our assumption that the reference earth model is in a state of hydrostatic equilibrium, and we ignore the time dependence of these directions. From equation (2.33), we see that

$$\dot{S} = C \left(\dot{S}L - \frac{\rho_i}{\rho_w} \dot{I} \right) + \dot{C} \left(SL - \frac{\rho_i}{\rho_w} I \right). \quad (2.43)$$

In appendix A, we find that \dot{C} is given by

$$\dot{C} = \frac{\rho_w \dot{S}L - \rho_i \dot{I}}{\rho_w \partial_{\perp} SL - \rho_i \partial_{\perp} I} \delta_{\partial\mathcal{O}_t}, \quad (2.44)$$

where $\partial\mathcal{O}_t$ is the boundary of the ocean set given by equation (2.35), $\delta_{\partial\mathcal{O}_t}$ is the Dirac delta function which is only non-zero on the ocean set boundary and ∂_{\perp} is a derivative in the direction perpendicular to this boundary, pointing into the ocean. The derivation is complicated by the fact that this derivative is a distribution rather than an ordinary function; in appendix A, we also sketch a simpler, less formal argument.

Equation (2.44) is only non-zero on $\partial\mathcal{O}_t$, but this is, by definition, where $SL - \frac{\rho_i}{\rho_w} I = 0$. Therefore, the second term on the right hand side of equation (2.43) vanishes and so

$$\dot{S} = C \left(\dot{S}L - \frac{\rho_i}{\rho_w} \dot{I} \right). \quad (2.45)$$

Substituting equation (2.45) into equation (2.42), we find

$$\int_{\partial M} [\rho_w C \dot{S}L + \rho_i (1 - C) \dot{I}] \, dS = 0. \quad (2.46)$$

Using equation (2.34), this can also be written

$$\int_{\partial M} \dot{\sigma} \, dS = 0, \quad (2.47)$$

where, as above, the terms in $\dot{\sigma}$ involving \dot{C} vanish, and so we can see that the rate of change of load has a mean value of zero. Substituting equation (2.41) into equation (2.46) and rearranging, we see that

$$\frac{\dot{\Phi}_G}{g} = \frac{1}{gA} \int_{\partial M} C(\dot{\mathbf{u}} \cdot \nabla \Phi + \dot{\phi}) \, dS - \frac{\rho_i}{\rho_w A} \int_{\partial M} (1 - C)\dot{I} \, dS, \tag{2.48}$$

where A is the surface area of the ocean basin, which is given by

$$A = \int_{\partial M} C \, dS. \tag{2.49}$$

Substituting this result into equation (2.41), we find

$$\dot{S}L = -\frac{1}{g}(\dot{\mathbf{u}} \cdot \nabla \Phi + \dot{\phi}) + \frac{1}{gA} \int_{\partial M} C(\dot{\mathbf{u}} \cdot \nabla \Phi + \dot{\phi}) \, dS - \frac{\rho_i}{\rho_w A} \int_{\partial M} (1 - C)\dot{I} \, dS, \tag{2.50}$$

and, from equation (2.34)

$$\dot{\sigma} = -\frac{\rho_w C}{g}(\dot{\mathbf{u}} \cdot \nabla \Phi + \dot{\phi}) + \frac{\rho_w C}{gA} \int_{\partial M} C(\dot{\mathbf{u}} \cdot \nabla \Phi + \dot{\phi}) \, dS + \rho_i(1 - C)\dot{I} - \frac{\rho_i C}{A} \int_{\partial M} (1 - C)\dot{I} \, dS. \tag{2.51}$$

These equations explicitly relate the time derivatives of the sea level and surface load to the deformation of the solid Earth. In obtaining these results, we have fully accounted for shoreline migration, but this is expressed simply through the dependence of the ocean function on SL and I . This dependence introduces non-linearity into the problem.

2.3 Weak formulation of the GIA problem

It will be useful to derive the weak form of the GIA problem. This enables us to implement the forward equations using a finite-element-type method and is necessary in deriving the adjoint equations, which we will need later when considering the inverse problem.

From Al-Attar & Tromp (2014), the weak form of the viscoelastic loading problem can be written as

$$\mathcal{A}(\dot{\mathbf{u}}, \dot{\phi} | \mathbf{u}', \phi') - \int_{M_S} 2\mu_0 \left[\dot{\mathbf{m}} : \mathbf{m}' + \frac{1}{\tau}(\mathbf{d} - \mathbf{m}) : (\mathbf{d}' - \mathbf{m}') \right] \, dV + \int_{\partial M} (\mathbf{u}' \cdot \nabla \Phi + \phi') \dot{\sigma} \, dS = 0, \tag{2.52}$$

which must hold for all sufficiently smooth test functions \mathbf{u}' , ϕ' and \mathbf{m}' that satisfy

$$[\mathbf{u}']_{-}^{+} = \mathbf{0}, \quad \mathbf{x} \in \Sigma_{SS}, \tag{2.53}$$

$$[\phi']_{-}^{+} = 0, \quad \mathbf{x} \in \Sigma, \tag{2.54}$$

and

$$\lim_{\|\mathbf{x}\| \rightarrow \infty} \phi' = 0. \tag{2.55}$$

Here, \mathcal{A} is the bilinear form

$$\begin{aligned} \mathcal{A}(\mathbf{u}, \phi | \mathbf{u}', \phi') &= \int_{M_S} \kappa \nabla \cdot \mathbf{u} \nabla \cdot \mathbf{u}' \, dV + \int_{M_S} 2\mu_0 \mathbf{d} : \mathbf{d}' \, dV + \frac{1}{2} \int_{M_S} \rho [\nabla(\mathbf{u} \cdot \nabla \Phi) \cdot \mathbf{u}' + \nabla(\mathbf{u}' \cdot \nabla \Phi) \cdot \mathbf{u}] \, dV \\ &\quad - \frac{1}{2} \int_{M_S} \rho (\nabla \cdot \mathbf{u} \nabla \Phi \cdot \mathbf{u}' + \nabla \cdot \mathbf{u}' \nabla \Phi \cdot \mathbf{u}) \, dV + \int_{M_S} \rho (\nabla \phi \cdot \mathbf{u}' + \mathbf{u} \cdot \nabla \phi') \, dV + \frac{1}{4\pi G} \int_{\mathbb{R}^3} \nabla \phi \cdot \nabla \phi' \, dV \\ &\quad + \int_{M_F} g^{-1} \phi \phi' \partial_n \rho \, dV + \int_{\Sigma_{FS}} \rho^{-} g \hat{\nu} \cdot \mathbf{u} \hat{\nu} \cdot \mathbf{u}' \, dS - \int_{\Sigma_{SF}} \rho^{+} g \hat{\nu} \cdot \mathbf{u} \hat{\nu} \cdot \mathbf{u}' \, dS \\ &\quad + \int_{\Sigma_{FS}} \rho^{-} (\phi \mathbf{u}' + \phi' \mathbf{u}) \cdot \hat{\nu} \, dS - \int_{\Sigma_{SF}} \rho^{+} (\phi \mathbf{u}' + \phi' \mathbf{u}) \cdot \hat{\nu} \, dS. \end{aligned} \tag{2.56}$$

This weak form of the problem is completely equivalent to the rate formulation of the linear viscoelastic problem described in section 2.1.3, including all associated boundary conditions.

We now wish to combine the equations for the surface load and the evolution of sea level with this weak form. Firstly, we can substitute equation (2.51) for the surface load term, $\dot{\sigma}$, into the above weak form to find

$$\begin{aligned} \mathcal{A}(\dot{\mathbf{u}}, \dot{\phi} | \mathbf{u}', \phi') &- \int_{M_S} 2\mu_0 \left[\dot{\mathbf{m}} : \mathbf{m}' + \frac{1}{\tau}(\mathbf{d} - \mathbf{m}) : (\mathbf{d}' - \mathbf{m}') \right] \, dV \\ &- \frac{\rho_w}{g} \int_{\partial M} \left[\dot{\mathbf{u}} \cdot \nabla \Phi + \dot{\phi} - \frac{1}{A} \int_{\partial M} C(\dot{\mathbf{u}} \cdot \nabla \Phi + \dot{\phi}) \, dS \right] C(\mathbf{u}' \cdot \nabla \Phi + \phi') \, dS \\ &+ \rho_i \int_{\partial M} (1 - C)\dot{I} \left[\mathbf{u}' \cdot \nabla \Phi + \phi' - \frac{1}{A} \int_{\partial M} C(\mathbf{u}' \cdot \nabla \Phi + \phi') \, dS \right] \, dS = 0. \end{aligned} \tag{2.57}$$

We will now derive the weak form of equation (2.50) and combine it with equation (2.57). We introduce the test function SL' which is defined on ∂M , multiply equation (2.50) by this test function and then integrate over the surface to find

$$\rho_w g \int_{\partial M} \dot{S}L SL' \, dS + \int_{\partial M} \left\{ \rho_w \left[\dot{\mathbf{u}} \cdot \nabla \Phi + \dot{\phi} - \frac{1}{A} \int_{\partial M} C(\dot{\mathbf{u}} \cdot \nabla \Phi + \dot{\phi}) \, dS \right] + \frac{\rho_i g}{A} \int_{\partial M} (1 - C)\dot{I} \, dS \right\} SL' \, dS = 0, \tag{2.58}$$

where a factor of $\rho_w g$ has been introduced for convenience. Adding this to equation (2.57), the weak form becomes

$$\begin{aligned} & \mathcal{A}(\dot{\mathbf{u}}, \dot{\phi}|\mathbf{u}', \phi') - \int_{M_S} 2\mu_0 \left[\dot{\mathbf{m}} : \mathbf{m}' + \frac{1}{\tau}(\mathbf{d} - \mathbf{m}) : (\mathbf{d}' - \mathbf{m}') \right] dV - \rho_w g \int_{\partial M} \dot{S}L SL' dS \\ & - \frac{\rho_w}{g} \int_{\partial M} \left[\dot{\mathbf{u}} \cdot \nabla \Phi + \dot{\phi} - \frac{1}{A} \int_{\partial M} C(\dot{\mathbf{u}} \cdot \nabla \Phi + \dot{\phi}) dS \right] [gSL' + C(\mathbf{u}' \cdot \nabla \Phi + \phi')] dS \\ & + \rho_i \int_{\partial M} (1 - C) \dot{I}_1 \left[\mathbf{u}' \cdot \nabla \Phi + \phi' - \frac{1}{A} \int_{\partial M} [gSL' + C(\mathbf{u}' \cdot \nabla \Phi + \phi')] dS \right] dS = 0, \end{aligned} \quad (2.59)$$

and we also require the initial condition given by equation (2.40). We will finally add the weak form of equation (2.38), which, introducing the test function I' defined on ∂M , is

$$\rho_i g \int_{\partial M} (\dot{I} - \dot{I}_1) I' dS = 0, \quad (2.60)$$

where, again, we have introduced a factor of $\rho_i g$ for convenience. We also have the initial condition from equation (2.37). Therefore, the overall weak form for the GIA problem, which we recall must hold for all \mathbf{u}' , ϕ' , \mathbf{m}' , SL' and I' , is

$$\begin{aligned} & \mathcal{A}(\dot{\mathbf{u}}, \dot{\phi}|\mathbf{u}', \phi') - \int_{M_S} 2\mu_0 \left[\dot{\mathbf{m}} : \mathbf{m}' + \frac{1}{\tau}(\mathbf{d} - \mathbf{m}) : (\mathbf{d}' - \mathbf{m}') \right] dV - \rho_w g \int_{\partial M} \dot{S}L SL' dS \\ & - \frac{\rho_w}{g} \int_{\partial M} \left[\dot{\mathbf{u}} \cdot \nabla \Phi + \dot{\phi} - \frac{1}{A} \int_{\partial M} C(\dot{\mathbf{u}} \cdot \nabla \Phi + \dot{\phi}) dS \right] [gSL' + C(\mathbf{u}' \cdot \nabla \Phi + \phi')] dS - \rho_i g \int_{\partial M} (\dot{I}_1 - \dot{I}) I' dS \\ & + \rho_i \int_{\partial M} (1 - C) \dot{I}_1 \left[\mathbf{u}' \cdot \nabla \Phi + \phi' - \frac{1}{A} \int_{\partial M} [gSL' + C(\mathbf{u}' \cdot \nabla \Phi + \phi')] dS \right] dS = 0, \end{aligned} \quad (2.61)$$

with the initial conditions

$$\mathbf{u}(\mathbf{x}, t_0) = \mathbf{0}, \quad (2.62)$$

$$\phi(\mathbf{x}, t_0) = 0, \quad (2.63)$$

$$\mathbf{m}(\mathbf{x}, t_0) = \mathbf{0}, \quad (2.64)$$

$$SL(\mathbf{x}, t_0) = 0, \quad (2.65)$$

$$I(\mathbf{x}, t_0) = I_0(\mathbf{x}). \quad (2.66)$$

The equations are equivalent to the formulation using the sea level equation, but are expressed independently of any numerical or iterative scheme. Through equation (2.61), the time derivatives of the variables of the forward problem (\mathbf{u} , ϕ , \mathbf{m} , SL , I) are related to the current state of the system. In order to solve the forward problem, the current state of the system is used to calculate the time derivatives of the variables and combined with some time-stepping scheme to find the state of the system at the next time step.

2.4 Numerical examples in spherically symmetric earth models

We now have the equations of motion for the GIA problem and can implement them numerically in order to solve the forward problem. Given the current state of the system, it is possible to calculate the time derivatives of the forward variables and, along with some suitable time-stepping scheme, use them to update the system. In appendix B, we outline how to implement the forward problem numerically in spherically symmetric earth models. In this section, we will give some examples of forward calculations in such models. However, we note that the theory presented above is valid in models with laterally varying structure.

Within the forward problem, we require a model of ice sheet history and of earth structure. We use the ice model ICE-5G (Peltier 2004), which gives the ice thickness globally at 500 or 1000 year intervals for the last 21000 years. However, our formulation of the forward problem takes the rate of change of ice thickness, and so we assume that this is constant between time slices. The earth model has the elastic structure of the Preliminary Reference Earth Model (PREM; Dziewonski & Anderson 1981) and a simple three-layer viscosity structure – there is a 120km thick elastic lid on top of an upper mantle with a viscosity of 5×10^{20} Pa s and a lower mantle (below 670 km depth) with a viscosity of 5×10^{21} Pa s.

We benchmarked our implementation against a code which calculates post-glacial sea level in the Laplace domain using a Love number approach and the sea level equation (Peltier 1974; Kendall et al. 2005). In figure 1 we show the difference between the change in sea level from 21000 years ago to the present day calculated using the two methods. The maximum difference in sea level change calculated is two metres which, as these differences are in regions of large sea level change, is less than 0.5 percent of the change in sea level at these locations. We also plot the sea level change as a function of time using the two methods at two locations (as marked in figure 1) in figure 2, and can see that the differences are negligible. In figure 3, we show the total sea level change from 21000 years ago to the present day calculated using the new method and also mark the locations of sea level measurements that are used when considering the inverse problem; these are (1) a formerly glaciated location to the north on the border between Alberta and Saskatchewan in Canada, (2) on the peripheral bulge (the area just

outside the former ice extent which sees the largest increases in sea level) in north west Nebraska in the US and (3) in the far-field of the ice melt in Tahiti.

3 THE GIA INVERSE PROBLEM

We now wish to turn our attention to the inverse problem, that is, using measurements of GIA to learn about the model parameters η , I_0 , \dot{I}_1 and SL_0 . In considering the inverse problem, it will be useful to calculate the derivative of a particular measurement with respect to a model parameter. This derivative is the linearised sensitivity of the measurement to a change in the parameter, and can also be used as part of a gradient-based optimisation scheme to find best-fitting model parameters. In order to calculate the derivatives, we will use the adjoint method.

3.1 The adjoint method

When considering the inverse problem, a simple approach is to calculate derivatives using a finite differencing method (e.g., Mitrovica & Peltier 1991; Paulson et al. 2005; Wu 2006). For an n -dimensional parameter space, construction of the derivative using such a method requires $n + 1$ solutions of the forward problem. For laterally varying earth models, which require a large number of model parameters and time-consuming forward calculations, it clearly becomes prohibitively expensive to calculate kernels in this way. In contrast, the adjoint method allows the exact derivative to be constructed using just one solution of the forward problem and one of the corresponding adjoint problem, even for an infinite-dimensional model space. Here, we will briefly present the theory of the adjoint method and illustrate it schematically.

We consider an observable, J , of which we wish to calculate the derivative with respect to a model parameter. This will typically be a function of the forward variables, \mathbf{u} , ϕ and SL , but may also involve an explicit dependence on model parameters (for example, through a regularisation term). We call J the objective functional, and, schematically, can write $J(u, p)$ where u represents the forward variables and p the model parameters. As the forward variables depend on the model parameters through the equations of motion, we can define the reduced objective functional through

$$\hat{J}(p) = J(u, p). \tag{3.1}$$

It is the derivative of this quantity with respect to p that we wish to calculate. We will write this derivative as $D\hat{J}$, and it is defined such that

$$\hat{J}(p + \delta p) = \hat{J}(p) + \langle D\hat{J}(p), \delta p \rangle + O(\delta p^2), \tag{3.2}$$

where $\langle \cdot, \cdot \rangle$ is an appropriate inner product. From this definition, $\delta\hat{J}(p)$, the linearised change in $\hat{J}(p)$ due to a perturbation of p , is given by

$$\delta\hat{J}(p) = \langle D\hat{J}(p), \delta p \rangle. \tag{3.3}$$

However, this derivative is difficult to calculate directly. Instead, we calculate the derivative of the objective functional $J(u, p)$ subject to the constraint that the forward variables are solutions of the equations of motion. For the class of problems we wish to consider, this constraint can be written schematically as $a(u, p) = 0$. Therefore, in order to calculate $D\hat{J}(p)$, we introduce a Lagrangian functional

$$L(u, u^\dagger, p) = J(u, p) + \langle a(u, p), u^\dagger \rangle, \tag{3.4}$$

where u^\dagger is a Lagrange multiplier used to enforce the constraint $a(u, p) = 0$. It can be shown (e.g., Tröltzsch 2005) that

$$D\hat{J}(p) = D_p L(u, u^\dagger, p), \tag{3.5}$$

provided

$$D_u L = 0, \tag{3.6}$$

$$D_{u^\dagger} L = 0, \tag{3.7}$$

where $D_p L$ is the partial derivative of L with respect to p , and similarly for $D_u L$ and $D_{u^\dagger} L$. Evaluation of equation (3.7) will simply return the forward equations and equation (3.6) gives the corresponding adjoint equations. Therefore, in order to calculate $D\hat{J}(p)$, we see that we must

- (i) for the given observable, write down $J(u, p)$;
- (ii) construct the Lagrangian using equation (3.4);
- (iii) solve the forward equations which are given by equation (3.7);
- (iv) solve the adjoint equations which are given by equation (3.6);
- (v) calculate $D\hat{J}(p)$ using equation (3.5). $D_p L(u, u^\dagger, p)$ will in general be some function of the solutions of the forward and adjoint equations.

The choice of J only changes the force terms in the adjoint equations, and so we do not have to rederive the entire set of equations for each type of measurement.

3.2 Example objective functional

There are a variety of measurements of which we might wish to calculate the derivative. In general, for the GIA problem, we can write $J(\mathbf{u}, \phi, SL)$ and so the first-order perturbation of the objective functional with respect to the forward variables is

$$\delta J = \int_{t_0}^{t_1} \int_{\partial M} \left(\dot{\mathbf{h}}_{\mathbf{u}} \cdot \delta \mathbf{u} + \dot{h}_{\phi} \delta \phi + \dot{h}_{SL} \delta SL \right) dS dt, \tag{3.8}$$

where $\dot{\mathbf{h}}_{\mathbf{u}}$, \dot{h}_{ϕ} and \dot{h}_{SL} are the Fréchet derivatives of J with respect to \mathbf{u} , ϕ and SL respectively. We note that these are written as time derivatives for later convenience. We are ignoring any possible explicit dependence of the objective functional on the model parameters, as might be introduced through regularisation, but its addition would be trivial.

As an example, we will consider the case of a sea level point measurement – the sea level at a particular time and location. In this case, the objective functional can be written as

$$J(SL) = \int_{t_0}^{t_1} \int_{\partial M} SL(\mathbf{x}, t) \delta(\mathbf{x} - \mathbf{x}_d) \delta(t - t_d) dS dt, \tag{3.9}$$

where \mathbf{x}_d and t_d are the location and time of the measurement respectively. Therefore,

$$\delta J = \int_{t_0}^{t_1} \int_{\partial M} \delta SL(\mathbf{x}, t) \delta(\mathbf{x} - \mathbf{x}_d) \delta(t - t_d) dS dt, \tag{3.10}$$

and so the Fréchet derivatives are

$$\dot{\mathbf{h}}_{\mathbf{u}} = \mathbf{0}, \quad \dot{h}_{\phi} = 0, \quad \dot{h}_{SL} = \delta(\mathbf{x} - \mathbf{x}_d) \delta(t - t_d). \tag{3.11}$$

Further examples of objective functionals are considered in appendix C of Al-Attar & Tromp (2014).

3.3 The Lagrangian

We now need to construct the Lagrangian, as in equation (3.4), for the GIA problem. We find that it is

$$\begin{aligned} L = & J(\mathbf{u}, \phi, SL) - \rho_w g \int_{\partial M} [SL(t_0) - SL_0] SL'_0 dS + \rho_i g \int_{\partial M} [I(t_0) - I_0] I'_0 dS \\ & + \int_{t_0}^{t_1} \left\{ \mathcal{A}(\dot{\mathbf{u}}, \dot{\phi} | \mathbf{u}', \phi') - \int_{M_S} 2\mu_0 \left[\dot{\mathbf{m}} : \mathbf{m}' + \frac{1}{\tau} (\mathbf{d} - \mathbf{m}) : (\mathbf{d}' - \mathbf{m}') \right] dV - \rho_w g \int_{\partial M} \dot{S} L SL' dS \right. \\ & - \frac{\rho_w}{g} \int_{\partial M} \left[\dot{\mathbf{u}} \cdot \nabla \Phi + \dot{\phi} - \frac{1}{A} \int_{\partial M} C(\dot{\mathbf{u}} \cdot \nabla \Phi + \dot{\phi}) dS \right] [gSL' + C(\mathbf{u}' \cdot \nabla \Phi + \phi')] dS - \rho_i g \int_{\partial M} (\dot{I}_1 - \dot{I}) I' dS \\ & \left. + \rho_i \int_{\partial M} (1 - C) \dot{I}_1 \left[\mathbf{u}' \cdot \nabla \Phi + \phi' - \frac{1}{A} \int_{\partial M} [gSL' + C(\mathbf{u}' \cdot \nabla \Phi + \phi')] dS \right] dS \right\} dt, \tag{3.12} \end{aligned}$$

where $J(\mathbf{u}, \phi, SL)$ is the chosen observable, the weak form is inside the time integral and we have introduced the test functions SL'_0 and I'_0 to impose the initial conditions given by equations (2.40) and (2.37).

3.4 The adjoint equations

By solving the forward problem as described in the previous section, we have found the solution to equation (3.7). In order to construct the derivative of our measurement, we must also find the solution of (3.6), that is, solve the adjoint equations. We must first derive the adjoint equations by perturbing the Lagrangian with respect to each of the forward variables and setting the perturbations equal to zero. Our forward variables are \mathbf{u} , ϕ , \mathbf{m} , SL and I . The full derivation of the adjoint equations is given in appendix C; here, we simply state the results. In doing so, it will be useful to introduce the adjoint variables, defined such that

$$\mathbf{u}^\dagger(t) = \mathbf{u}'(t_1 - t + t_0), \tag{3.13}$$

$$\phi^\dagger(t) = \phi'(t_1 - t + t_0), \tag{3.14}$$

$$\mathbf{m}^\dagger(t) = \mathbf{m}'(t_1 - t + t_0), \tag{3.15}$$

$$SL^\dagger(t) = SL'(t_1 - t + t_0), \tag{3.16}$$

$$I^\dagger(t) = I'(t_1 - t + t_0). \tag{3.17}$$

It is also convenient to define the adjoint ocean function and associated adjoint ocean area through

$$C^\dagger(t) = C(t_1 - t + t_0), \quad (3.18)$$

$$A^\dagger(t) = A(t_1 - t + t_0), \quad (3.19)$$

and the adjoint sources

$$\mathbf{h}_\mathbf{u}^\dagger(t) = \mathbf{h}_\mathbf{u}(t_1 - t + t_0), \quad (3.20)$$

$$h_\phi^\dagger(t) = h_\phi(t_1 - t + t_0), \quad (3.21)$$

$$h_{SL}^\dagger(t) = h_{SL}(t_1 - t + t_0). \quad (3.22)$$

With these definitions, we find that the adjoint equations are

$$\begin{aligned} & \mathcal{A}(\dot{\mathbf{u}}^\dagger, \dot{\phi}^\dagger | \delta \mathbf{u}, \delta \phi) - \int_{\partial M} 2\mu_0 \left[\dot{\mathbf{m}}^\dagger : \delta \mathbf{m} + \frac{1}{\tau} (\mathbf{d}^\dagger - \mathbf{m}^\dagger) : (\delta \mathbf{d} - \delta \mathbf{m}) \right] dV - \int_{\partial M} (\dot{\mathbf{h}}_\mathbf{u}^\dagger \cdot \delta \mathbf{u} + \dot{h}_\phi^\dagger \delta \phi) dS \\ & - \frac{\rho_w}{g} \int_{\partial M} \left[\dot{\mathbf{u}}^\dagger \cdot \nabla \Phi + \dot{\phi}^\dagger - \frac{1}{A^\dagger} \int_{\partial M} C^\dagger (\dot{\mathbf{u}}^\dagger \cdot \nabla \Phi + \dot{\phi}^\dagger) dS \right] C^\dagger (\delta \mathbf{u} \cdot \nabla \Phi + \delta \phi) dS \\ & + \frac{1}{g} \int_{\partial M} \dot{h}_{SL}^\dagger \left[\delta \mathbf{u} \cdot \nabla \Phi + \delta \phi - \frac{1}{A^\dagger} \int_{\partial M} C^\dagger (\delta \mathbf{u} \cdot \nabla \Phi + \delta \phi) dS \right] dS = 0, \end{aligned} \quad (3.23)$$

$$\dot{S}L^\dagger = -\frac{\dot{h}_{SL}^\dagger}{\rho_w g} - \frac{\dot{C}^\dagger}{g} \left[\dot{\mathbf{u}}^\dagger \cdot \nabla \Phi + \dot{\phi}^\dagger - \frac{1}{A^\dagger} \int_{\partial M} [gSL^\dagger + C^\dagger (\dot{\mathbf{u}}^\dagger \cdot \nabla \Phi + \dot{\phi}^\dagger)] dS \right], \quad (3.24)$$

$$\dot{I}^\dagger = -\frac{\dot{C}^\dagger}{g} \left[\dot{\mathbf{u}}^\dagger \cdot \nabla \Phi + \dot{\phi}^\dagger - \frac{1}{A^\dagger} \int_{\partial M} [gSL^\dagger + C^\dagger (\dot{\mathbf{u}}^\dagger \cdot \nabla \Phi + \dot{\phi}^\dagger)] dS \right] = \dot{S}L^\dagger + \frac{\dot{h}_{SL}^\dagger}{\rho_w g}, \quad (3.25)$$

where $\delta \mathbf{u}$, $\delta \phi$ and $\delta \mathbf{m}$ now act as time-independent test functions. The adjoint variables satisfy the initial conditions

$$\mathbf{u}^\dagger(t_0) = \mathbf{0}, \quad \phi^\dagger(t_0) = 0, \quad \mathbf{m}^\dagger(t_0) = \mathbf{0}, \quad SL^\dagger(t_0) = 0, \quad I^\dagger(t_0) = 0, \quad (3.26)$$

and we also find that SL'_0 and I'_0 satisfy

$$SL'_0 = SL^\dagger(t_1), \quad I'_0 = I^\dagger(t_1). \quad (3.27)$$

In deriving the sensitivity kernels, we will find it useful to use the adjoint definitions to rewrite the Lagrangian in equation (3.12) as

$$\begin{aligned} L = J + \int_{t_0}^{t_1} & \left\{ \mathcal{A}(\dot{\mathbf{u}}, \dot{\phi} | \mathbf{u}^\dagger, \phi^\dagger) - \int_{M_S} 2\mu_0 \left[\dot{\mathbf{m}} : \mathbf{m}^\dagger + \frac{1}{\tau} (\mathbf{d} - \mathbf{m}) : (\mathbf{d}^\dagger - \mathbf{m}^\dagger) \right] dV - \rho_w g \int_{\partial M} \dot{S}L SL^\dagger dS \right. \\ & - \frac{\rho_w}{g} \int_{\partial M} \left[\dot{\mathbf{u}} \cdot \nabla \Phi + \dot{\phi} - \frac{1}{A} \int_{\partial M} C (\dot{\mathbf{u}} \cdot \nabla \Phi + \dot{\phi}) dS \right] [gSL^\dagger + C^\dagger (\mathbf{u}^\dagger \cdot \nabla \Phi + \phi^\dagger)] dS - \rho_i g \int_{\partial M} (\dot{I}_1 - \dot{I}) I^\dagger dS \\ & + \rho_i \int_{\partial M} (1 - C) \dot{I}_1 \left[\mathbf{u}^\dagger \cdot \nabla \Phi + \phi^\dagger - \frac{1}{A^\dagger} \int_{\partial M} [gSL^\dagger + C^\dagger (\mathbf{u}^\dagger \cdot \nabla \Phi + \phi^\dagger)] dS \right] dS \left. \right\} dt \\ & - \rho_w g \int_{\partial M} [SL(t_0) - SL_0] SL^\dagger(t_1) dS + \rho_i g \int_{\partial M} [I(t_0) - I_0] I^\dagger(t_1) dS, \end{aligned} \quad (3.28)$$

where, within the time integral, it is understood that all forward variables are evaluated at time t and all adjoint variables are evaluated at time $t_1 - t + t_0$.

3.5 Sensitivity kernels

Given the solutions of the forward and adjoint problems, we are able to calculate the sensitivity of particular measurements (such as the example given in section 3.2) to the parameters. We now need to derive the form of the sensitivity kernels for the different parameters using equation (3.5). In what follows, we write the kernel for the model parameter p as K_p . We calculate the form of the kernels for viscosity, ice sheet thickness and initial sea level, but we could also consider the kernels for other parameters. For example, we could calculate the sensitivity to boundary perturbations, such as the thickness of the elastic lid, using a method similar to Liu & Tromp (2008).

3.5.1 Viscosity kernels

Perturbing the Lagrangian in equation (3.28) with respect to η , we find

$$\delta \hat{J} = \int_{t_0}^{t_1} \int_{M_S} \frac{2\mu_0}{\tau} (\mathbf{d} - \mathbf{m}) : (\mathbf{d}^\dagger - \mathbf{m}^\dagger) \frac{\delta \eta}{\eta} dV dt. \quad (3.29)$$

It will be useful to consider relative changes in viscosity, and so we define the viscosity sensitivity kernel such that

$$\delta \hat{J} = \int_{M_S} K_\eta \frac{\delta \eta}{\eta} dV. \quad (3.30)$$

We therefore see that

$$K_\eta = \int_{t_0}^{t_1} \frac{2\mu_0}{\tau} (\mathbf{d} - \mathbf{m}) : (\mathbf{d}^\dagger - \mathbf{m}^\dagger) dt = \int_{t_0}^{t_1} \frac{1}{2\eta} \boldsymbol{\tau}(t) : \boldsymbol{\tau}^\dagger(t_1 - t + t_0) dt, \quad (3.31)$$

where we recall that the deviatoric stress, $\boldsymbol{\tau}$, is given by equation (2.25). It will also be useful to define the radial viscosity sensitivity kernel, \overline{K}_η , which is given by

$$\overline{K}_\eta = \int_{\mathbb{S}^2} r^2 K_\eta dS = \int_{t_1}^{t_2} \int_{\mathbb{S}^2} \frac{1}{2\eta} \boldsymbol{\tau}(t) : \boldsymbol{\tau}^\dagger(t_1 - t + t_0) r^2 dS dt, \quad (3.32)$$

where \mathbb{S}^2 is the unit two-sphere. These equations have the same form as the equivalents in Al-Attar & Tromp (2014) and Crawford et al. (2017).

3.5.2 Ice kernels

We can first calculate the sensitivity of the objective functional to the initial ice thickness. This is defined such that

$$\delta \hat{J} = \int_{\partial M} K_{I_0} \delta I_0 dS. \quad (3.33)$$

Perturbing the Lagrangian with respect to I_0 , we find

$$\delta \hat{J} = -\rho_i g \int_{\partial M} I^\dagger(t_1) \delta I_0 dS, \quad (3.34)$$

and so

$$K_{I_0} = -\rho_i g I^\dagger(t_1). \quad (3.35)$$

As discussed in Al-Attar & Tromp (2014), the kernel for the ice thickness at later times will be singular whenever there is a jump in the adjoint loads (as is the case when considering, for example, a point sea level measurement). However, the kernel for the rate of change of ice thickness remains non-singular with such loads. In deriving the kernel for ice coverage at later times, it is therefore most convenient to define it with respect to the rate of change of ice thickness, and so we write

$$\delta \hat{J} = \int_{t_0}^{t_1} \int_{\partial M} K_{\dot{I}_1} \delta \dot{I}_1 dS dt. \quad (3.36)$$

Perturbing the Lagrangian with respect to \dot{I}_1 , we find

$$\delta \hat{J} = \int_{t_0}^{t_1} \int_{\partial M} \rho_i \left\{ (1 - C) \left[\mathbf{u}^\dagger \cdot \nabla \Phi + \phi^\dagger - \frac{1}{A} \int_{\partial M} [gSL^\dagger + C^\dagger(\mathbf{u}^\dagger \cdot \nabla \Phi + \phi^\dagger)] dS \right] - gI^\dagger \right\} \delta \dot{I}_1 dS dt, \quad (3.37)$$

and so

$$K_{\dot{I}_1} = \rho_i (1 - C) \left[\mathbf{u}^\dagger \cdot \nabla \Phi + \phi^\dagger - \frac{1}{A^\dagger} \int_{\partial M} [gSL^\dagger + C^\dagger(\mathbf{u}^\dagger \cdot \nabla \Phi + \phi^\dagger)] dS \right] - \rho_i g I^\dagger, \quad (3.38)$$

where we again recall that forward variables are evaluated at time t whereas adjoint variables are evaluated at time $t_1 - t + t_0$.

3.5.3 Initial sea level kernel

Finally, we consider the sensitivity of the objective functional to the initial sea level. Perturbing the Lagrangian with respect to SL_0 , we find that

$$\delta \hat{J} = \int_{\partial M} \rho_w g SL^\dagger(t_1) \delta SL_0 dS, \quad (3.39)$$

and so

$$K_{SL_0} = \rho_w g SL^\dagger(t_1), \quad (3.40)$$

where we have chosen to define the kernel such that

$$\delta \hat{J} = \int_{\partial M} K_{SL_0} \delta SL_0 dS. \quad (3.41)$$

One possible application of this kernel is to find the initial sea level such that the final sea level matches present day sea level as closely as possible. We define a misfit

$$J(SL) = \int_{\partial M} \frac{1}{2} [SL(\mathbf{x}, t_p) - SL_p(\mathbf{x})]^2 dS, \quad (3.42)$$

where t_p is the time at the present day and SL_p is the measured sea level at this time. We would like to find the initial sea level, SL_0 , that minimises this misfit. In order to do so, we require the gradient of equation (3.42) combined with some

gradient-based optimisation method. We can use the adjoint method in order to calculate this gradient. Equation (3.42) is the objective functional and, perturbing it with respect to the forward variables, we see that

$$\delta J(SL) = \int_{\partial M} [SL(\mathbf{x}, t_p) - SL_p(\mathbf{x})] \delta SL(\mathbf{x}, t_p) dS = \int_{t_0}^{t_1} \int_{\partial M} [SL(\mathbf{x}, t) - SL_p(\mathbf{x})] \delta SL(\mathbf{x}, t) \delta(t - t_p) dS dt, \quad (3.43)$$

and so,

$$\dot{\mathbf{h}}_{\mathbf{u}} = \mathbf{0}, \quad \dot{h}_\phi = 0, \quad \dot{h}_{SL} = [SL(\mathbf{x}, t_p) - SL_p(\mathbf{x})] \delta(t - t_p). \quad (3.44)$$

Therefore, in order to calculate the initial sea level which best fits the present day sea level, we

- (i) choose some first estimate of the initial sea level;
- (ii) solve the forward problem to find the final sea level;
- (iii) calculate the misfit given by equation (3.42) and the adjoint loads given by equation (3.44);
- (iv) solve the elastic adjoint equations for the given load, as the kernel in equation (3.40) only requires the adjoint solution at time t_1 ;
- (v) construct the derivative given by equation (3.40);
- (vi) using the derivative and some gradient-based optimisation method (e.g., the conjugate gradient method), calculate an updated initial sea level;
- (vii) repeat steps (ii) to (vi) until the misfit in equation (3.42) is sufficiently small.

Numerical tests have shown that this process converges in only a few iterations. This process is similar to, for example, the outer iteration loop in Kendall et al. (2005).

3.6 Inverse modelling in spherically symmetric earth models

In this section, we present several examples of sensitivity kernels calculated in spherically symmetric earth models. In order to calculate these kernels, we require the solutions to both the forward and adjoint problems in such models. The numerical implementation of both problems in spherically symmetric earth models is discussed in detail in appendices B and D.

3.6.1 Viscosity sensitivity kernels

We calculated the radial sensitivity kernels, given by equation (3.32) for the sea level at locations in Canada, the US and Tahiti at three different times since the Last Glacial Maximum (as indicated in figure 3). These are shown in figure 4. A positive (negative) value of the kernel at a particular depth means that an increase in viscosity at this depth would lead to an increase (decrease) in the sea level measurement. We note that the magnitude of the sensitivity is much smaller in Tahiti than it is for the North American measurements – as the Laurentide ice sheet has melted from North America, there has been a significant fall in sea level due to rebound and the magnitude of this rebound will depend quite strongly on the viscosity structure of the model. However, relative to the values in the upper mantle, we can see that the measurement in Tahiti has greater sensitivity in the lower mantle. This is because the ocean load which affects deformation in Tahiti has a larger spatial scale than the ice load over North America.

The laterally varying sensitivities, given by equation (3.31), have also been calculated for sea level measurements at different times and at the above locations to the viscosity at depths of 635 km and 1756 km. These depths are indicated on the radial kernels in figure 4 with black dashed lines. A positive (negative) value of the kernel at a particular location means that an increase in viscosity at this location would lead to an increase (decrease) in the sea level measurement. Figures 5 and 6 show the kernels for measurements at a location in Canada which was under the ice sheet at the LGM. The sensitivity broadens with depth, as we would expect. We note that the sensitivity to viscosity structure is small until approximately 12000 years ago. This is in part due to the ice sheet model, as ICE-5G has only a small amount of ice melt from the Laurentide ice sheet until this time. There is a small amount of sensitivity outside the region shown, particularly in northern Europe while the Fennoscandian ice sheet is melting. Figures 7 and 8 show the equivalent kernels for measurements at a location in the US which is on the peripheral bulge, the region of land just outside the edge of the former ice sheet that has seen the greatest increase in sea level. We see similar features in these kernels.

We also present figures for the sensitivity of the sea level in Tahiti (figures 9 and 10). At both depths, we see that the magnitude of the sensitivity is similar at the measurement location as it is in the regions of ice melt and, again, broadens with depth. However, as in figure 4, we see that the maximum amplitude of the sensitivity is much smaller here than for measurements in North America.

As mentioned above, the kernels give the linearised sensitivity of a measurement, and we would like to examine the magnitude of perturbations for which this is a good approximation of the total sensitivity. In figure 11, we show the magnitude of the calculated change in sea level at a location in Canada and that predicted by the kernels for viscosity perturbations of different magnitudes and sea level measurements made at different times. We can see that the kernels predict the change very

well for perturbations of up to 10 percent, and this is true for sea level measurements at all times and perturbations at all depths shown. For perturbations of a larger magnitude, the change predicted is still of the right sign and order of magnitude.

3.6.2 Ice sensitivity kernels

In figures 12 and 13 we show the sensitivity of the present-day sea level in central North America and Tahiti respectively to the rate of change of ice thickness at different times. These sensitivities are given by equation (3.38). The kernels presented in panel (f) of each figure are equivalent to the results presented in Larour et al. (2017); however, we are also able to account fully for viscoelasticity in our kernel calculations, as required for the other figure panels. A positive (negative) value of the ice kernel at a particular location means that an increase in the rate of change of ice thickness at this location would result in an increase (decrease) in the present-day sea level at the measurement location. We note that, in both of these figures, we do not place any restrictions on where the ice sheet thickness can change.

From figure 12, we can firstly see that the sensitivity of present day sea level to the rate of change of ice thickness in the past is roughly constant until about 9000 years before the present. This is because, for the viscosity model we have adopted, the Earth has essentially relaxed in response to any ice melting or growth prior to this time. Thus melting of a given amount prior to 9000 years ago will contribute the same sea level change regardless of the precise timing of the melt. As we get closer to the present day, the sensitivity to the rate of change of ice thickness decreases in magnitude because the level of relaxation in response to the change progressively decreases. The largest positive sensitivity is evident at the location of the sea level measurement. As ice melts (forms) here, the ground rebounds (subsides) and sea level falls (rises). On land away from the measurement location, the kernel is negative. The dominant effect in these locations is simply the change in water volume in the oceans due to a change in ice thickness. For example, ice melting in the far-field adds water to the oceans, increasing sea level at the measurement location.

The pattern of sensitivity for a present day sea level measurement in Tahiti, as shown in figure 13, is quite different. As the sea level measurement is on a small island in the ocean, there is essentially no sensitivity in the vicinity of the measurement. As before, the sensitivity does not vary with time for changes in ice volume more than 9000 years before the measurement. The sensitivity is negative everywhere – wherever ice melts (forms) on land, the volume of water in the oceans will increase (decrease) and sea level will rise (fall). The largest amplitude negative sensitivity is on the shorelines as, if ice forms at these locations, the shoreline will subside, increasing the volume of the ocean basin and hence lowering sea level even further. In contrast, the smallest amplitude negative sensitivity is slightly in land of the coast. If ice forms in such a location, the ground under the ice will subside, causing uplift on the coast and so the volume of the ocean basin will decrease; this effect will negate some of the fall in sea level due to the formation of ice. As we get closer to the present day, the solid Earth has had less time to rebound due to the change in ice load, and so the kernel is dominated by gravitational effects.

In figure 14, we show the sensitivity of the sea level at the Sunda Shelf (figure 14a) and Barbados (figure 14b) 14200 years ago to the rate of change of ice thickness at this time, only in locations where there was ice present. This is the time of Melt Water Pulse 1A, when a large increase in sea level is observed due to a sudden ice melting event (Clark et al. 2002). From our sensitivity kernels, we can see that the sea level at the two locations has similar sensitivity to the rate of change of ice thickness in Antarctica, but quite different sensitivity to that in North America. Clark et al. (2002) calculated the sea level change at the Sunda Shelf and Barbados due to ice melting in different regions and, in agreement with our kernels, found that the change at the two locations would be similar for an Antarctic source but different for a North American source. However, they only considered melting of entire ice sheets, while our kernels reveal the full spatial dependence. Using these kernels, we can also construct a measurement that is relatively insensitive to the rate of change of ice thickness in Antarctica. In figure 14c, we show the ice sensitivity kernel for the measurement that is equal to the sea level at the Sunda Shelf minus 0.95 times the sea level in Barbados. We can see that this measurement is most sensitive to the rate of change of ice sheet thickness in the south-eastern part of the Laurentide ice sheet. This is an example of how we can use the sensitivity kernels to find a combination of measurements that localises the sensitivity in a particular way. In this case, the value of 0.95 was chosen by trial and error; in practice, a combination of data which minimises or maximises sensitivity in a particular region could be found more systematically using Backus-Gilbert methods (?Backus & Gilbert 1968; ?).

4 CONCLUSION

In this paper, we presented a method for calculating the sensitivity of measurements of glacial isostatic adjustment to the viscosity structure of the Earth and the ice sheet history. We use the adjoint method, which enables the linearised sensitivities, or kernels, to be calculated quickly and efficiently, even in the case of laterally heterogeneous earth models. To apply this approach, we found it useful to formulate a new method for solving the forward GIA problem which does not make use of the sea level equation and should be well suited to three-dimensional calculations. Through application of this approach, we have also presented the first three-dimensional examples of such sensitivities. These results give physical insight into which

parts of the model space affect the GIA signal at a given location. We note that whilst the numerical examples presented in this paper are calculated with respect to a spherically symmetric background model, the theory is valid in models with lateral variations.

The kernels have a number of potential applications within the GIA inverse problem and can be used to further our understanding of the viscosity structure and ice sheet history of the Earth. Currently, ice sheet models are generally constructed in spherically symmetric earth models (e.g., Peltier et al. 2015). One possible use of the methods described in this paper would be to take a three-dimensional viscosity structure (such as one inferred from a seismic tomography model; e.g., Priestley & McKenzie 2013) and use the ice kernels to invert for an ice sheet history which fits the data with such a viscosity structure. In this manner, the impact of realistic lateral variations on ice sheet history could be quantitatively assessed. The addition of the viscosity kernels would enable simultaneous inversion for the ice sheet history and viscosity structure, and both sets of kernels provide a method for quantifying how well the outcome of the inversion is constrained.

ACKNOWLEDGEMENTS

OC is supported by a NERC studentship and a CASE award from British Antarctic Survey. JA acknowledges funding from the Royal Society. We thank John Woodhouse for providing a new routine for efficient computation of generalised Legendre functions. We are grateful to Anthony Purcell, an anonymous reviewer and editor Duncan Agnew for their helpful comments and suggestions.

REFERENCES

- A, G., Wahr, J., & Zhong, S., 2013. Computations of the viscoelastic response of a 3-D compressible Earth to surface loading: an application to Glacial Isostatic Adjustment in Antarctica and Canada, *Geophys. J. Int.*, **192**(2), 557–572.
- Al-Attar, D. & Tromp, J., 2014. Sensitivity kernels for viscoelastic loading based on adjoint methods, *Geophys. J. Int.*, **196**(1), 34–77.
- Argus, D. F., Peltier, W. R., Drummond, R., & Moore, A. W., 2012. The Antarctica component of postglacial rebound model ICE-6G_C (VM5a) based on GPS positioning, exposure age dating of ice thicknesses, and relative sea level histories, *Geophys. J. Int.*, **198**(1), 537–563.
- Backus, G. & Gilbert, F., 1968. The resolving power of gross Earth data, *Geophys. J. Int.*, **16**(2), 169–205.
- Boschi, L., Tromp, J., & O’Connell, R. J., 1999. On Maxwell singularities in postglacial rebound, *Geophys. J. Int.*, **136**(2), 492–498.
- Bunge, H. P., Hagelberg, C. R., & Travis, B. J., 2003. Mantle circulation models with variational data assimilation: inferring past mantle flow and structure from plate motion histories and seismic tomography, *Geophys. J. Int.*, **152**(2), 280–301.
- Clark, P. U., Mitrovica, J. X., Milne, G. A., & Tamisiea, M. E., 2002. Sea-level fingerprinting as a direct test for the source of Global Meltwater Pulse 1A, *Science*, **295**(5564), 2438–2441.
- Crawford, O., Al-Attar, D., Tromp, J., & Mitrovica, J. X., 2017. Forward and inverse modelling of post-seismic deformation, *Geophys. J. Int.*, **208**(2), 845–876.
- Creveling, J. R., Mitrovica, J. X., Clark, P. U., Waelbroeck, C., & Pico, T., 2017. Predicted bounds on peak global mean sea level during marine isotope stages 5a and 5c, *Quaternary Sci Rev*, **163**, 193–208.
- Dahlen, F. A., 1974. On the static deformation of an earth model with a fluid core, *Geophys. J. Int.*, **36**(2), 461–485.
- Dahlen, F. A. & Tromp, J., 1998. *Theoretical Global Seismology*, Princeton University Press.
- Duistermaat, J. J. & Kolk, J. A. C., 2010. *Distributions*, Birkhauser.
- Dziewonski, A. M. & Anderson, D. L., 1981. Preliminary reference Earth model, *Phys. Earth Planet. In.*, **25**(4), 297–356.
- Fang, M. & Hager, B. H., 1995. The singularity mystery associated with a radially continuous Maxwell viscoelastic structure, *Geophys. J. Int.*, **123**(3), 849–865.
- Farrell, W. E. & Clark, J. A., 1976. On postglacial sea level, *Geophys. J. Int.*, **46**(3), 647–667.
- Han, D. & Wahr, J., 1995. The viscoelastic relaxation of a realistically stratified earth, and a further analysis of postglacial rebound, *Geophys. J. Int.*, **120**(2), 287–311.
- Haskell, N. A., 1935. The motion of a viscous fluid under a surface load, *J. Appl. Phys.*, **6**(8), 265–269.
- Johnston, P., 1993. The effect of spatially non-uniform water loads on prediction of sea-level change, *Geophys. J. Int.*, **114**(1), 615–634.
- Kendall, R. A., Mitrovica, J. X., & Milne, G. A., 2005. On post-glacial sea level – II. Numerical formulation and comparative results on spherically symmetric models, *Geophys. J. Int.*, **161**(3), 679–706.
- Lambeck, K. & Chappell, J., 2001. Sea level change through the last glacial cycle, *Science*, **292**(5517), 679–686.
- Lambeck, K., Smither, C., & Johnston, P., 1998. Sea-level change, glacial rebound and mantle viscosity for northern Europe, *Geophys. J. Int.*, **134**(1), 102–144.
- Larour, E., Ivins, E., & Adhikari, S., 2017. Should coastal planners have concern over where land ice is melting?, *Sci Adv*, **3**(11), doi:10.1029/2010JB007405.
- Latychev, K., Mitrovica, J. X., Tromp, J., Tamisiea, M. E., Komatitsch, D., & Christara, C. C., 2005. Glacial isostatic adjustment of 3-D Earth models: a finite-volume formulation, *Geophys. J. Int.*, **161**(1), 421–444.
- Lau, H. C. P., Mitrovica, J. X., Austermann, J., Crawford, O., Al-Attar, D., & Latychev, K., 2016. Inferences of mantle viscosity based on ice age data sets: Radial structure, *J. Geophys. Res.*, **121**(10), 6991–7012.
- Li, K., Jackson, A., & Livermore, P. W., 2011. Variational data assimilation for the initial-value dynamo problem, *Phys. Rev. E.*, **84**(5), 056321.
- Lions, J. L., 1970. *Optimal Control of Systems Governed by Partial Differential Equations*, Springer-Verlag.

- Liu, Q. & Tromp, J., 2008. Finite-frequency sensitivity kernels for global seismic wave propagation based upon adjoint methods, *Geophys. J. Int.*, **174**(1), 265–286.
- Martínez, Z., Sasgen, I., & Velínský, J., 2015. The forward sensitivity and adjoint-state methods of glacial isostatic adjustment, *Geophys. J. Int.*, **200**(1), 77–105.
- Milne, G. A. & Mitrovica, J. X., 1998. Postglacial sea-level change on a rotating Earth, *Geophys. J. Int.*, **133**(1), 1–19.
- Milne, G. A., Mitrovica, J. X., & Davis, J. L., 1999. Near-field hydro-isostasy: the implementation of a revised sea-level equation, *Geophys. J. Int.*, **139**(2), 464–482.
- Misner, C. W., Thorne, K. S., & Wheeler, J. A., 1973. *Gravitation*, W. H. Freeman and Company.
- Mitrovica, J. X., 1996. Haskell [1935] revisited, *J. Geophys. Res.*, **101**(B1), 555–569.
- Mitrovica, J. X. & Milne, G. A., 2003. On post-glacial sea level: I. General theory, *Geophys. J. Int.*, **154**(2), 253–267.
- Mitrovica, J. X. & Peltier, W. R., 1991. A complete formalism for the inversion of post-glacial rebound data: resolving power analysis, *Geophys. J. Int.*, **104**(2), 267–288.
- Nakada, M. & Lambeck, K., 1989. Late Pleistocene and Holocene sea-level change in the Australian region and mantle rheology, *Geophys. J. Int.*, **96**(3), 497–517.
- Nakada, M., Okuno, J., Lambeck, K., & Purcell, A., 2015. Viscosity structure of Earth's mantle inferred from rotational variations due to GIA process and recent melting events, *Geophys. J. Int.*, **202**(2), 976–992.
- Nocedal, J. & Wright, S. J., 1999. *Numerical Optimization*, Springer-Verlag.
- Paulson, A., Zhong, S., & Wahr, J., 2005. Modelling post-glacial rebound with lateral viscosity variations, *Geophys. J. Int.*, **163**(1), 357–371.
- Peltier, W. R., 1974. The impulse response of a Maxwell Earth, *Rev. Geophys.*, **12**(4), 649–669.
- Peltier, W. R., 2004. Global glacial isostasy and the surface of the ice-age Earth: The ICE-5G (VM2) model and GRACE, *Annu. Rev. Earth Pl. Sc.*, **32**, 111–149.
- Peltier, W. R., Argus, D. F., & Drummond, R., 2015. Space geodesy constrains ice age terminal deglaciation: The global ICE-6G_C (VM5a) model, *J. Geophys. Res.*, **120**(1), 450–487.
- Phinney, R. A. & Burridge, R., 1973. Representation of the elastic-gravitational excitation of a spherical earth model by generalised spherical harmonics, *Geophys. J. Int.*, **34**(4), 451–487.
- Priestley, K. & McKenzie, D., 2013. The relationship between shear wave velocity, temperature, attenuation and viscosity in the shallow part of the mantle, *Earth Planet. Sci. Letters*, **381**, 78–91.
- Schoof, C., 2007. Ice sheet grounding line dynamics: Steady states, stability, and hysteresis, *J. Geophys. Res.*, **112**(F3).
- Spivak, M., 1970. *A Comprehensive Introduction to Differential Geometry*, vol. 1, Publish or Perish, Inc.
- Tröltzsch, F., 2005. *Optimal Control of Partial Differential Equations*, American Mathematical Society.
- Tromp, J. & Mitrovica, J. X., 1999. Surface loading of a viscoelastic earth - I. General theory, *Geophys. J. Int.*, **137**(3), 847–855.
- Tromp, J., Tape, C., & Liu, Q., 2005. Seismic tomography, adjoint methods, time reversal and banana-doughnut kernels, *Geophys. J. Int.*, **160**(1), 195–216.
- Van der Wal, W., Whitehouse, P., & Schrama, E. J. O., 2015. Effect of GIA models with 3D composite mantle viscosity on GRACE mass balance estimates for Antarctica, *Earth Planet. Sc. Lett.*, **414**, 134–143.
- Wu, P., 2004. Using commercial finite element packages for the study of earth deformations, sea levels and the state of stress, *Geophys. J. Int.*, **158**(2), 401–408.
- Wu, P., 2006. Sensitivity of relative sea levels and crustal velocities in Laurentide to radial and lateral viscosity variations in the mantle, *Geophys. J. Int.*, **165**(2), 401–413.
- Zhong, S., Paulson, A., & Wahr, J., 2003. Three-dimensional finite-element modelling of Earth's viscoelastic deformation: effects of lateral variations in lithospheric thickness, *Geophys. J. Int.*, **155**(2), 679–695.

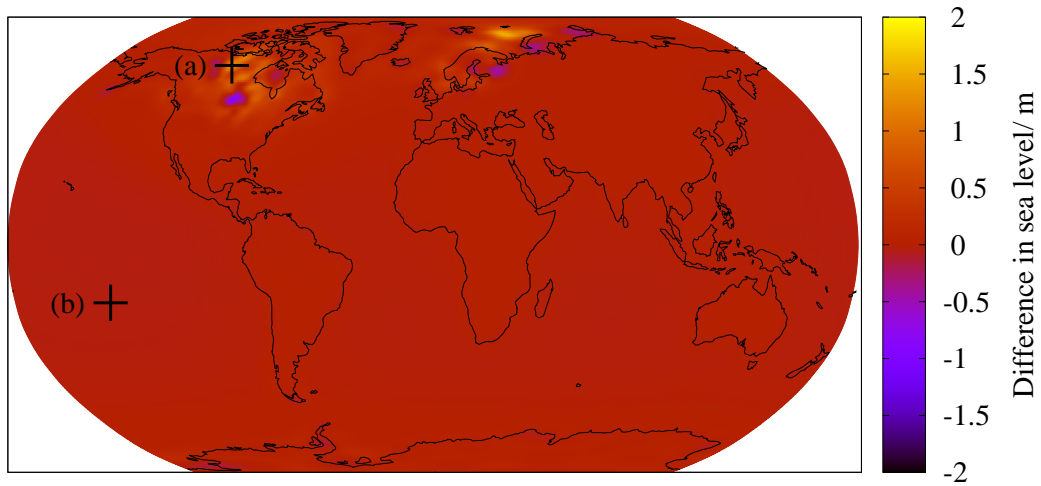


Figure 1. Difference in sea level change from 21000 years ago to the present calculated using the two methods. The crosses indicate the locations of the two time series plotted in figure 2.

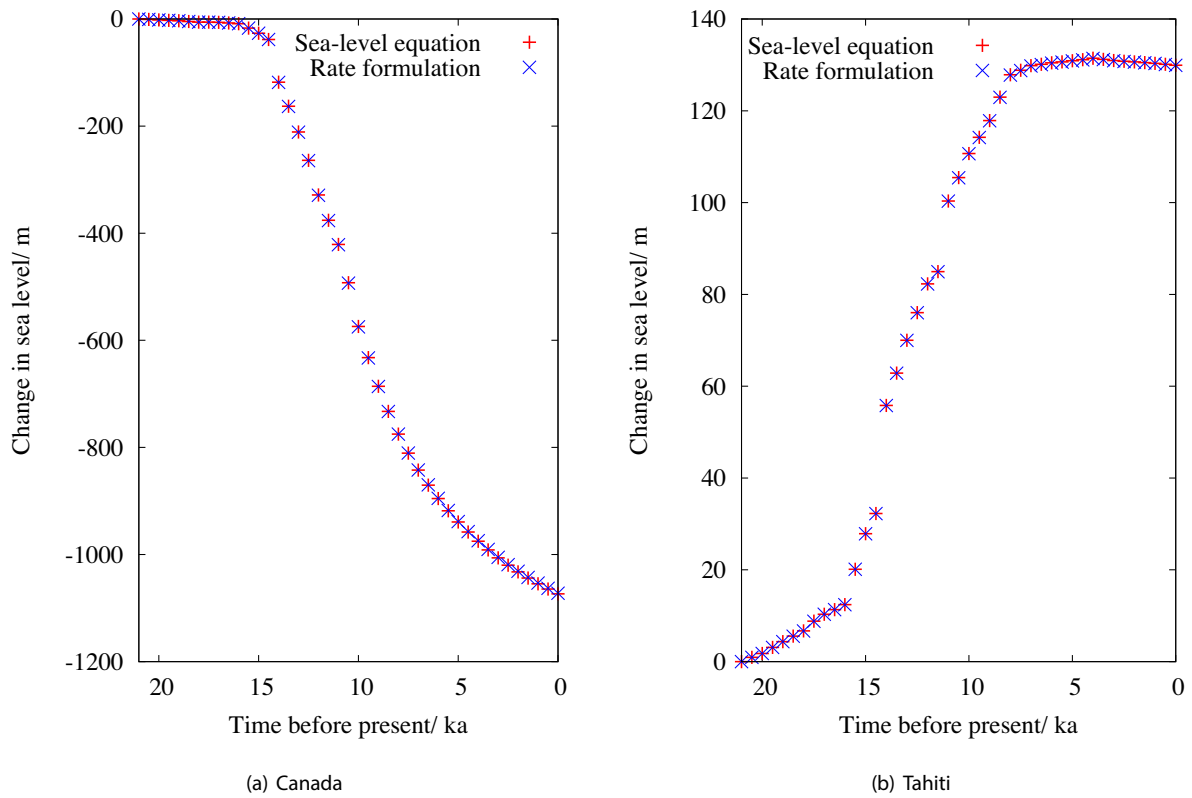


Figure 2. Time series showing the change in sea level from 21000 years ago at two locations for the two methods. The locations are marked by crosses in figure 1.

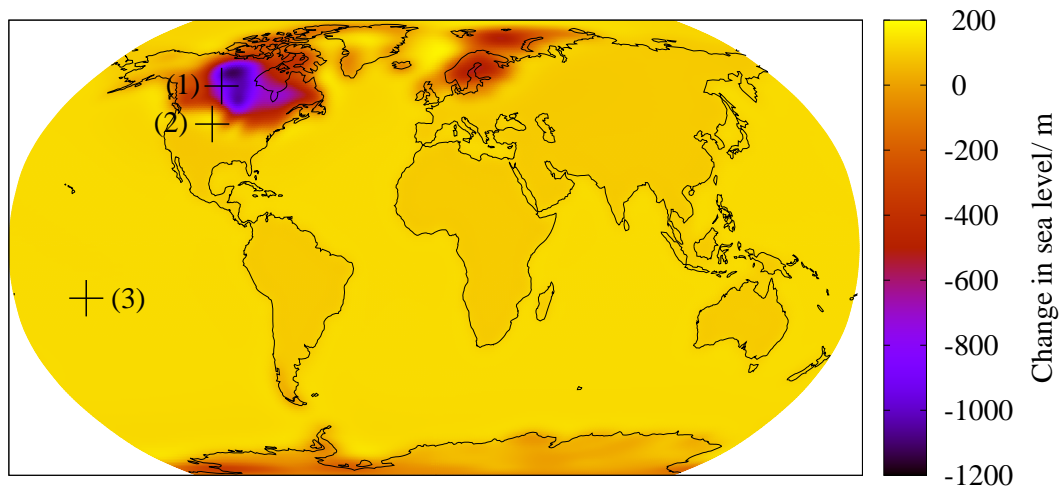


Figure 3. Sea level change from 21000 years ago to present calculated using the new rate formulation method presented in this paper. The crosses indicate locations of sea level measurements that are used when considering the inverse problem. Location (1) is in Canada (near-field site), (2) is in the US (peripheral bulge site) and (3) is in Tahiti (far-field site). We note that, whilst the sea level appears to change discontinuously at the coast lines, the change is in fact continuous but occurs over a small distance.

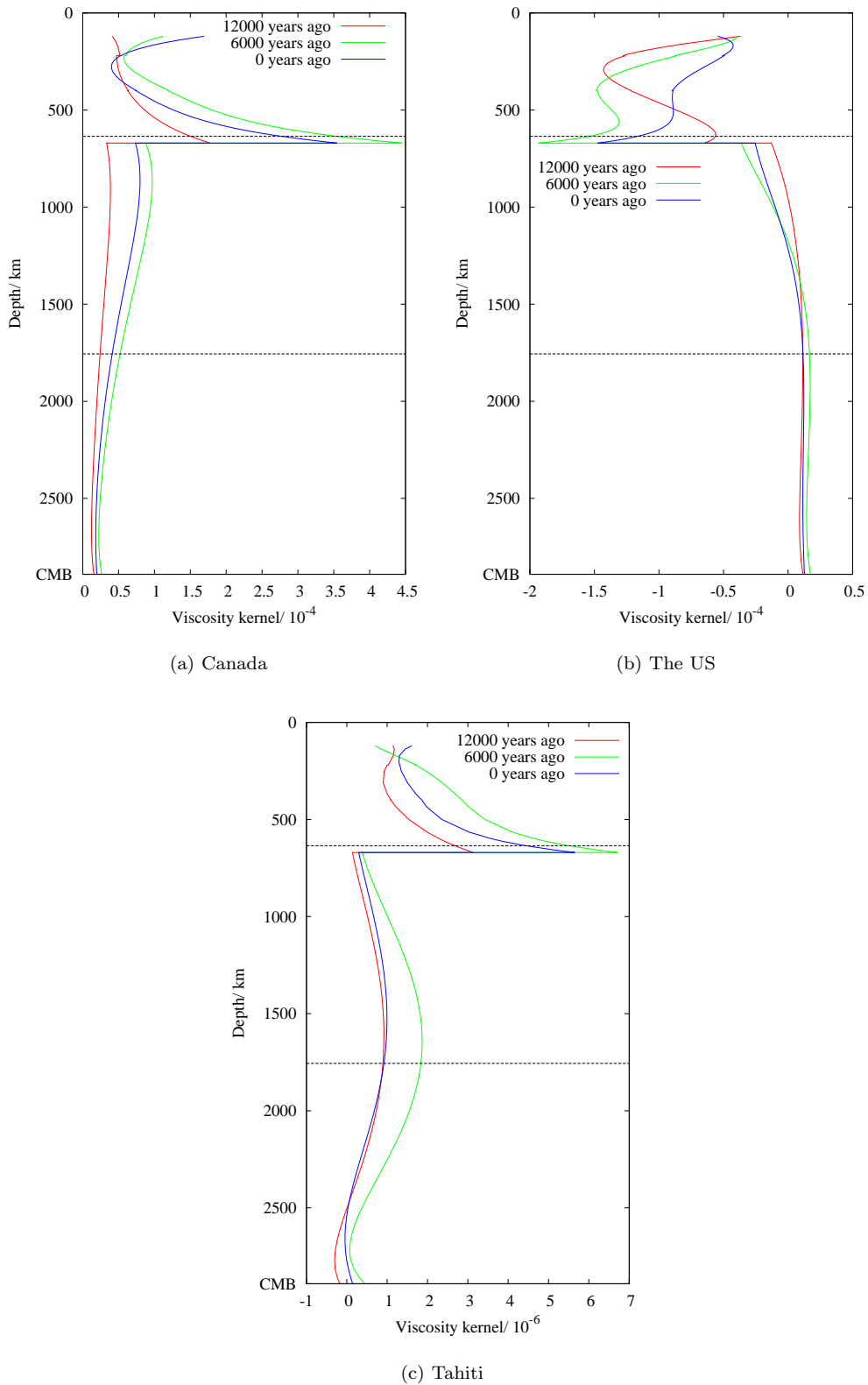


Figure 4. The radial sensitivity kernels for the sea level at three different times since the LGM at locations in (a) Canada (indicated by (1) in figure 3), (b) the US (indicated by (2) in figure 3) and (c) Tahiti (indicated by (3) in figure 3). There is a discontinuity in the kernels at a depth of 670 km due to the jump in viscosity structure at this depth. The kernels are not defined at depths shallower than 120 km as the earth model is elastic in this region. The horizontal black dashed lines indicate the depths at which we plot the laterally varying sensitivity kernels for the same measurements in figures 5 and 6 for Canada, 7 and 8 for the US and 9 and 10 for Tahiti.

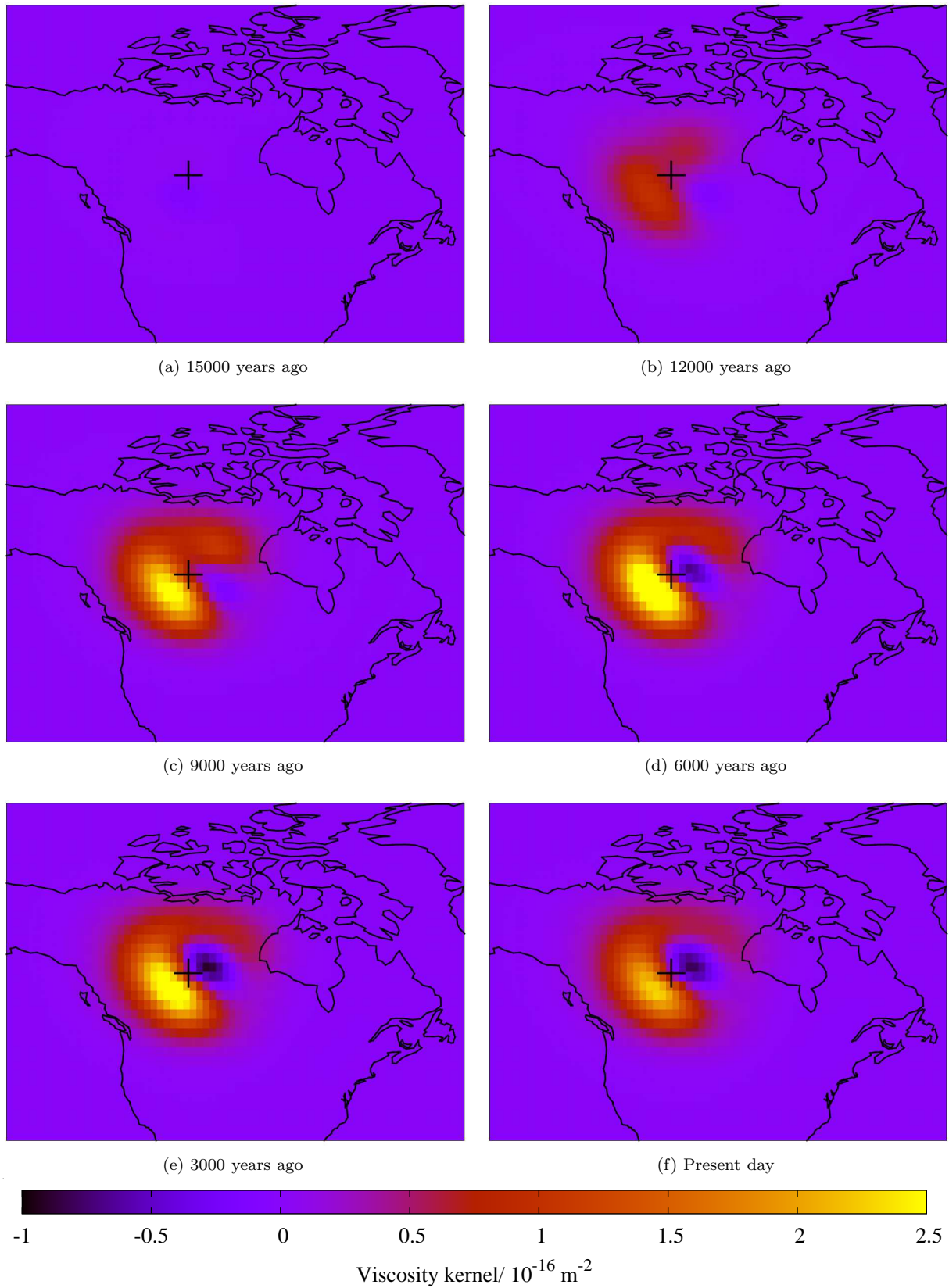


Figure 5. The sensitivity of the sea level at a location in Canada (as marked by the cross here and labelled (1) in figure 3) at different times to the viscosity at a depth of 635 km. The sensitivity is shown for sea level measurements (a) 15000 years ago, (b) 12000 years ago, (c) 9000 years ago, (d) 6000 years ago, (e) 3000 years ago and (f) at the present day.

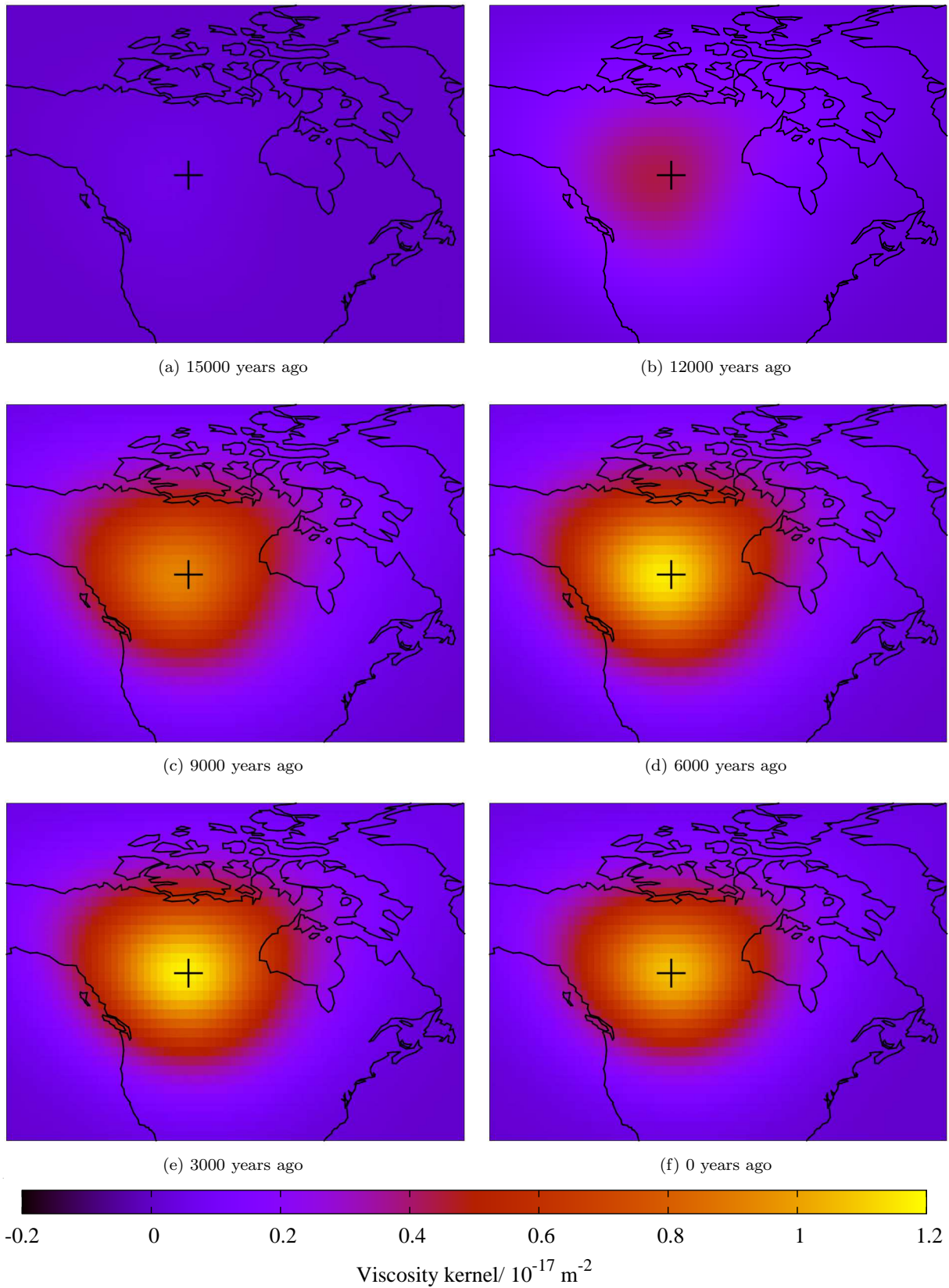


Figure 6. The sensitivity of the sea level at a location in Canada (as marked by the cross here and labelled (1) in figure 3) at different times to the viscosity at a depth of 1756 km. The sensitivity is shown for sea level measurements (a) 15000 years ago, (b) 12000 years ago, (c) 9000 years ago, (d) 6000 years ago, (e) 3000 years ago and (f) at the present day.

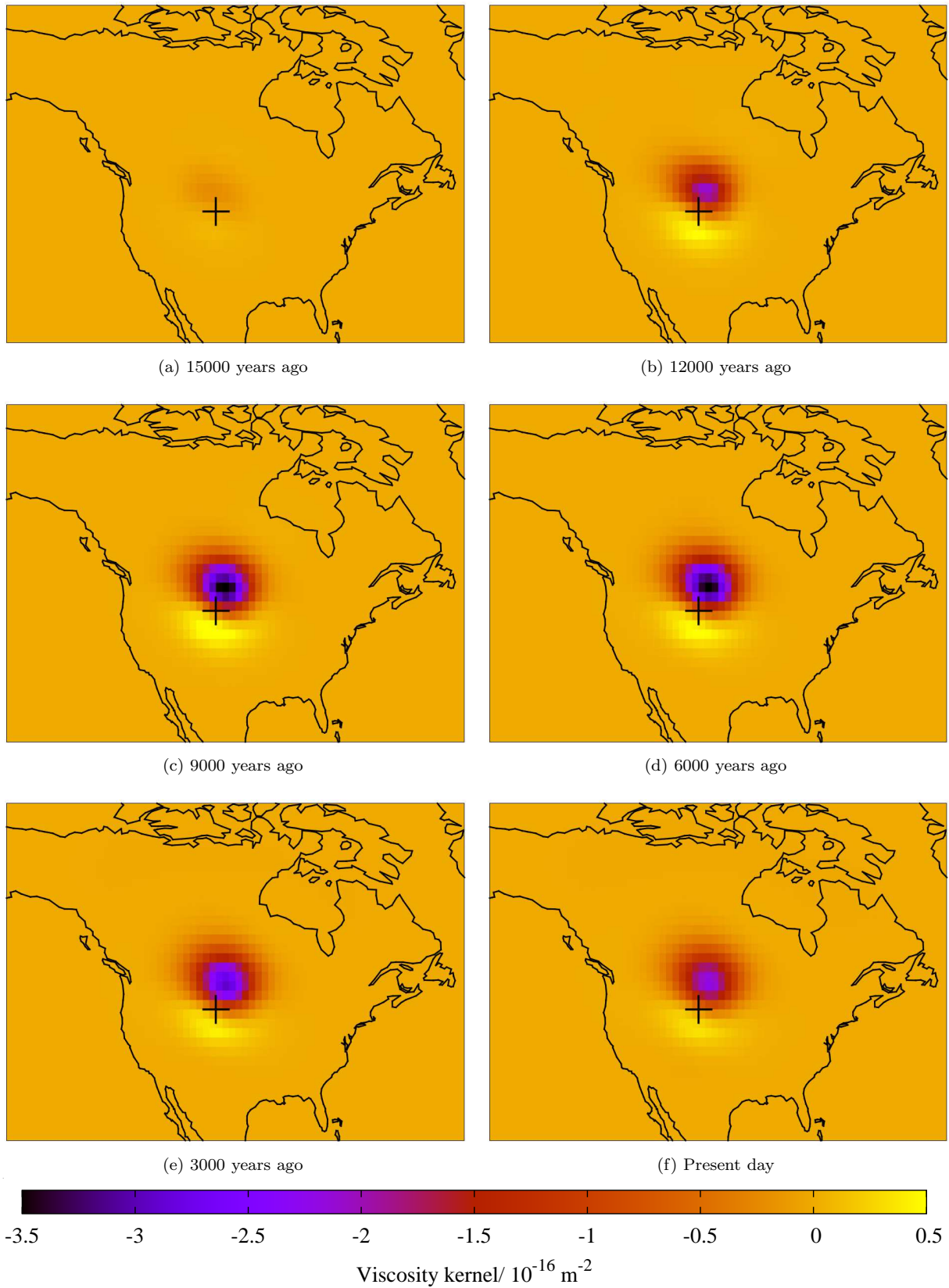


Figure 7. The sensitivity of the sea level at a location in the US (as marked by the cross here and labelled (2) in figure 3) at different times to the viscosity at a depth of 635 km. The sensitivity is shown for sea level measurements (a) 15000 years ago, (b) 12000 years ago, (c) 9000 years ago, (d) 6000 years ago, (e) 3000 years ago and (f) at the present day.

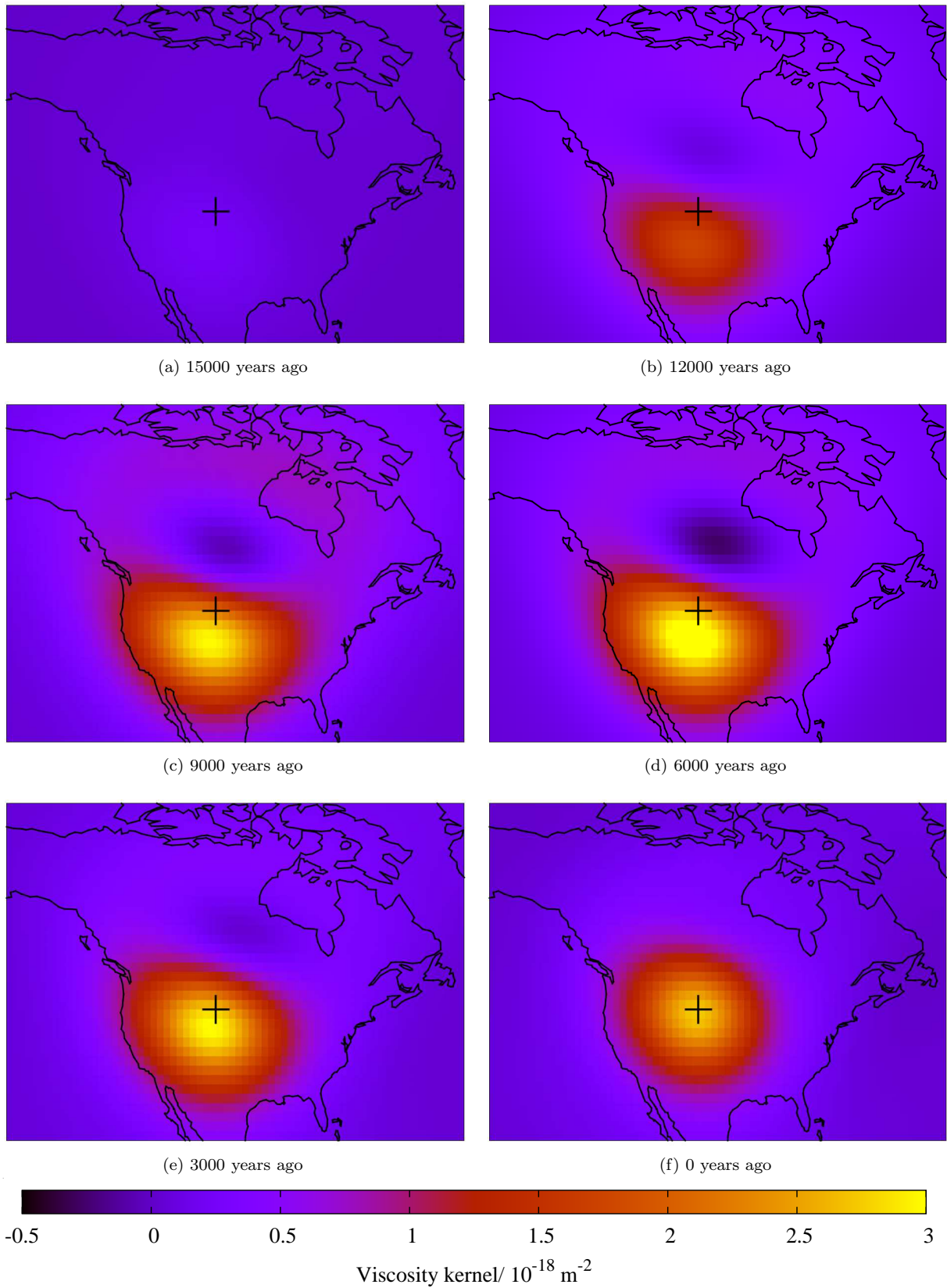


Figure 8. The sensitivity of the sea level at a location in the US (as marked by the cross here and labelled (2) in figure 3) at different times to the viscosity at a depth of 1756 km. The sensitivity is shown for sea level measurements (a) 15000 years ago, (b) 12000 years ago, (c) 9000 years ago, (d) 6000 years ago, (e) 3000 years ago and (f) at the present day.

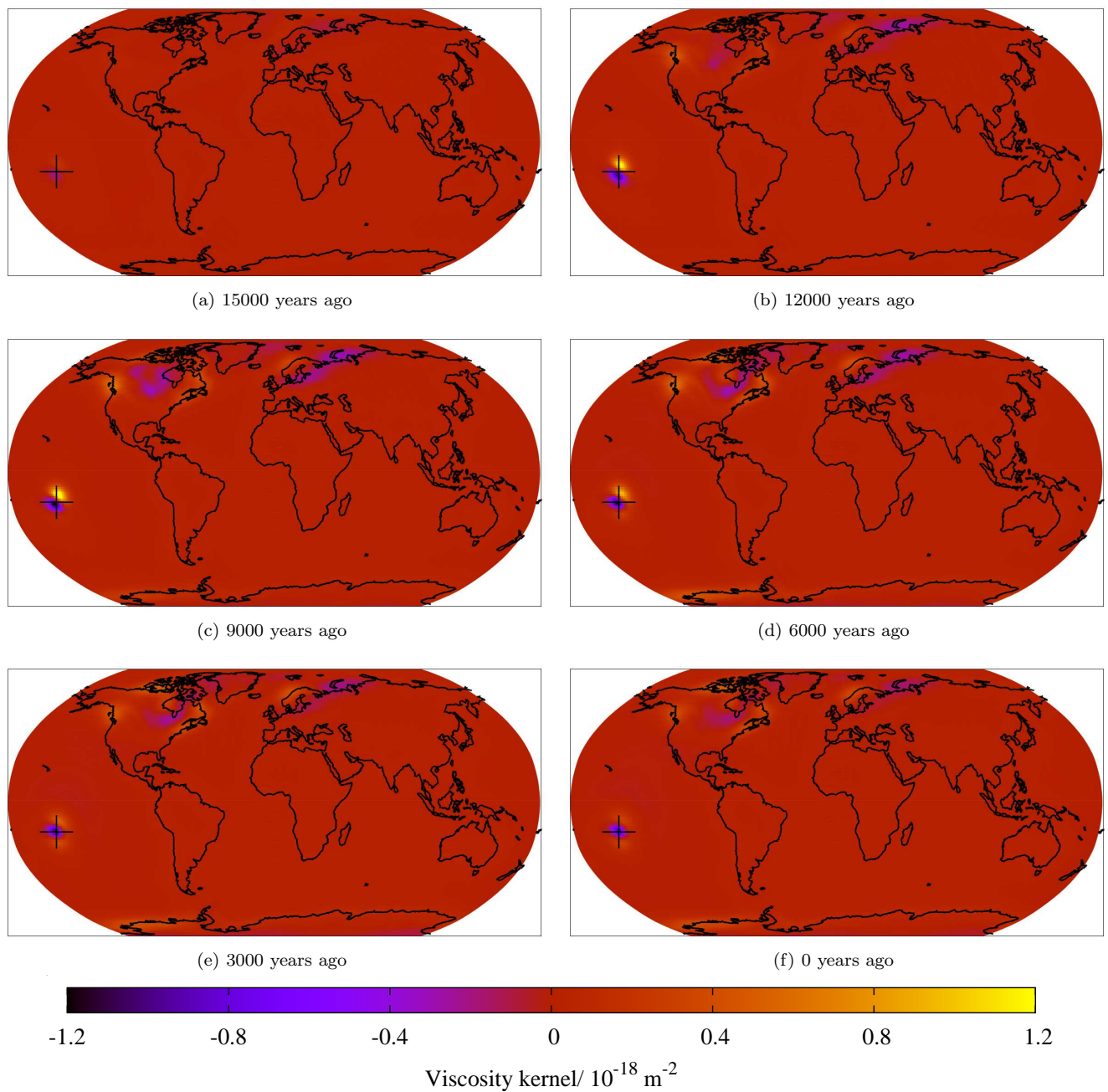


Figure 9. The sensitivity of the sea level in Tahiti (as marked by the cross here and labelled (3) in figure 3) at different times to the viscosity at a depth of 635 km. The sensitivity is shown for sea level measurements (a) 15000 years ago, (b) 12000 years ago, (c) 9000 years ago, (d) 6000 years ago, (e) 3000 years ago and (f) at the present day.

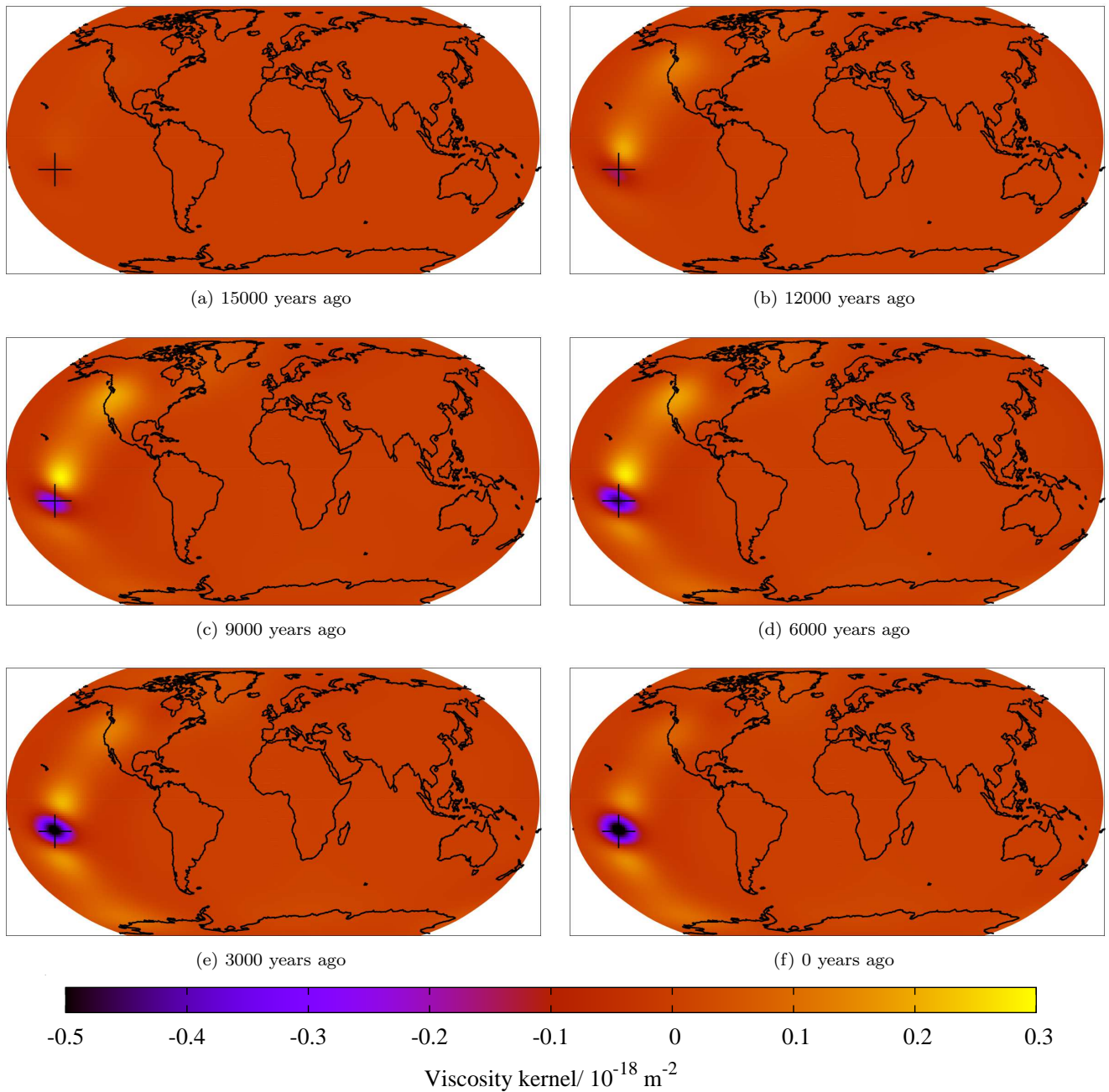


Figure 10. The sensitivity of the sea level in Tahiti (as marked by the cross here and labelled (3) in figure 3) at different times to the viscosity at a depth of 1756 km. The sensitivity is shown for sea level measurements (a) 15000 years ago, (b) 12000 years ago, (c) 9000 years ago, (d) 6000 years ago, (e) 3000 years ago and (f) at the present day.

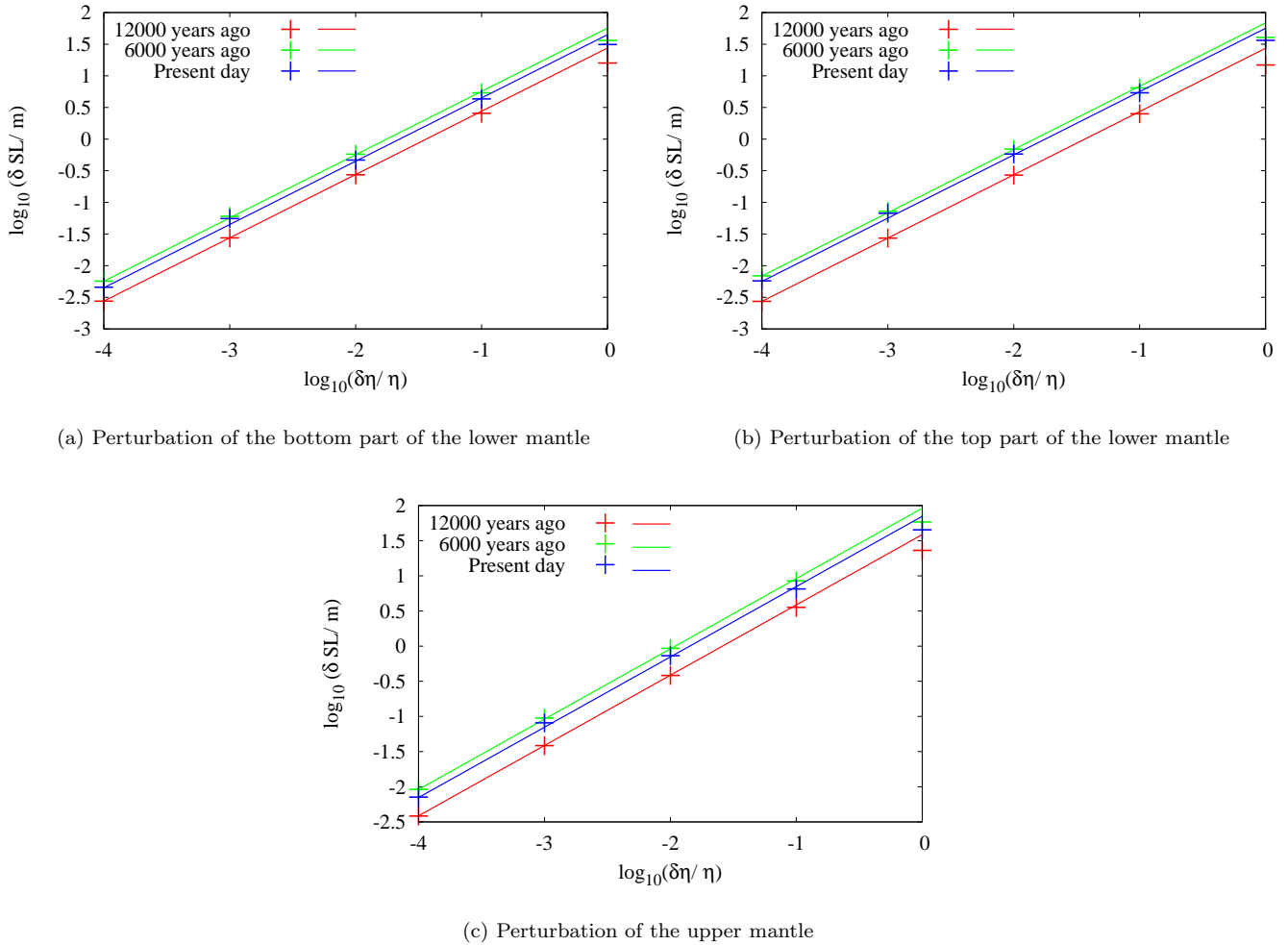


Figure 11. Comparison of the magnitude of the change in sea level at a location in Canada (indicated by (1) in figure 3) predicted by the kernels to the magnitude of the actual change for several different viscosity perturbations and sea level measurement times. We consider the sea level 12000 years ago (shown in red), 6000 years ago (shown in green) and at the present day (shown in blue) and examine how they respond to viscosity perturbations of different magnitudes in three different regions of the mantle. We perturb the viscosity between (a) 1428 and the core-mantle boundary at 2891 km depth (bottom part of the lower mantle), (b) 670 km and 1428 km depth (top part of the lower mantle) and (c) 120 km and 670 km depth (the upper mantle). The calculated changes in sea level are plotted in crosses of the appropriate colour, whilst the linearised changes predicted by the kernels are shown with the straight lines. At all times, all perturbations in the viscosity lead to an increase in sea level. We see that the kernels predict the change in sea level very well up to a perturbation of about 10%, and for perturbations larger than this still predict a change of the correct sign and order of magnitude.

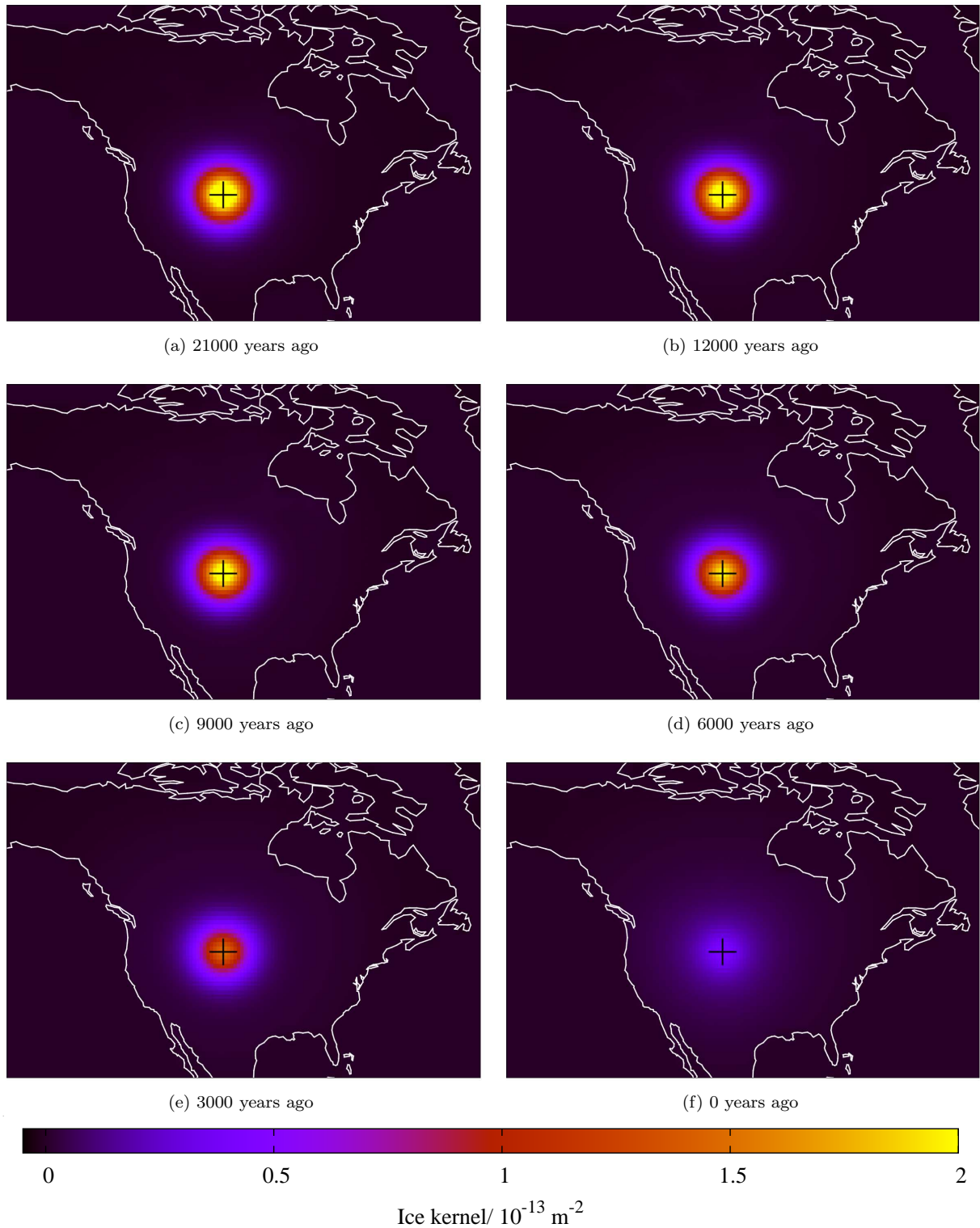


Figure 12. The sensitivity of the sea level at a location in the US (as marked by the cross here and labelled (2) in figure 3) at the present day to the rate of change of ice thickness at several times since the LGM. The sensitivity is shown to the rate of change of ice thickness (a) 21000 years ago, (b) 12000 years ago, (c) 9000 years ago, (d) 6000 years ago, (e) 3000 years ago and (f) at the present day. We show only the sensitivity in the vicinity of North America; however, there is a small negative sensitivity on the rest of the continents.

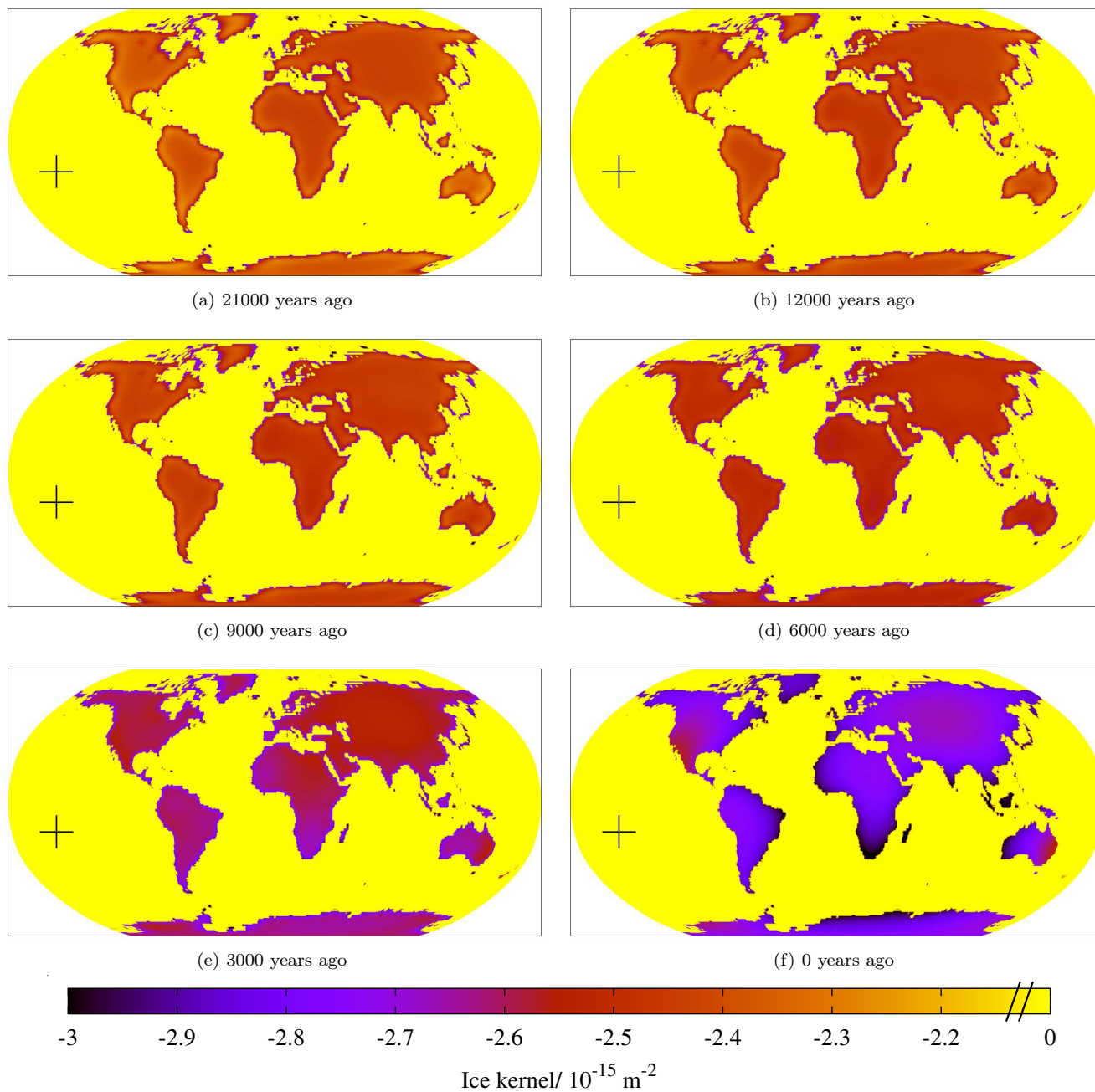
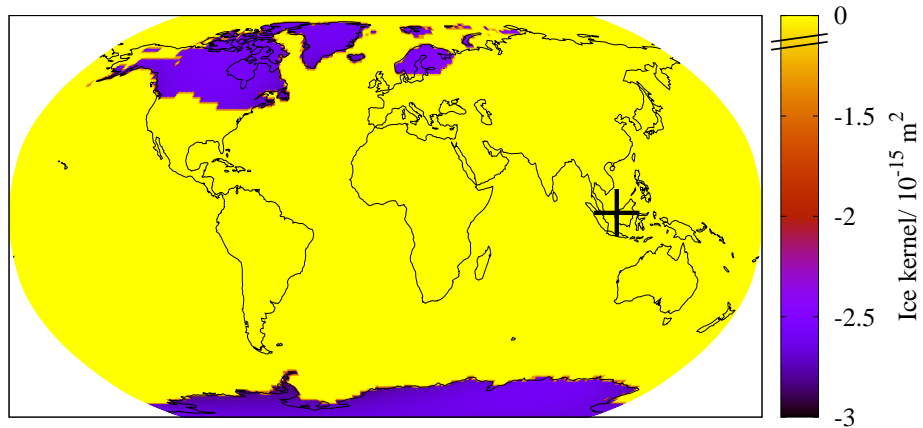
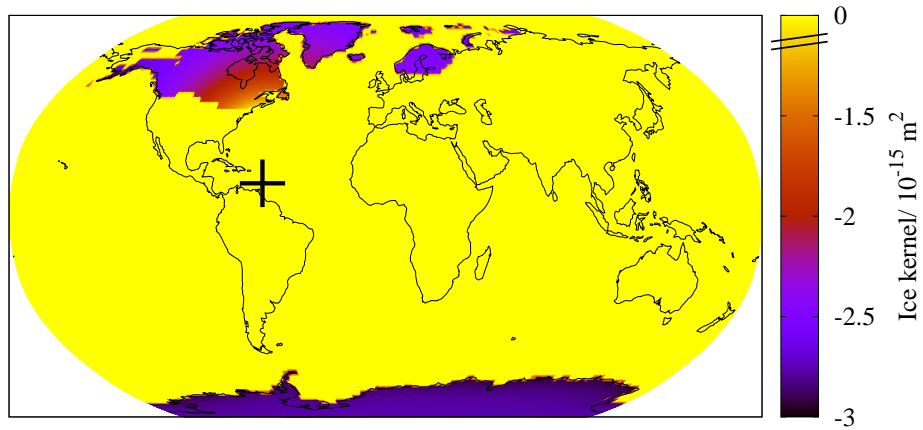


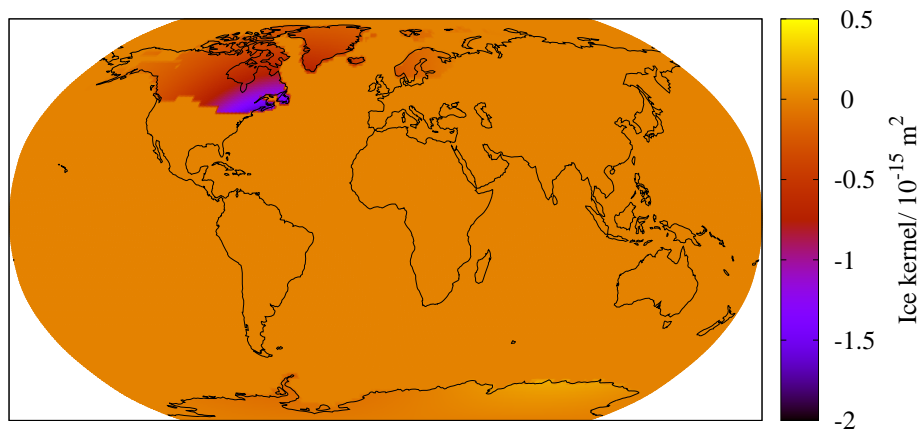
Figure 13. The sensitivity of the sea level in Tahiti (as marked by the cross here and labelled (3) in figure 3) at the present day to the rate of change of ice thickness at several times since the LGM. The sensitivity is shown to the rate of change of ice thickness (a) 21000 years ago, (b) 12000 years ago, (c) 9000 years ago, (d) 6000 years ago, (e) 3000 years ago and (f) at the present day.



(a) Measurement in the Sunda Shelf



(b) Measurement in Barbados



(c) Composite measurement – the sea level in the Sunda Shelf minus 95% of the sea level in Barbados

Figure 14. The sensitivity of the sea level 14200 years ago to the rate of change of ice thickness at that time in locations where there was ice present. We show the sensitivities for (a) the Sunda Shelf and (b) Barbados, which are indicated by the crosses. We also show (c) the sensitivity of a composite measurement, constructed to be relatively insensitive to the rate of change of ice thickness in Antarctica, which is 95% of the sea level in Barbados subtracted from the sea level in the Sunda Shelf.

APPENDIX A: DERIVATIVE OF THE OCEAN FUNCTION

In this appendix we obtain an expression for the time derivative of the ocean function defined in equation (2.32), and obtain similar relations for the first-order perturbation of the ocean function required in the derivation of the adjoint GIA problem. The details of this calculation are somewhat involved, requiring use of the theory of distributions. We also include a simpler heuristic derivation to help provide intuition about the result.

A1 Formal derivation

In order to simplify the presentation, we define the function f such that

$$f = \rho_w SL - \rho_i I. \quad (\text{A.1})$$

In terms of this function, we define \mathcal{F} , a subset of points on the surface of the Earth, by

$$\mathcal{F} = \{\mathbf{x} \in \partial M \mid f(\mathbf{x}) > 0\} \subseteq \partial M, \quad (\text{A.2})$$

and the corresponding indicator function

$$C(\mathbf{x}) = \begin{cases} 1, & \mathbf{x} \in \mathcal{F}, \\ 0, & \mathbf{x} \notin \mathcal{F}. \end{cases} \quad (\text{A.3})$$

For f defined as in equation (A.1), \mathcal{F} is the ocean set and C is the ocean function. We shall assume that f is smooth, and that

$$\nabla_1 f \neq \mathbf{0} \quad (\text{A.4})$$

whenever $f(\mathbf{x}) = 0$, where ∇_1 denotes the tangential gradient operator on ∂M . From this assumption, we see using the regular value theorem (e.g., Spivak 1970) that the boundary

$$\partial \mathcal{F} = \{\mathbf{x} \in \partial M \mid f(\mathbf{x}) = 0\}, \quad (\text{A.5})$$

which in our case is the shoreline, forms a one-dimensional sub-manifold on ∂M , but will not, in general, be connected. This assumption is necessary for the following analysis, but can be seen, physically, to exclude shoreline configurations which do not form a closed loop, such as the example shown in figure A1.

A1.1 Fermi normal co-ordinates on the boundary $\partial \mathcal{F}$

Given a point $\mathbf{x} \in \partial \mathcal{F}$, it will be useful to define a local co-ordinate system near the boundary. At \mathbf{x} we define basis vectors

$$\hat{\mathbf{x}}_{\perp} = \frac{\nabla_1 f}{\|\nabla_1 f\|}, \quad \hat{\mathbf{x}}_{\parallel} = \frac{\hat{\nu} \times \nabla_1 f}{\|\hat{\nu} \times \nabla_1 f\|}, \quad (\text{A.6})$$

where $\hat{\nu}$ is the outward unit normal vector to ∂M at this point, and \times denotes the usual cross-product in \mathbb{R}^3 . It is readily seen that $\hat{\mathbf{x}}_{\perp}$ is a unit tangent vector on ∂M that is normal to $\partial \mathcal{F}$ and pointing into \mathcal{F} , that is, perpendicular to the shoreline and pointing into the ocean. $\hat{\mathbf{x}}_{\parallel}$ is a unit tangent vector to ∂M that is tangent to $\partial \mathcal{F}$ at \mathbf{x} and so points along the shoreline. Using these definitions, we see that for $\mathbf{x} \in \partial \mathcal{F}$ we can write

$$\nabla_1 f = \partial_{\perp} f \hat{\mathbf{x}}_{\perp}, \quad (\text{A.7})$$

where, by definition $\partial_{\perp} f = \hat{\mathbf{x}}_{\perp} \cdot \nabla_1 f$, and we note that $\partial_{\perp} f > 0$ for all $\mathbf{x} \in \partial \mathcal{F}$ due to the chosen orientation of $\hat{\mathbf{x}}_{\perp}$.

Starting at \mathbf{x} , we can move along the boundary $\partial \mathcal{F}$ in the direction initially parallel to $\hat{\mathbf{x}}_{\parallel}$ a small distance l , and so arrive at a new point $\mathbf{x}' \in \partial \mathcal{F}$. We can define local basis vectors $\hat{\mathbf{x}}'_{\perp}$ and $\hat{\mathbf{x}}'_{\parallel}$ at \mathbf{x}' in the same manner as above, and so then move a distance n along the unique geodesic curve on ∂M starting at \mathbf{x}' that is initially tangent to $\hat{\mathbf{x}}'_{\perp}$ to arrive at a point $\mathbf{x}'' \in \partial M$. In this way, we have constructed a mapping from $(n, l) \in \mathbb{R}^2$ into ∂M , and it is clear that for (n, l) in a sufficiently small neighbourhood of zero this mapping is a diffeomorphism that defines the desired local co-ordinate system about the point $\mathbf{x} \in \partial M$.

This construction defines the so-called ‘Fermi normal co-ordinates’ associated with the submanifold $\partial \mathcal{F} \subseteq \partial M$ (e.g., Misner et al. 1973), and will be of great use below. Within these co-ordinates it may be shown that the metric tensor on ∂M has components equal to the Kronecker delta tensor δ_{ij} at the point \mathbf{x} , and so it follows that within a suitably small neighbourhood of \mathbf{x} we can write the surface element dS on ∂M as $dn dl$ which is accurate to first-order in the distance of the given point from \mathbf{x} .

A1.2 One-parameter families of indicator functions

Let now $(\mathbf{x}, \epsilon) \mapsto f(\mathbf{x}, \epsilon) \in \mathbb{R}$ be a smooth one-parameter family of scalar functions on ∂M defined for $\epsilon \in \mathbb{R}$ in some neighbourhood of zero. Associated with this one-parameter family, we can similarly define the sets \mathcal{F}_{ϵ} , and $\partial \mathcal{F}_{\epsilon}$, along with

the index functions

$$C(\mathbf{x}, \epsilon) = \begin{cases} 1, & \mathbf{x} \in \mathcal{F}_\epsilon, \\ 0, & \mathbf{x} \notin \mathcal{F}_\epsilon. \end{cases} \tag{A.8}$$

If we assume that

$$\nabla_1 f(\mathbf{x}, 0) \neq \mathbf{0} \tag{A.9}$$

for all $\mathbf{x} \in \partial\mathcal{F}_0$, then it readily follows that the same is true for all ϵ in some neighbourhood of zero, and that for such values of ϵ the boundary sets $\partial\mathcal{F}_\epsilon$ define embedded submanifolds on ∂M that are diffeomorphic to one another.

Let \mathbf{x}_0 be an arbitrary point on $\partial\mathcal{F}_0$, and let (n, l) be the Fermi normal co-ordinates defined in some neighbourhood of this point with respect to the boundary $\partial\mathcal{F}_0$. For ϵ sufficiently close to zero, we can use these co-ordinates to define locally the boundary $\partial\mathcal{F}_\epsilon$ implicitly through

$$f(n, l, \epsilon) = 0. \tag{A.10}$$

For $\epsilon = 0$ we see, in particular, that we must have $f(n, l, 0) = 0$, and, by definition of the co-ordinate system, this implies $n = 0$. For sufficiently small ϵ we know from eq.(A.9) that

$$\partial_n f(n, l, \epsilon) > 0, \tag{A.11}$$

and from the implicit function theorem (Spivak 1970) can conclude that there is a function $(l, \epsilon) \mapsto n(l, \epsilon)$ such that

$$f(n(l, \epsilon), l, \epsilon) = 0. \tag{A.12}$$

For fixed l , we can consider the mapping $\epsilon \mapsto n(l, \epsilon)$ to describe the trajectory of a point initially on $\partial\mathcal{F}_0$ as ϵ is varied. Differentiating eq.(A.12) with respect to ϵ and evaluating the result at $\epsilon = 0$, we obtain

$$\partial_\epsilon n(l, 0) = -\frac{\partial_\epsilon f(0, l, 0)}{\partial_n f(0, l, 0)}, \tag{A.13}$$

and so conclude that to first-order in ϵ the diffeomorphism from $\partial\mathcal{F}_0$ onto $\partial\mathcal{F}_\epsilon$ can be expressed in the local co-ordinates as

$$(0, l) \mapsto \left(-\frac{\partial_\epsilon f(0, l, 0)}{\partial_n f(0, l, 0)} \epsilon, l \right). \tag{A.14}$$

A1.3 Derivative of the one-parameter family of index functions

We now consider the calculation of $\partial_\epsilon C(\mathbf{x}, \epsilon)|_{\epsilon=0}$. Clearly this derivative will not define a regular function on ∂M , and we will have to interpret this derivative in the sense of distributions (e.g., Duistermaat & Kolk 2010). To do so, let $\Psi_h : \mathbb{R} \rightarrow \mathbb{R}$ be a smooth function depending smoothly on a parameter $h \in \mathbb{R}$, such that $\Psi_h(t) = 0$ for $t > -h$, and $\Psi_h(t) = 1$ for $t > h$. Such a function could be constructed explicitly, but this will not be necessary, and all we require is that

$$\lim_{h \rightarrow 0} \Psi_h = H, \tag{A.15}$$

where H is the Heaviside step function, and this limit is understood in the sense of distributions. Noting that the index function $C(\mathbf{x}, \epsilon)$ can be written

$$C(\mathbf{x}, \epsilon) = H[f(\mathbf{x}, \epsilon)], \tag{A.16}$$

in the sense of distributions, we can then write

$$C(\mathbf{x}, \epsilon) = \lim_{h \rightarrow 0} \Psi_h[f(\mathbf{x}, \epsilon)]. \tag{A.17}$$

When differentiating this expression in the sense of distributions, we are free to interchange the order of differentiation and the limit on the right hand side, and so obtain

$$\partial_\epsilon C(\mathbf{x}, \epsilon)|_{\epsilon=0} = \lim_{h \rightarrow 0} \Psi'_h[f(\mathbf{x}, 0)] \partial_\epsilon f(\mathbf{x}, \epsilon)|_{\epsilon=0}. \tag{A.18}$$

To reduce this expression further, we must evaluate the limit

$$\lim_{h \rightarrow 0} \Psi'_h[f(\mathbf{x}, 0)], \tag{A.19}$$

in the sense of distributions on ∂M . Letting φ be an arbitrary smooth test function on ∂M , we must have

$$\int_{\partial M} \lim_{h \rightarrow 0} \Psi'_h[f(\mathbf{x}, 0)] \varphi(\mathbf{x}) \, dS = \lim_{h \rightarrow 0} \int_{\partial M} \Psi'_h[f(\mathbf{x}, 0)] \varphi(\mathbf{x}) \, dS, \tag{A.20}$$

where the integral on the left hand side is interpreted as a duality product. For small values of h , $\Psi'_h[f(\mathbf{x}, 0)]$ will be non-zero in a thin ribbon enclosing $\partial\mathcal{F}_0$, and so we need only consider test functions whose support has non-empty intersection with this boundary. Furthermore, we can suppose that φ has support contained in an arbitrarily small neighbourhood of a point $\mathbf{x}_0 \in \partial\mathcal{F}_0$, and then pass to a global result using a suitable partition of unity. In particular, we suppose that the support of φ

is such that for each of its points \mathbf{x} , the geodesic distance from \mathbf{x}_0 is less than some $a > 0$. Within such a neighbourhood of \mathbf{x}_0 , we can employ the Fermi normal co-ordinates defined above, and so write

$$\int_{\partial M} \Psi'_h[f(\mathbf{x}, 0)]\varphi(\mathbf{x}) \, dS = \int_{-a}^a \int_{-a}^a \Psi'_h[f(n, l, 0)]\varphi(n, l) \, dn \, dl, \tag{A.21}$$

which is accurate to first order in the distance a . Expanding $f(n, l, 0)$ and $\varphi(n, l)$ in Taylor series about $n = 0$, recalling that $f(0, l, 0) = 0$ by construction, and retaining only lowest-order terms we obtain

$$\int_{\partial M} \Psi'_h[f(\mathbf{x}, 0)]\varphi(\mathbf{x}) \, dS = \int_{-a}^a \int_{-a}^a \Psi'_h[\partial_n f(0, l, 0)n]\varphi(0, l) \, dn \, dl, \tag{A.22}$$

which is now accurate to zeroth order in a . Introducing a dummy variable $t = \partial_n f(0, l, 0)n$ the integral on the right hand side can be alternatively written

$$\int_{-a}^a \int_{-a}^a \Psi'_h[\partial_n f(0, l, 0)n]\varphi(0, l) \, dn \, dl = \int_{-a}^a \left(\int_{-T}^T \Psi'_h(t) \, dt \right) \frac{\varphi(0, l)}{\partial_n f(0, l, 0)} \, dl, \tag{A.23}$$

where the integration limit $T > 0$ is readily determined but not needed. By taking $h < T$, we see that, by construction, $\int_{-T}^T \Psi'_h(t) \, dt = 1$, and so obtain

$$\lim_{h \rightarrow 0} \int_{\partial M} \Psi'_h[f(\mathbf{x}, 0)]\varphi(\mathbf{x}) \, dS = \int_{-a}^a \frac{\varphi(0, l)}{\partial_n f(0, l, 0)} \, dl, \tag{A.24}$$

which is accurate to zeroth order in the length a , which we recall determines the dimensions of the support of the test function φ . As, however, the test function is arbitrary, we can take a as small as we like, and so can conclude that eq.(A.24) holds exactly. Passing to a general test function using a suitable partition of unity, we then obtain the global result

$$\lim_{h \rightarrow 0} \int_{\partial M} \Psi'_h[f(\mathbf{x}, 0)]\varphi(\mathbf{x}) \, dS = \int_{\partial \mathcal{F}_0} \frac{1}{\partial_\perp f(\mathbf{x}, 0)} \varphi(\mathbf{x}) \, dl, \tag{A.25}$$

where dl now denotes the standard line element on ∂M . Combining this with eq.(A.18) we see that

$$\int_{\partial M} \partial_\epsilon C(\mathbf{x}, \epsilon)|_{\epsilon=0} \varphi(\mathbf{x}) \, dS = \int_{\partial \mathcal{F}_0} \frac{\partial_\epsilon f(\mathbf{x}, \epsilon)|_{\epsilon=0}}{\partial_\perp f(\mathbf{x}, 0)} \varphi(\mathbf{x}) \, dl, \tag{A.26}$$

and so can conclude that

$$\partial_\epsilon C(\mathbf{x}, \epsilon)|_{\epsilon=0} = \frac{\partial_\epsilon f(\mathbf{x}, \epsilon)|_{\epsilon=0}}{\partial_\perp f(\mathbf{x}, 0)} \delta_{\partial \mathcal{F}_0}(\mathbf{x}), \tag{A.27}$$

where $\delta_{\partial \mathcal{F}_0}$ is the delta line-distribution on $\partial \mathcal{F}_0$.

A1.4 Application to the ocean function

To calculate the time derivative of the ocean function we simply apply eq.(A.27) in the case that

$$f(\mathbf{x}, \epsilon) = \rho_w SL(\mathbf{x}, t + \epsilon) - \rho_i I(\mathbf{x}, t + \epsilon), \tag{A.28}$$

with ϵ denoting a time increment defined about some reference time t . This then leads to the desired result

$$\dot{C} = \frac{\rho_w \dot{S}L - \rho_i \dot{I}}{\rho_w \partial_\perp SL - \rho_i \partial_\perp I} \delta_{\partial \mathcal{O}_t}. \tag{A.29}$$

Similarly, if we wish to determine the first-order perturbation to the ocean function corresponding to given perturbations in SL and I , we immediately obtain

$$\delta C = \frac{\rho_w \delta SL - \rho_i \delta I}{\rho_w \partial_\perp SL - \rho_i \partial_\perp I} \delta_{\partial \mathcal{O}_t}. \tag{A.30}$$

We note that this equation is somewhat similar to equation (21) in Martinec et al. (2015), but their result is incorrect.

A2 Heuristic derivation

Here, we sketch a simpler and less formal derivation of the time derivative of the ocean function than is described in the previous section.

Figure A2 shows schematically, in one dimension, a shoreline with an ice sheet. At time t , the ice configuration is shown by solid black lines and the sea surface by the dashed black line. At a time Δt later, some of the ice sheet has melted and the sea level has risen, resulting in the ice sheet configuration shown by the solid blue lines and the sea surface by the dashed blue line. By the definition of derivatives, \dot{C} is given by

$$\dot{C}(x, t) = \lim_{\Delta t \rightarrow 0} \frac{C(x, t + \Delta t) - C(x, t)}{\Delta t}, \tag{A.31}$$

where, in our schematic, x is the direction perpendicular to the shoreline. At time t , the ocean function is zero for $x \leq 0$ and one for $x > 0$ and so we can write

$$C(x, t) = H(x), \tag{A.32}$$

where H is the Heaviside step function. At time $t + \Delta t$, the grounding line of the ice sheet has moved to $x = -h$, and so we have

$$C(x, t + \Delta t) = H(x + h). \tag{A.33}$$

We can therefore write equation (A.31) as

$$\dot{C}(x, t) = \lim_{\Delta t \rightarrow 0} \frac{H(x + h) - H(x)}{\Delta t}. \tag{A.34}$$

Using figure A2, we can calculate the value of h . In the region $-h \leq x \leq 0$, the vertical distance between the ocean floor (the solid black horizontal line) and the base of the ice sheet at time $t + \Delta t$ (the lower solid blue line) is equal to the change in thickness of the water load, $\Delta S(x)$, from time t to $t + \Delta t$. We can also see that this gradient of the solid blue line is the derivative of the water load with respect to x , which we will write as $\partial_{\perp} S$ to indicate that the derivative is in the direction perpendicular to the shoreline. Assuming that h is small enough that we can consider the gradient of S to be constant in the region $-h \leq x \leq 0$, we can therefore write

$$h = \frac{\Delta S(0)}{\partial_{\perp} S(0, t)} = \frac{\dot{S}(0, t)\Delta t}{\partial_{\perp} S(0, t)}, \tag{A.35}$$

where we have performed a Taylor expansion to first order in Δt . Using equation (2.30), we find

$$\rho_w \dot{S} = \rho_w \dot{S}L - \rho_i \dot{I}, \tag{A.36}$$

$$\rho_w \partial_{\perp} S = \rho_w \partial_{\perp} SL - \rho_i \partial_{\perp} I, \tag{A.37}$$

and so

$$h = \frac{\rho_w \dot{S}L(0, t) - \rho_i \dot{I}(0, t)}{\rho_w \partial_{\perp} SL(0, t) - \rho_i \partial_{\perp} I(0, t)} \Delta t, \tag{A.38}$$

which leads to

$$\dot{C}(x, t) = \lim_{\Delta t \rightarrow 0} \frac{1}{\Delta t} \left[H \left(x + \frac{\rho_w \dot{S}L(0, t) - \rho_i \dot{I}(0, t)}{\rho_w \partial_{\perp} SL(x, t) - \rho_i \partial_{\perp} I(x, t)} \Delta t \right) - H(x) \right]. \tag{A.39}$$

This function is plotted in figure A3. As Δt gets smaller, the non-zero region gets narrower and taller with constant area. As $\Delta t \rightarrow 0$, the function approaches a Dirac delta function multiplied by this area. We therefore find that

$$\dot{C}(x, t) = \frac{\rho_w \dot{S}L(x, t) - \rho_i \dot{I}(x, t)}{\rho_w \partial_{\perp} SL(x, t) - \rho_i \partial_{\perp} I(x, t)} \delta(x), \tag{A.40}$$

and, by extension, the full formula for the entire surface of the Earth is

$$\dot{C} = \frac{\rho_w \dot{S}L - \rho_i \dot{I}}{\rho_w \partial_{\perp} SL - \rho_i \partial_{\perp} I} \delta_{\partial \mathcal{O}_t}, \tag{A.41}$$

as stated in equation (2.44) and derived more rigorously in the previous section.

APPENDIX B: NUMERICAL IMPLEMENTATION OF THE FORWARD EQUATIONS IN SPHERICALLY SYMMETRIC EARTH MODELS

For the numerical examples presented in this paper, we assume that the earth model is spherically symmetric, that is, the structure is a function of depth only. However, our formulation of the forward problem is valid in models which are not spherically symmetric, and could be implemented in such a model using, for example, a three-dimensional finite element method.

For a spherically symmetric earth model, the outward unit normal vector will be in the radial direction. Therefore,

$$\nabla \Phi = g \hat{\mathbf{r}}, \tag{B.1}$$

and so

$$\mathbf{u} \cdot \nabla \Phi = g u_r, \tag{B.2}$$

where u_r is the component of the displacement in the radial direction.

B1 Generalised spherical harmonics

We will find it useful to adopt a pseudo-spectral method in calculating the time derivatives – we transform back and forth between the spatial and spherical harmonic domains depending on which is most useful for the particular step. To do so, we will expand some fields in generalised spherical harmonics. Using this approach, a scalar field, ϕ can simply be written

$$\phi = \sum_{l,m} \phi_{lm} Y_{lm}^0, \quad (\text{B.3})$$

where Y_{lm}^N are the generalised spherical harmonics defined in appendix C of Dahlen & Tromp (1998) and here, and in what follows, the summation is over integer values for $0 \leq l \leq \infty$ and $-l \leq m \leq l$. In considering higher order fields, we first recall the canonical basis vectors (Phinney & Burridge 1973),

$$\hat{\mathbf{e}}_- = \frac{1}{\sqrt{2}}(\hat{\boldsymbol{\theta}} - i\hat{\boldsymbol{\phi}}), \quad (\text{B.4})$$

$$\hat{\mathbf{e}}_0 = \hat{\mathbf{r}} \quad (\text{B.5})$$

$$\hat{\mathbf{e}}_+ = -\frac{1}{\sqrt{2}}(\hat{\boldsymbol{\theta}} + i\hat{\boldsymbol{\phi}}), \quad (\text{B.6})$$

defined relative to the basis vectors in spherical polar coordinates. The so-called contravariant components of the displacement, \mathbf{u} , in this basis are

$$u^- = \frac{1}{\sqrt{2}}(u_\theta + iu_\phi), \quad (\text{B.7})$$

$$u^0 = u_r, \quad (\text{B.8})$$

$$u^+ = -\frac{1}{\sqrt{2}}(u_\theta - iu_\phi). \quad (\text{B.9})$$

In order to expand these components using generalised spherical harmonics, we write

$$u_{lm}^\alpha = \sum_{l,m} u_{lm}^\alpha Y_{lm}^\alpha. \quad (\text{B.10})$$

We will find it useful to introduce coefficients U_{lm} , V_{lm} and W_{lm} , defined such that

$$u_{lm}^0 = U_{lm}, \quad (\text{B.11})$$

$$u_{lm}^\pm = \frac{k}{\sqrt{2}}(V_{lm} \pm iW_{lm}), \quad (\text{B.12})$$

where $k = \sqrt{l(l+1)}$. We can also write a second-order tensor field, \mathbf{T} , as

$$\mathbf{T} = \sum_{l,m} T_{lm}^{\alpha\beta} Y_{lm}^{\alpha+\beta} \hat{\mathbf{e}}_\alpha \otimes \hat{\mathbf{e}}_\beta, \quad (\text{B.13})$$

where \otimes is the tensor product. The main tensor we wish to consider is \mathbf{m} ; however, from equation (2.23), we can see that \mathbf{m} is a symmetric second-order tensor with zero trace. We therefore will find it useful to introduce the coefficients M_{lm} , N_{lm} , R_{lm} , S_{lm} and T_{lm} , defined such that

$$m_{lm}^{\pm\pm} = \frac{k\sqrt{k^2-2}}{2r}(M_{lm} \pm iN_{lm}), \quad (\text{B.14})$$

$$m_{lm}^{00} = \frac{2}{3r}R_{lm}, \quad (\text{B.15})$$

$$m_{lm}^{0\pm} = m_{lm}^{\pm 0} = \frac{k}{2\sqrt{2}r}(S_{lm} \pm iT_{lm}), \quad (\text{B.16})$$

$$m_{lm}^{\pm\mp} = \frac{1}{3r}R_{lm}. \quad (\text{B.17})$$

As shown in Al-Attar & Tromp (2014), the system naturally decouples into two sets of equations, the spheroidal system, which involves the coefficients U_{lm} , V_{lm} , ϕ_{lm} , M_{lm} , R_{lm} and S_{lm} , and the toroidal system, which involves W_{lm} , N_{lm} and T_{lm} . As our force term is purely in the radial direction, it only excites the spheroidal system.

B2 Calculation of \mathbf{m}

We can calculate \mathbf{m} using equation (2.23). The tensor components can be expanded using generalised spherical harmonics. As the spherical harmonics are orthogonal, the equations decouple for each l and m , and so each can be considered separately.

We find that

$$\dot{M}_{lm} = \frac{1}{\tau}(V_{lm} - M_{lm}), \quad (\text{B.18})$$

$$\dot{R}_{lm} = \frac{1}{\tau} \left(r \partial_r U_{lm} - U_{lm} + \frac{k^2}{2} V_{lm} - R_{lm} \right), \quad (\text{B.19})$$

$$\dot{S}_{lm} = \frac{1}{\tau} (r \partial_r V_{lm} - V_{lm} + U_{lm} - S_{lm}). \quad (\text{B.20})$$

B3 Calculation of $\dot{\mathbf{u}}$ and $\dot{\phi}$

Given the current ice distribution and sea level, we first calculate the ocean function spatially. We then calculate the spherical harmonic coefficients of C and hence the ocean area, which is given by

$$A = \sqrt{4\pi} R^2 C_{00}. \quad (\text{B.21})$$

In order to find $\dot{\mathbf{u}}$ and $\dot{\phi}$, we must solve

$$\begin{aligned} & \mathcal{A}(\dot{\mathbf{u}}, \dot{\phi} | \mathbf{u}', \phi') - \frac{\rho_w}{g} \int_{\partial M} \left[\dot{\mathbf{u}} \cdot \nabla \Phi + \dot{\phi} - \frac{1}{A} \int_{\partial M} C(\dot{\mathbf{u}} \cdot \nabla \Phi + \dot{\phi}) \, dS \right] C(\mathbf{u}' \cdot \nabla \Phi + \phi') \, dS \\ &= \int_{M_S} \frac{2\mu_0}{\tau} (\mathbf{d} - \mathbf{m}) : \mathbf{d}' \, dV - \rho_i \int_{\partial M} (1 - C) \dot{I} \left[\mathbf{u}' \cdot \nabla \Phi + \phi' - \frac{1}{A} \int_{\partial M} C(\mathbf{u}' \cdot \nabla \Phi + \phi') \, dS \right] \, dS, \end{aligned} \quad (\text{B.22})$$

where we have written all terms that are independent of $\dot{\mathbf{u}}$ and $\dot{\phi}$ on the right hand side, whereas those on the left hand side are linear in these time derivatives. However, we will first find it useful to consider the simpler equation

$$\mathcal{A}(\dot{\mathbf{u}}, \dot{\phi} | \mathbf{u}', \phi') = \int_{M_S} \frac{2\mu_0}{\tau} (\mathbf{d} - \mathbf{m}) : \mathbf{d}' \, dV - \rho_i \int_{\partial M} (1 - C) \dot{I} \left[\mathbf{u}' \cdot \nabla \Phi + \phi' - \frac{1}{A} \int_{\partial M} C(\mathbf{u}' \cdot \nabla \Phi + \phi') \, dS \right] \, dS. \quad (\text{B.23})$$

We recall that the equations of motion must hold for all choices of the test functions \mathbf{u}' and ϕ' . We will find it useful to choose

$$u'^{\alpha} = u_{lm}^{*\alpha} Y_{lm}^{*\alpha}, \quad (\text{B.24})$$

$$\phi' = \phi_{lm}^{*0} Y_{lm}^{*0}, \quad (\text{B.25})$$

for a particular l and m . As shown in Al-Attar & Tromp (2014), this choice results in the decoupling of the spherical harmonic components of $\dot{\mathbf{u}}$ and $\dot{\phi}$ for each different l and m . We can write these equations schematically as

$$\mathbf{A}_l \dot{\mathbf{w}}_{lm}^0 = \mathbf{f}_{lm}. \quad (\text{B.26})$$

For a model with no fluid regions and N radial nodes, \mathbf{A}_l is a matrix of size $3N \times 3N$ and \mathbf{w}_{lm}^0 and \mathbf{f}_{lm} are vectors of length $3N$. $\dot{\mathbf{w}}_{lm}^0$ contains, for particular values of l and m , the coefficients $\dot{\phi}_{lm}^0$, \dot{U}_{lm}^0 and \dot{V}_{lm}^0 at each radial node that satisfy equation (B.23), so that

$$(\mathbf{w}_{lm}^0)_{3n-2} = \dot{\phi}_{lm}^0(r_n), \quad (\text{B.27})$$

$$(\mathbf{w}_{lm}^0)_{3n-1} = \dot{U}_{lm}^0(r_n), \quad (\text{B.28})$$

$$(\mathbf{w}_{lm}^0)_{3n} = \dot{V}_{lm}^0(r_n). \quad (\text{B.29})$$

\mathbf{A}_l and \mathbf{f}_{lm} are constructed by taking U_{lm}^{*0} , V_{lm}^{*0} and ϕ_{lm}^{*0} to be equal to one at each radial node in turn and zero elsewhere. Therefore, the solution to equation (B.23) is

$$\dot{\mathbf{w}}_{lm}^0 = [\mathbf{A}_l]^{-1} \mathbf{f}_{lm}, \quad (\text{B.30})$$

for each l and m . We note that in fluid regions, this formulation requires some modification as only the gravitational potential coefficients are defined.

With the addition of the remaining terms on the left hand side of equation (B.22), the system no longer has the form of equation (B.26). The extra terms mean the equations no longer decouple for each l and m . Equation (B.22) can be written

$$\mathbf{A}_l \dot{\mathbf{w}}_{lm} + \mathbf{g}_{lm}(\dot{\mathbf{u}}, \dot{\phi}) = \mathbf{f}_{lm}, \quad (\text{B.31})$$

where $\mathbf{g}_{lm}(\dot{\mathbf{u}}, \dot{\phi})$ is a vector of length $3N$ formed by taking U_{lm}^{*0} , V_{lm}^{*0} and ϕ_{lm}^{*0} to be equal to one at each radial node in turn and zero elsewhere. We can therefore see that the components of \mathbf{g}_{lm} are

$$g_{lm}^{3N-2}(\dot{\mathbf{u}}, \dot{\phi}) = \frac{\rho_w}{gA} \left[C(g\dot{u}_r + \dot{\phi}) \right]_{00} C_{lm} - \frac{\rho_w}{g} \left[C(g\dot{u}_r + \dot{\phi}) \right]_{lm}, \quad (\text{B.32})$$

$$g_{lm}^{3N-1}(\dot{\mathbf{u}}, \dot{\phi}) = \frac{\rho_w}{A} \left[C(g\dot{u}_r + \dot{\phi}) \right]_{00} C_{lm} - \rho_w \left[C(g\dot{u}_r + \dot{\phi}) \right]_{lm}, \quad (\text{B.33})$$

and $g_{lm}^n(\dot{\mathbf{u}}, \dot{\phi}) = 0$ for $n \neq 3N - 2, 3N - 1$. Here we can explicitly see how \mathbf{g}_{lm} depends on the total $\dot{\mathbf{u}}$ and $\dot{\phi}$ fields, not just the coefficients for l and m . We can therefore not solve equation (B.22) by simply acting a matrix on a vector. Instead, we will use an iterative method, the steps of which are

- (i) use equation (B.30) to find $\dot{\mathbf{w}}_{lm}^0$, an initial estimate of \dot{U}_{lm} , \dot{V}_{lm} and $\dot{\phi}_{lm}$, for all l and m ;
- (ii) find the current estimate of the spatial fields $\dot{\mathbf{u}}$ and $\dot{\phi}$;
- (iii) construct the product $C(g\dot{u}_r + \dot{\phi})$ and take its spherical harmonic transform;
- (iv) calculate $\mathbf{g}_{lm}^i(\dot{\mathbf{u}}, \dot{\phi})$, the current estimate of $\mathbf{g}(\dot{\mathbf{u}}, \dot{\phi})$;
- (v) calculate $\dot{\mathbf{w}}_{lm}^{i+1}$ by rearranging equation (B.31) to find

$$\dot{\mathbf{w}}_{lm}^{i+1} = A_l^{-1}[\mathbf{f}_{lm} - \mathbf{g}_{lm}(\dot{\mathbf{u}}^i, \dot{\phi}^i)] = \dot{\mathbf{w}}_{lm}^0 - \mathbf{A}_l^{-1}\mathbf{g}_{lm}(\dot{\mathbf{u}}^i, \dot{\phi}^i); \tag{B.34}$$

- (vi) repeat steps (ii) - (v) until a suitable level of convergence is reached.

This method looks somewhat like the iteration required to solve the sea level equation; however, shoreline migration is handled trivially and iteration would not be required in a three-dimensional model.

B4 Calculation of $\dot{S}L$

We finally calculate $\dot{S}L$ in the spatial domain using equation (2.41). In order to do so, we must

- (i) calculate the spatial variation of $\dot{\mathbf{u}}$ and $\dot{\phi}$ at the surface from their spherical harmonic coefficients;
- (ii) construct the products $C(\dot{\mathbf{u}} \cdot \nabla\Phi + \dot{\phi})$ and $(1 - C)\dot{I}$;
- (iii) transform these products to the spherical harmonic domain in order to find $[C(\dot{\mathbf{u}} \cdot \nabla\Phi + \dot{\phi})]_{00}$ and $[(1 - C)\dot{I}]_{00}$;
- (iv) calculate $\dot{S}L$, which is given by

$$\dot{S}L = -\left(\dot{u}_r + \frac{\dot{\phi}}{g}\right) + \frac{\sqrt{4\pi}R^2}{A} \left[C\left(\dot{u}_r + \frac{\dot{\phi}}{g}\right) \right]_{00} - \frac{\sqrt{4\pi}R^2\rho_i}{\rho_w A} [(1 - C)\dot{I}]_{00}. \tag{B.35}$$

APPENDIX C: DERIVATION OF THE ADJOINT EQUATIONS

In this appendix, we derive the adjoint equations stated in section 3.4.

C1 Perturbation of the Lagrangian

The Lagrangian has the form

$$\begin{aligned} L = & J - \rho_w g \int_{\partial M} [SL(t_0) - SL_0]SL'_0 \, dS + \rho_i g \int_{\partial M} [I(t_0) - I_0]I'_0 \, dS \\ & + \int_{t_0}^{t_1} \left\{ \mathcal{A}(\dot{\mathbf{u}}, \dot{\phi}|\mathbf{u}', \phi') - \int_{M_S} 2\mu_0 \left[\dot{\mathbf{m}} : \mathbf{m}' + \frac{1}{\tau}(\mathbf{d} - \mathbf{m}) : (\mathbf{d}' - \mathbf{m}') \right] \, dV - \rho_w g \int_{\partial M} \dot{S}L SL' \, dS \right. \\ & - \frac{\rho_w}{g} \int_{\partial M} \left[\dot{\mathbf{u}} \cdot \nabla\Phi + \dot{\phi} - \frac{1}{A} \int_{\partial M} C(\dot{\mathbf{u}} \cdot \nabla\Phi + \dot{\phi}) \, dS \right] [gSL' + C(\mathbf{u}' \cdot \nabla\Phi + \phi')] \, dS - \rho_i g \int_{\partial M} (\dot{I}_1 - \dot{I})I' \, dS \\ & \left. + \rho_i \int_{\partial M} (1 - C)\dot{I}_1 \left[\mathbf{u}' \cdot \nabla\Phi + \phi' - \frac{1}{A} \int_{\partial M} [gSL' + C(\mathbf{u}' \cdot \nabla\Phi + \phi')] \, dS \right] \, dS \right\} dt. \tag{C.1} \end{aligned}$$

In order to calculate the adjoint equations, we must perturb the Lagrangian with respect to \mathbf{u} , ϕ , \mathbf{m} , SL and I . In doing so, it will be useful to write

$$\delta J = \int_{t_0}^{t_1} \int_{\partial M} (\dot{h}_{\mathbf{u}} \cdot \delta\mathbf{u} + \dot{h}_{\phi} \delta\phi + \dot{h}_{SL} \delta SL) \, dS \, dt, \tag{C.2}$$

where we are assuming the objective functional is a function of displacement, gravitational potential and sea level only.

C1.1 Perturbation with respect to SL

We first consider perturbations of the Lagrangian with respect to SL , and find

$$\begin{aligned} \delta L = & \int_{t_0}^{t_1} \int_{\partial M} \dot{h}_{SL} \delta SL \, dS \, dt - \rho_w g \int_{\partial M} \delta SL(t_0) SL'_0 \, dS - \rho_w g \int_{\partial M} \delta \dot{S} L SL' \, dS \\ & + \int_{t_0}^{t_1} \left\{ \frac{\rho_w}{g} \left[\int_{\partial M} \delta C(\dot{\mathbf{u}} \cdot \nabla \Phi + \dot{\phi}) \, dS \right] \left[\int_{\partial M} \frac{1}{A} [gSL' + C(\mathbf{u}' \cdot \nabla \Phi + \phi')] \, dS \right] \right. \\ & - \frac{\rho_w}{g} \left[\int_{\partial M} C(\dot{\mathbf{u}} \cdot \nabla \Phi + \dot{\phi}) \, dS \right] \left[\int_{\partial M} \frac{1}{A^2} [gSL' + C(\mathbf{u}' \cdot \nabla \Phi + \phi')] \, dS \right] \left[\int_{\partial M} \delta C \, dS \right] \\ & - \frac{\rho_w}{g} \int_{\partial M} \left[\dot{\mathbf{u}} \cdot \nabla \Phi + \dot{\phi} - \frac{1}{A} \int_{\partial M} C(\dot{\mathbf{u}} \cdot \nabla \Phi + \dot{\phi}) \, dS \right] \delta C(\mathbf{u}' \cdot \nabla \Phi + \phi') \, dS \\ & - \rho_i \int_{\partial M} \delta C \dot{I}_1 \left[\mathbf{u}' \cdot \nabla \Phi + \phi' - \frac{1}{A} \int_{\partial M} [gSL' + C(\mathbf{u}' \cdot \nabla \Phi + \phi')] \, dS \right] \, dS \\ & - \rho_i \left[\int_{\partial M} \frac{(1-C)}{A} \dot{I}_1 \, dS \right] \left[\int_{\partial M} \delta C(\mathbf{u}' \cdot \nabla \Phi + \phi') \, dS \right] \\ & \left. + \rho_i \left[\int_{\partial M} \frac{(1-C)}{A^2} \dot{I}_1 \, dS \right] \left[\int_{\partial M} [gSL' + C(\mathbf{u}' \cdot \nabla \Phi + \phi')] \, dS \right] \left[\int_{\partial M} \delta C \, dS \right] \right\} dt, \end{aligned} \tag{C.3}$$

where δC denotes the first order perturbation of C with respect to SL . Collecting terms and integrating by parts with respect to time to remove the time derivative of the perturbation, we find

$$\begin{aligned} \delta L = & \rho_w g \int_{\partial M} \{ \delta SL(t_0)[SL'(t_0) - SL'_0] - \delta SL(t_1)SL'(t_1) \} \, dS + \int_{t_0}^{t_1} \left\{ \int_{\partial M} \delta SL(\dot{h}_{SL} + \rho_w g \dot{S} L') \, dS \right. \\ & - \int_{\partial M} \delta C \left[\frac{\rho_w}{g}(\dot{\mathbf{u}} \cdot \nabla \Phi + \dot{\phi}) - \frac{\rho_w}{gA} \int_{\partial M} C(\dot{\mathbf{u}} \cdot \nabla \Phi + \dot{\phi}) \, dS + \rho_i \dot{I}_1 + \frac{\rho_i}{A} \int_{\partial M} (1-C)\dot{I}_1 \, dS \right] \\ & \left. \left[\mathbf{u}' \cdot \nabla \Phi + \phi' - \frac{1}{A} \int_{\partial M} [gSL' + C(\mathbf{u}' \cdot \nabla \Phi + \phi')] \, dS \right] \, dS \right\} dt. \end{aligned} \tag{C.4}$$

In order to eliminate the terms outside the time integral, we impose the conditions

$$SL'(t_1) = 0, \quad SL'_0 = SL'(t_0). \tag{C.5}$$

We recall that

$$\dot{S}L = -\frac{1}{g}(\dot{\mathbf{u}} \cdot \nabla \Phi + \dot{\phi}) + \frac{1}{gA} \int_{\partial M} C(\dot{\mathbf{u}} \cdot \nabla \Phi + \dot{\phi}) \, dS - \frac{\rho_i}{\rho_w} \int_{\partial M} (1-C)\dot{I}_1 \, dS, \tag{C.6}$$

and so equation (C.4) can be written as

$$\begin{aligned} \delta L = & \int_{t_0}^{t_1} \left\{ \int_{\partial M} (\dot{h}_{SL} + \rho_w g \dot{S} L') \delta SL \, dS \right. \\ & \left. - \int_{\partial M} \delta C(\rho_i \dot{I}_1 - \rho_w \dot{S} L) \left[\mathbf{u}' \cdot \nabla \Phi + \phi' - \frac{1}{A} \int_{\partial M} [gSL' + C(\mathbf{u}' \cdot \nabla \Phi + \phi')] \, dS \right] \, dS \right\} dt. \end{aligned} \tag{C.7}$$

Using equations (2.38), (A.29) and (A.30), we can write

$$(\rho_w \dot{S} L - \rho_i \dot{I}_1) \delta C = (\rho_w \dot{S} L - \rho_i \dot{I}_1) \delta C = \rho_w \dot{C} \delta SL \tag{C.8}$$

and so

$$\delta L = \int_{t_0}^{t_1} \int_{\partial M} \left\{ \dot{h}_{SL} + \rho_w g \dot{S} L' + \rho_w \dot{C} \left[\mathbf{u}' \cdot \nabla \Phi + \phi' - \frac{1}{A} \int_{\partial M} [gSL' + C(\mathbf{u}' \cdot \nabla \Phi + \phi')] \, dS \right] \right\} \, dS \, dt. \tag{C.9}$$

Therefore, setting the variation of L with respect to SL to be equal to zero, we have

$$\dot{S} L' + \frac{\dot{h}_{SL}}{\rho_w g} + \frac{\dot{C}}{g} \left[\mathbf{u}' \cdot \nabla \Phi + \phi' - \frac{1}{A} \int_{\partial M} [gSL' + C(\mathbf{u}' \cdot \nabla \Phi + \phi')] \, dS \right] = 0. \tag{C.10}$$

C1.2 Perturbation with respect to I

We now consider perturbations of the Lagrangian with respect to I . In this case,

$$\begin{aligned} \delta L = & \rho_i g \int_{\partial M} \{ \delta I(t_0)[I'_0 - I'(t_0)] + \delta I(t_1)I'(t_1) \} \, dS \\ & + \int_{t_0}^{t_1} \left\{ -\rho_i g \int_{\partial M} \delta I \dot{I}' \, dS - \int_{\partial M} \delta C(\rho_i \dot{I}_1 - \rho_w \dot{S} L) \left[\mathbf{u}' \cdot \nabla \Phi + \phi' - \frac{1}{A} \int_{\partial M} [gSL' + C(\mathbf{u}' \cdot \nabla \Phi + \phi')] \, dS \right] \right\} dt. \end{aligned} \tag{C.11}$$

where δC denotes the first order perturbation of C with respect to I , we have used equation (C.6) and we have integrated by parts with respect to time. In order to eliminate the terms outside the time integral, we impose the conditions

$$I'(t_1) = 0, \quad I'_0 = I'(t_0). \tag{C.12}$$

Using equations (2.38), (A.29) and (A.30), we can write

$$(\rho_w \dot{S}L - \rho_i \dot{I}_1) \delta C = (\rho_w \dot{S}L - \rho_i \dot{I}) \delta C = -\rho_i \dot{C} \delta I, \tag{C.13}$$

and so

$$\delta L = \int_{t_0}^{t_1} \left\{ -\rho_i g \int_{\partial M} \delta I \dot{I}' \, dS - \int_{\partial M} \rho_i \dot{C} \delta I \left[\mathbf{u}' \cdot \nabla \Phi + \phi' - \frac{1}{A} \int_{\partial M} [gSL' + C(\mathbf{u}' \cdot \nabla \Phi + \phi')] \, dS \right] \right\} dt. \tag{C.14}$$

Setting the variation of L with respect to I to be equal to zero, we therefore have

$$\dot{I}' + \frac{\dot{C}}{g} \left[\mathbf{u}' \cdot \nabla \Phi + \phi' - \frac{1}{A} \int_{\partial M} [gSL' + C(\mathbf{u}' \cdot \nabla \Phi + \phi')] \, dS \right] = 0. \tag{C.15}$$

C1.3 Perturbation with respect to \mathbf{u} , ϕ and \mathbf{m}

Finally, we consider perturbations of the Lagrangian with respect to \mathbf{u} , ϕ and \mathbf{m} , and so find

$$\delta L = \int_{t_0}^{t_1} \left\{ \int_{\partial M} (\dot{\mathbf{h}}_{\mathbf{u}} \cdot \delta \mathbf{u} + \dot{h}_\phi \delta \phi) \, dS + \mathcal{A}(\delta \mathbf{u}, \delta \phi | \dot{\mathbf{u}}', \phi') - \int_{\partial M} 2\mu_0 \left[\delta \dot{\mathbf{m}} : \dot{\mathbf{m}}' + \frac{1}{\tau} (\delta \mathbf{d} - \delta \mathbf{m}) : (\mathbf{d}' - \mathbf{m}') \right] \, dV \right. \\ \left. - \frac{\rho_w}{g} \int_{\partial M} \left[\delta \dot{\mathbf{u}} \cdot \nabla \Phi + \delta \dot{\phi} - \frac{1}{A} \int_{\partial M} C(\delta \dot{\mathbf{u}} \cdot \nabla \Phi + \delta \dot{\phi}) \, dS \right] [gSL' + C(\mathbf{u}' \cdot \nabla \Phi + \phi')] \, dS \right\} dt. \tag{C.16}$$

To eliminate the time derivatives of the perturbations, we can integrate this equation by parts with respect to time. We find

$$\delta L = \int_{t_0}^{t_1} \left\{ \int_{\partial M} (\dot{\mathbf{h}}_{\mathbf{u}} \cdot \delta \mathbf{u} + \dot{h}_\phi \delta \phi) \, dS - \mathcal{A}(\delta \mathbf{u}, \delta \phi | \dot{\mathbf{u}}', \phi') + \int_{\partial M} 2\mu_0 \left[\delta \mathbf{m} : \dot{\mathbf{m}}' - \frac{1}{\tau} (\delta \mathbf{d} - \delta \mathbf{m}) : (\mathbf{d}' - \mathbf{m}') \right] \, dV \right. \\ \left. + \frac{\rho_w}{g} \int_{\partial M} \left[\delta \mathbf{u} \cdot \nabla \Phi + \delta \phi - \frac{1}{A} \int_{\partial M} C(\delta \mathbf{u} \cdot \nabla \Phi + \delta \phi) \, dS \right] [g\dot{S}L' + C(\dot{\mathbf{u}}' \cdot \nabla \Phi + \dot{\phi}') + \dot{C}(\mathbf{u}' \cdot \nabla \Phi + \phi')] \, dS \right. \\ \left. - \frac{\rho_w}{gA} \int_{\partial M} \dot{C} \left[\delta \mathbf{u} \cdot \nabla \Phi + \delta \phi - \frac{1}{A} \int_{\partial M} C(\delta \mathbf{u} \cdot \nabla \Phi + \delta \phi) \, dS \right] [gSL' + C(\mathbf{u}' \cdot \nabla \Phi + \phi')] \, dS \right\} dt, \tag{C.17}$$

where we have imposed the terminal conditions

$$\mathbf{u}'(t_1) = \mathbf{0}, \quad \phi'(t_1) = 0, \quad \mathbf{m}'(t_1) = \mathbf{0}. \tag{C.18}$$

The terms in the second and third rows of equation (C.17) arise because

$$\int_{t_0}^{t_1} \left[\delta \dot{\mathbf{u}} \cdot \nabla \Phi + \delta \dot{\phi} - \frac{1}{A} \int_{\partial M} C(\delta \dot{\mathbf{u}} \cdot \nabla \Phi + \delta \dot{\phi}) \, dS \right] dt = \left[\delta \mathbf{u} \cdot \nabla \Phi + \delta \phi - \frac{1}{A} \int_{\partial M} C(\delta \mathbf{u} \cdot \nabla \Phi + \delta \phi) \, dS \right]_{t_0}^{t_1} \\ + \int_{t_0}^{t_1} \frac{1}{A} \int_{\partial M} \dot{C} \left[\delta \mathbf{u} \cdot \nabla \Phi + \delta \phi - \frac{1}{A} \int_{\partial M} C(\delta \mathbf{u} \cdot \nabla \Phi + \delta \phi) \, dS \right] \, dS dt. \tag{C.19}$$

Using equation (C.10), we can write

$$g\dot{S}L' + \dot{C}(\mathbf{u}' \cdot \nabla \Phi + \phi') = -\frac{\dot{h}_{SL}}{\rho_w} + \frac{\dot{C}}{A} \int_{\partial M} [gSL' + C(\mathbf{u}' \cdot \nabla \Phi + \phi')] \, dS. \tag{C.20}$$

Substituting this into equation (C.17), and after some rearrangement and cancelling of terms, we find

$$\delta L = \int_{t_0}^{t_1} \left\{ \int_{\partial M} (\dot{\mathbf{h}}_{\mathbf{u}} \cdot \delta \mathbf{u} + \dot{h}_\phi \delta \phi) \, dS - \mathcal{A}(\delta \mathbf{u}, \delta \phi | \dot{\mathbf{u}}', \phi') + \int_{\partial M} 2\mu_0 \left[\delta \mathbf{m} : \dot{\mathbf{m}}' - \frac{1}{\tau} (\delta \mathbf{d} - \delta \mathbf{m}) : (\mathbf{d}' - \mathbf{m}') \right] \, dV \right. \\ \left. - \frac{\rho_w}{g} \int_{\partial M} \left[\delta \mathbf{u} \cdot \nabla \Phi + \delta \phi - \frac{1}{A} \int_{\partial M} C(\delta \mathbf{u} \cdot \nabla \Phi + \delta \phi) \, dS \right] \left[\frac{\dot{h}_{SL}}{\rho_w} - C(\dot{\mathbf{u}}' \cdot \nabla \Phi + \dot{\phi}') \right] \, dS \right\} dt, \tag{C.21}$$

and so, setting this variation equal to zero, we have

$$\int_{\partial M} (\dot{\mathbf{h}}_{\mathbf{u}} \cdot \delta \mathbf{u} + \dot{h}_\phi \delta \phi) \, dS - \mathcal{A}(\delta \mathbf{u}, \delta \phi | \dot{\mathbf{u}}', \phi') + \int_{\partial M} 2\mu_0 \left[\delta \mathbf{m} : \dot{\mathbf{m}}' - \frac{1}{\tau} (\delta \mathbf{d} - \delta \mathbf{m}) : (\mathbf{d}' - \mathbf{m}') \right] \, dV \\ + \frac{\rho_w}{g} \int_{\partial M} \left[\dot{\mathbf{u}}' \cdot \nabla \Phi + \dot{\phi}' - \frac{1}{A} \int_{\partial M} C(\dot{\mathbf{u}}' \cdot \nabla \Phi + \dot{\phi}') \, dS \right] C(\delta \mathbf{u} \cdot \nabla \Phi + \delta \phi) \, dS \\ - \frac{1}{g} \int_{\partial M} \dot{h}_{SL} \left[\delta \mathbf{u} \cdot \nabla \Phi + \delta \phi - \frac{1}{A} \int_{\partial M} C(\delta \mathbf{u} \cdot \nabla \Phi + \delta \phi) \, dS \right] \, dS = 0. \tag{C.22}$$

C2 The adjoint equations

It is convenient to introduce adjoint variables, defined by

$$\mathbf{u}^\dagger(t) = \mathbf{u}'(t_1 - t + t_0), \quad (\text{C.23})$$

$$\phi^\dagger(t) = \phi'(t_1 - t + t_0), \quad (\text{C.24})$$

$$\mathbf{m}^\dagger(t) = \mathbf{m}'(t_1 - t + t_0), \quad (\text{C.25})$$

$$SL^\dagger(t) = SL'(t_1 - t + t_0), \quad (\text{C.26})$$

$$I^\dagger(t) = I'(t_1 - t + t_0), \quad (\text{C.27})$$

which satisfy the initial conditions

$$\mathbf{u}^\dagger(t_0) = \mathbf{0}, \quad \phi^\dagger(t_0) = 0, \quad \mathbf{m}^\dagger(t_0) = \mathbf{0}, \quad SL^\dagger(t_0) = 0, \quad I^\dagger(t_0) = 0. \quad (\text{C.28})$$

Similarly, we define the adjoint ocean function and adjoint ocean area through

$$C^\dagger(t) = C(t - t_1 + t_0), \quad (\text{C.29})$$

$$A^\dagger(t) = A(t - t_1 + t_0), \quad (\text{C.30})$$

and finally define adjoint sources as

$$\mathbf{h}_\mathbf{u}^\dagger(t) = \mathbf{h}_\mathbf{u}(t_1 - t + t_0), \quad (\text{C.31})$$

$$h_\phi^\dagger(t) = h_\phi(t_1 - t + t_0), \quad (\text{C.32})$$

$$h_{SL}^\dagger(t) = h_{SL}(t_1 - t + t_0). \quad (\text{C.33})$$

Using these definitions, we can rewrite equations (C.10), (C.15) and (C.22) as

$$\dot{S}L^\dagger = -\frac{\dot{h}_{SL}^\dagger}{\rho_w g} - \frac{\dot{C}^\dagger}{g} \left[\mathbf{u}^\dagger \cdot \nabla \Phi + \phi^\dagger - \frac{1}{A^\dagger} \int_{\partial M} [gSL^\dagger + C^\dagger(\mathbf{u}^\dagger \cdot \nabla \Phi + \phi^\dagger)] dS \right], \quad (\text{C.34})$$

$$\dot{I}^\dagger = -\frac{\dot{C}^\dagger}{g} \left[\mathbf{u}^\dagger \cdot \nabla \Phi + \phi^\dagger - \frac{1}{A^\dagger} \int_{\partial M} [gSL^\dagger + C^\dagger(\mathbf{u}^\dagger \cdot \nabla \Phi + \phi^\dagger)] dS \right] = \dot{S}L^\dagger + \frac{\dot{h}_{SL}^\dagger}{\rho_w g}, \quad (\text{C.35})$$

$$\begin{aligned} \mathcal{A}(\dot{\mathbf{u}}^\dagger, \dot{\phi}^\dagger | \mathbf{u}, \phi) - \int_{\partial M} 2\mu_0 \left[\dot{\mathbf{m}}^\dagger : \mathbf{m} + \frac{1}{\tau} (\mathbf{d}^\dagger - \mathbf{m}^\dagger) : (\mathbf{d} - \mathbf{m}) \right] dV - \int_{\partial M} (\dot{\mathbf{h}}_\mathbf{u}^\dagger \cdot \mathbf{u} + \dot{h}_\phi^\dagger \phi) dS \\ - \frac{\rho_w}{g} \int_{\partial M} \left[\dot{\mathbf{u}}^\dagger \cdot \nabla \Phi + \dot{\phi}^\dagger - \frac{1}{A^\dagger} \int_{\partial M} C^\dagger(\dot{\mathbf{u}}^\dagger \cdot \nabla \Phi + \dot{\phi}^\dagger) dS \right] C^\dagger(\mathbf{u} \cdot \nabla \Phi + \phi) dS \\ + \frac{1}{g} \int_{\partial M} \dot{h}_{SL}^\dagger \left[\mathbf{u} \cdot \nabla \Phi + \phi - \frac{1}{A^\dagger} \int_{\partial M} C^\dagger(\mathbf{u} \cdot \nabla \Phi + \phi) dS \right] dS = 0, \end{aligned} \quad (\text{C.36})$$

where we have also replaced the test functions $\delta \mathbf{u}$, $\delta \phi$ and $\delta \mathbf{m}$ with \mathbf{u} , ϕ and \mathbf{m} . These equations, along with the initial conditions given in equation (C.28), constitute the adjoint problem. We can also rewrite the Lagrangian as

$$\begin{aligned} L = J + \int_{t_0}^{t_1} \left\{ \mathcal{A}(\dot{\mathbf{u}}, \dot{\phi} | \mathbf{u}^\dagger, \phi^\dagger) - \int_{M_S} 2\mu_0 \left[\dot{\mathbf{m}} : \mathbf{m}^\dagger + \frac{1}{\tau} (\mathbf{d} - \mathbf{m}) : (\mathbf{d}^\dagger - \mathbf{m}^\dagger) \right] dV - \rho_w g \int_{\partial M} \dot{S}L SL^\dagger dS \right. \\ \left. - \frac{\rho_w}{g} \int_{\partial M} \left[\dot{\mathbf{u}} \cdot \nabla \Phi + \dot{\phi} - \frac{1}{A} \int_{\partial M} C(\dot{\mathbf{u}} \cdot \nabla \Phi + \dot{\phi}) dS \right] [gSL^\dagger + C^\dagger(\mathbf{u}^\dagger \cdot \nabla \Phi + \phi^\dagger)] dS - \rho_i g \int_{\partial M} (\dot{I}_1 - \dot{I}) I^\dagger dS \right. \\ \left. + \rho_i \int_{\partial M} (1 - C) \dot{I}_1 \left[\mathbf{u}^\dagger \cdot \nabla \Phi + \phi^\dagger - \frac{1}{A^\dagger} \int_{\partial M} [gSL^\dagger + C^\dagger(\mathbf{u}^\dagger \cdot \nabla \Phi + \phi^\dagger)] dS \right] dS \right\} dt \\ - \rho_w g \int_{\partial M} [SL(t_0) - SL_0] SL^\dagger(t_1) dS + \rho_i g \int_{\partial M} [I(t_0) - I_0] I^\dagger(t_1) dS \end{aligned} \quad (\text{C.37})$$

where, within the time integral, all forward variables are evaluated at time t and all adjoint variables are evaluated at time $t_1 - t + t_0$.

C3 Solving the adjoint sea level and ice equations

Equations (C.34) and (C.35) are singular and so cannot be straightforwardly numerically integrated. Instead, we define a new variable, Q^\dagger , which satisfies

$$Q^\dagger = SL^\dagger + \frac{h_{SL}^\dagger}{\rho_w g} + \frac{C^\dagger}{g} \left[\mathbf{u}^\dagger \cdot \nabla \Phi + \phi^\dagger - \frac{1}{A^\dagger} \int_{\partial M} [gSL^\dagger + C^\dagger(\mathbf{u}^\dagger \cdot \nabla \Phi + \phi^\dagger)] dS \right]. \quad (\text{C.38})$$

Therefore,

$$\begin{aligned} \dot{Q}^\dagger = & SL^\dagger + \frac{h_{SL}^\dagger}{\rho_w g} + \frac{C^\dagger}{g} \left[\mathbf{u}^\dagger \cdot \nabla \Phi + \phi^\dagger - \frac{1}{A^\dagger} \int_{\partial M} [gSL^\dagger + C^\dagger(\mathbf{u}^\dagger \cdot \nabla \Phi + \phi^\dagger)] dS \right] \\ & + \frac{C^\dagger}{g} \left[\dot{\mathbf{u}}^\dagger \cdot \nabla \Phi + \dot{\phi}^\dagger - \frac{1}{A^\dagger} \int_{\partial M} [g\dot{S}L^\dagger + C^\dagger(\dot{\mathbf{u}}^\dagger \cdot \nabla \Phi + \dot{\phi}^\dagger) + \dot{C}^\dagger(\mathbf{u}^\dagger \cdot \nabla \Phi + \phi^\dagger)] dS \right] \\ & + \frac{C^\dagger}{gA^\dagger} \left[\int_{\partial M} \dot{C}^\dagger dS \right] \left[\frac{1}{A^\dagger} \int_{\partial M} [gSL^\dagger + C^\dagger(\mathbf{u}^\dagger \cdot \nabla \Phi + \phi^\dagger)] dS \right], \end{aligned} \tag{C.39}$$

which, using equation (C.6), simplifies to

$$\dot{Q}^\dagger = \frac{C^\dagger}{g} \left[\dot{\mathbf{u}}^\dagger \cdot \nabla \Phi + \dot{\phi}^\dagger + \frac{1}{\rho_w A^\dagger} \int_{\partial M} \dot{h}_{SL}^\dagger dS - \frac{1}{A^\dagger} \int_{\partial M} C^\dagger(\dot{\mathbf{u}}^\dagger \cdot \nabla \Phi + \dot{\phi}^\dagger) dS \right]. \tag{C.40}$$

We also note that

$$Q^\dagger(t_0) = \frac{h_{SL}^\dagger(t_0)}{\rho_w g}. \tag{C.41}$$

We further define P^\dagger to be

$$P^\dagger = \frac{1}{gA^\dagger} \int_{\partial M} [gSL^\dagger + C^\dagger(\mathbf{u}^\dagger \cdot \nabla \Phi + \phi^\dagger)] dS, \tag{C.42}$$

which satisfies

$$\begin{aligned} \dot{P}^\dagger = & \frac{1}{A^\dagger} \int_{\partial M} \dot{S}L^\dagger dS - \frac{1}{gA^\dagger} \left[\int_{\partial M} \dot{C} dS \right] \left[\frac{1}{A^\dagger} \int_{\partial M} [gSL^\dagger + C^\dagger(\mathbf{u}^\dagger \cdot \nabla \Phi + \phi^\dagger)] dS \right] \\ & + \frac{1}{gA^\dagger} \int_{\partial M} \dot{C}^\dagger(\mathbf{u}^\dagger \cdot \nabla \Phi + \phi^\dagger) dS + \frac{1}{gA^\dagger} \int_{\partial M} C^\dagger(\dot{\mathbf{u}}^\dagger \cdot \nabla \Phi + \dot{\phi}^\dagger) dS, \end{aligned} \tag{C.43}$$

and, again using equation (C.6), this simplifies to

$$\dot{P}^\dagger = \frac{1}{gA^\dagger} \int_{\partial M} C^\dagger(\dot{\mathbf{u}}^\dagger \cdot \nabla \Phi + \dot{\phi}^\dagger) dS - \frac{1}{\rho_w g A^\dagger} \int_{\partial M} \dot{h}_{SL}^\dagger dS. \tag{C.44}$$

We also see that

$$P^\dagger(t_0) = 0. \tag{C.45}$$

Both equation (C.40) and equation (C.44) can be straightforwardly integrated. It is therefore useful to write SL^\dagger in terms of these two fields, and so we find

$$SL^\dagger = Q^\dagger + C^\dagger P^\dagger - \frac{h_{SL}^\dagger}{\rho_w g} - \frac{C^\dagger}{g}(\mathbf{u}^\dagger \cdot \nabla \Phi + \phi^\dagger). \tag{C.46}$$

Using equation (C.35), we can also write

$$I^\dagger = Q^\dagger + C^\dagger P^\dagger - \frac{C^\dagger}{g}(\mathbf{u}^\dagger \cdot \nabla \Phi + \phi^\dagger) - \frac{h_{SL}^\dagger(t_0)}{\rho_w g}. \tag{C.47}$$

C4 Elastic adjoint equations

It will also be useful to form the equations for when there is a jump in adjoint load. In this case, the equations become

$$\Delta Q^\dagger = \frac{C^\dagger}{g} \left[\Delta \mathbf{u}^\dagger \cdot \nabla \Phi + \Delta \phi^\dagger + \frac{1}{\rho_w A^\dagger} \int_{\partial M} \Delta h_{SL}^\dagger dS - \frac{1}{A^\dagger} \int_{\partial M} C^\dagger(\Delta \mathbf{u}^\dagger \cdot \nabla \Phi + \Delta \phi^\dagger) dS \right], \tag{C.48}$$

$$\Delta P^\dagger = \frac{1}{gA^\dagger} \int_{\partial M} C^\dagger(\Delta \mathbf{u}^\dagger \cdot \nabla \Phi + \Delta \phi^\dagger) dS - \frac{1}{\rho_w g A^\dagger} \int_{\partial M} \Delta h_{SL}^\dagger dS, \tag{C.49}$$

$$\begin{aligned} & \mathcal{A}(\Delta \mathbf{u}^\dagger, \Delta \phi^\dagger | \delta \mathbf{u}, \delta \phi) - \int_{\partial M} (\Delta \mathbf{h}_{\mathbf{u}}^\dagger \cdot \delta \mathbf{u} + \Delta h_\phi^\dagger \delta \phi) dS, \\ & - \frac{\rho_w}{g} \int_{\partial M} \left[\Delta \mathbf{u}^\dagger \cdot \nabla \Phi + \Delta \phi^\dagger - \frac{1}{A^\dagger} \int_{\partial M} C^\dagger(\Delta \mathbf{u}^\dagger \cdot \nabla \Phi + \Delta \phi^\dagger) dS \right] C^\dagger(\delta \mathbf{u} \cdot \nabla \Phi + \delta \phi) dS, \\ & + \frac{1}{g} \int_{\partial M} \Delta h_{SL}^\dagger \left[\delta \mathbf{u} \cdot \nabla \Phi + \delta \phi - \frac{1}{A^\dagger} \int_{\partial M} C^\dagger(\delta \mathbf{u} \cdot \nabla \Phi + \delta \phi) dS \right] dS = 0, \end{aligned} \tag{C.50}$$

and we can calculate SL^\dagger and I^\dagger using equations (C.46) and (C.47) respectively.

APPENDIX D: NUMERICAL IMPLEMENTATION OF THE ADJOINT EQUATIONS IN SPHERICALLY SYMMETRIC EARTH MODELS

We can expand the adjoint fields in an analogous manner to the forward fields. Introducing coefficients ϕ_{lm}^\dagger , U_{lm}^\dagger , V_{lm}^\dagger and W_{lm}^\dagger , we write

$$\phi^\dagger = \sum_{l,m} \phi_{lm}^\dagger Y_{lm}^0, \quad (\text{D.1})$$

and

$$u_{lm}^{\dagger 0} = U_{lm}^\dagger, \quad (\text{D.2})$$

$$u_{lm}^{\dagger \pm} = \frac{k}{\sqrt{2}} (V_{lm}^\dagger \pm iW_{lm}^\dagger). \quad (\text{D.3})$$

We can also write

$$m_{lm}^{\dagger \pm \pm} = \frac{k\sqrt{k^2 - 2}}{2r} (M_{lm}^\dagger \pm iN_{lm}^\dagger), \quad (\text{D.4})$$

$$m_{lm}^{\dagger 00} = \frac{2}{3r} R_{lm}^\dagger, \quad (\text{D.5})$$

$$m_{lm}^{\dagger 0 \pm} = m_{lm}^{\dagger \pm 0} = \frac{k}{2\sqrt{2}r} (S_{lm}^\dagger \pm iT_{lm}^\dagger), \quad (\text{D.6})$$

$$m_{lm}^{\dagger \pm \mp} = \frac{1}{3r} R_{lm}^\dagger, \quad (\text{D.7})$$

where we have introduced the coefficients M_{lm}^\dagger , N_{lm}^\dagger , R_{lm}^\dagger , S_{lm}^\dagger and T_{lm}^\dagger . As in the forward case, the spheroidal and toroidal systems of equations decouple. In what follows, we will assume that only the spheroidal system is excited. For a measurement with no toroidal component (such as a sea level measurement), this is a valid assumption. However, if we were, for example, to make a measurement of the horizontal displacement, we would need to solve the toroidal system of equations. This is considered in Crawford et al. (2017).

D1 Calculation of \mathbf{m}^\dagger

We find that the components of \mathbf{m}^\dagger satisfy

$$\dot{M}_{lm}^\dagger = \frac{1}{\tau} (V_{lm}^\dagger - M_{lm}^\dagger), \quad (\text{D.8})$$

$$\dot{R}_{lm}^\dagger = \frac{1}{\tau} \left(r\partial_r U_{lm}^\dagger - U_{lm}^\dagger + \frac{k^2}{2} V_{lm}^\dagger - R_{lm}^\dagger \right), \quad (\text{D.9})$$

$$\dot{S}_{lm}^\dagger = \frac{1}{\tau} \left(r\partial_r V_{lm}^\dagger - V_{lm}^\dagger + U_{lm}^\dagger - S_{lm}^\dagger \right). \quad (\text{D.10})$$

These equations have exactly the same form as those for the forward variables, and so we can use the same numerical code.

D2 Calculation of $\dot{\mathbf{u}}^\dagger$ and $\dot{\phi}^\dagger$

In order to find $\dot{\mathbf{u}}^\dagger$ and $\dot{\phi}^\dagger$, we must solve

$$\begin{aligned} & \mathcal{A}(\dot{\mathbf{u}}^\dagger, \dot{\phi}^\dagger | \mathbf{u}, \phi) - \int_{\partial M} 2\mu_0 \left[\dot{\mathbf{m}}^\dagger : \mathbf{m} + \frac{1}{\tau} (\mathbf{d}^\dagger - \mathbf{m}^\dagger) : (\mathbf{d} - \mathbf{m}) \right] dV - \int_{\partial M} (\dot{\mathbf{h}}_{\mathbf{u}}^\dagger \cdot \mathbf{u} + \dot{h}_\phi^\dagger \phi) dS \\ & - \frac{\rho_w}{g} \int_{\partial M} \left[\dot{\mathbf{u}}^\dagger \cdot \nabla \Phi + \dot{\phi}^\dagger - \frac{1}{A^\dagger} \int_{\partial M} C^\dagger (\dot{\mathbf{u}}^\dagger \cdot \nabla \Phi + \dot{\phi}^\dagger) dS \right] C^\dagger (\mathbf{u} \cdot \nabla \Phi + \phi) dS \\ & = - \frac{1}{g} \int_{\partial M} \dot{h}_{SL}^\dagger \left[\mathbf{u} \cdot \nabla \Phi + \phi - \frac{1}{A^\dagger} \int_{\partial M} C^\dagger (\mathbf{u} \cdot \nabla \Phi + \phi) dS \right] dS, \end{aligned} \quad (\text{D.11})$$

where we have simply rearranged equation (C.36) to have the terms independent of $\dot{\mathbf{u}}^\dagger$ and $\dot{\phi}^\dagger$ on the right hand side. Comparing this to equation (B.22), we see that the two differ only in the terms on the right hand side. We recall that in equation (D.11), \mathbf{u} and ϕ are now the time-independent test functions, and the equation must hold for all choices. As in the forward case, we define the test functions in terms of the complex conjugates of the generalised spherical harmonics. We can now find $\dot{\mathbf{u}}^\dagger$ and $\dot{\phi}^\dagger$ by following the same method as outlined in section B3. We will find that the vector \mathbf{f}_{lm} will be different in the adjoint case, but that it can be constructed in exactly the same way as in the forward case. With the exception of the calculation of this vector, we can use exactly the same numerical routines to solve the equations for the adjoint variables $\dot{\mathbf{u}}^\dagger$ and $\dot{\phi}^\dagger$ as for the forward variables $\dot{\mathbf{u}}$ and $\dot{\phi}$.

D3 Calculation of I^\dagger and SL^\dagger

As described in section C3, we do not calculate \dot{I}^\dagger and \dot{SL}^\dagger . We instead calculate \dot{P}^\dagger and \dot{Q}^\dagger , the time derivatives of two different functions and, having time-stepped the system, calculate SL^\dagger and I^\dagger from P^\dagger and Q^\dagger .

\dot{P}^\dagger and \dot{Q}^\dagger are given by equations (C.44) and (C.40) respectively. We calculate them spatially and so simply calculate $\dot{\mathbf{u}}$ and $\dot{\phi}$ from their spherical harmonic coefficients and construct the required terms. Having time-stepped the system, we then calculate SL^\dagger and I^\dagger in the spatial domain using equations (C.46) and (C.47) respectively.

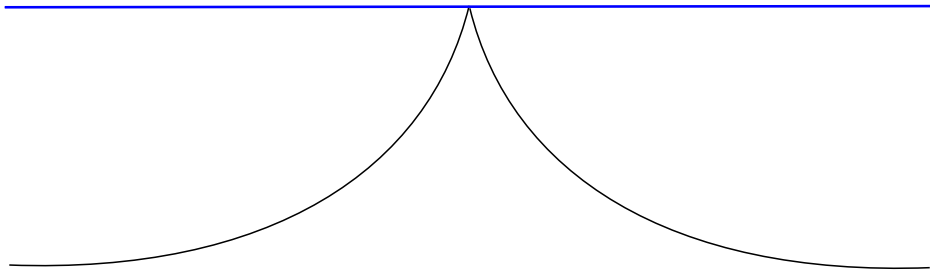


Figure A1. An example side view of a shoreline configuration which cannot be considered in our formulation of the problem. The black line is the surface of the solid Earth and the blue line is the ocean surface. The shoreline in this case does not form a closed loop but rather a single point or line where the ridge touches the ocean surface.

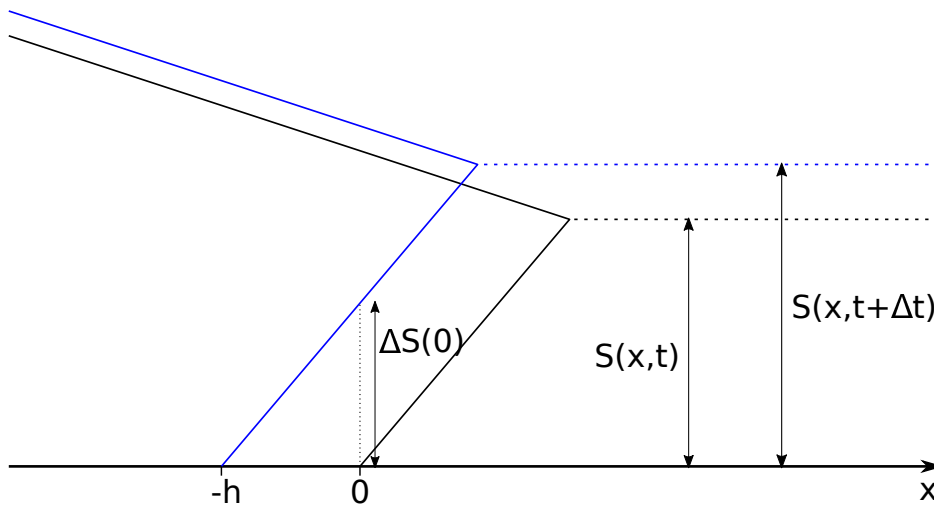


Figure A2. A schematic diagram showing a change in water and ice configuration. The x axis indicates the surface of the solid Earth. Initially, at time t , the edge of the ice sheet is shown by the solid black line and the surface of the ocean by the dashed black line. At a time Δt later, some of the ice has melted and sea level has risen so that at time $t + \Delta t$, the edge of the ice sheet is indicated by the solid blue line and the ocean surface is shown by the dashed blue line.

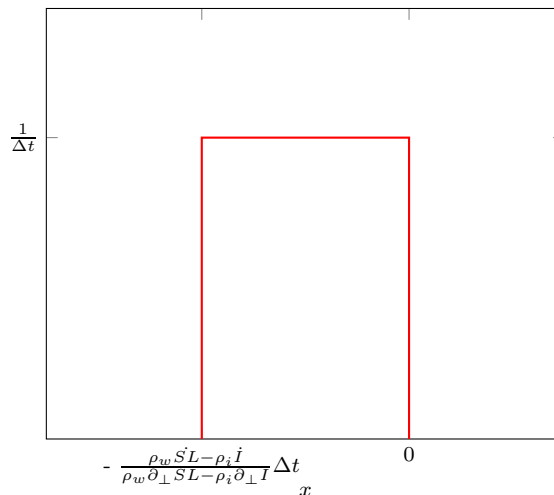


Figure A3. The function within the limit on the right hand side of equation (A.39). The time derivative of the ocean function, \dot{C} , is given by the limit of this function as Δt tends to zero, where x is in the direction perpendicular to the shoreline and pointing into the ocean.